Review

Synthesis of Inorganic-Organic Hybrid Thiometallate Materials with a Special Focus on Thioantimonates and Thiostannates and *in situ* X-Ray Scattering Studies of their Formation

Beatrix Seidlhofer, Nicole Pienack, and Wolfgang Bensch

Institute of Inorganic Chemistry, Christian-Albrechts-University of Kiel, Max-Eyth-Straße 2, 24118 Kiel, Germany

Reprint requests to Wolfgang Bensch. Phone: +49 431 880-2419. Fax: +49 431 880-1520. E-mail: wbensch@ac.uni-kiel.de

Z. Naturforsch. **2010**, *65b,* 937 – 975; received March 2, 2010

A rich variety of inorganic-organic hybrid thioantimonates and thiostannates were prepared during the last few years under solvothermal conditions applying organic amine molecules or transition metal complexes as structure directors. In this review synthetic approaches to and structural features of these thiometallates are discussed. For thioantimonates(III) the structures range from well isolated thioanions to three-dimensional networks, whereas the structural chemistry of thiostannates(IV) is strongly dominated by the $[Sn_2S_6]^{4-}$ anion, and no three-dimensional thiostannate has been reported so far. In the structures of thioantimonates(III) several primary building units like the $[SbS_3]$ trigonal pyramid, the $[SbS_4]$ unit or even the $[SbS_5]$ moiety are joined by vertex- and/or edge-linkages to form building blocks of higher structural hierarchy like $[Sb_3S_4]$ semi-cubes or Sb_xS_x heterocycles. A pronounced difference between thioantimonate and thiostannate chemistry is the tendency of Sb(III) to enhance the coordination geometry *via* so-called secondary bonds. In most cases the environment of Sb(III) is better described as a $3+n$ polyhedron with $n = 1-3$. The thioantimonate(V) structural chemistry is less rich than that of thioantimonates(III), and the $[SbS_4]^{3-}$ anion shows no tendency for further condensation. By applying suitable multidentate amine molecules, transition metal cations which normally prefer bonding to the N atoms of the amines can be incorporated into the thiometallate frameworks.

Key words: Thiometallates, Inorganic-Organic Hybrid Compounds, Solvothermal Synthesis, *in situ* X-Ray Scattering

Introduction

In the last few years several reviews appeared summarizing structural and synthetic work of thiometallate compounds prepared under solvothermal conditions [1 – 8]. Solvothermal or hydrothermal reactions are performed in closed reaction vessels applying polar solvents which are heated above their boiling points, *i. e.* temperatures in the range between 100 and about 250 °C. Under these conditions an autogeneous pressure is developed, and the properties of the solvents are drastically changed [9]. Typical solvents used are water, amines or alcohols, or mixtures of solvents. The advantages of the solvothermal approach are the dissolution of normally nearly insoluble starting materials like metals, chalcogens and metal chalcogenides in the strongly polar and polarizing solvents under conditions which are mild enough so that complex molecules like chains or rings can participate in the formation of the crystalline solids.

One should keep in mind that solvothermal reactions are heterogeneous reactions with complex equilibria of dissolved species, and small changes of synthesis parameters like temperature, pressure, solvent, viscosity, concentration and nature of the starting material, pH value, redox potential, reaction time, solubility of the reaction product, availability of protons, shape, size and charge of the charge compensating cations *etc.* can modify these equilibria. Several of these synthesis parameters influence each other in a not well understood way. Therefore, the successful preparation of a new compound under solvothermal conditions is mainly the result of a systematic variation of the parameters, and only few rules of thumb are at hand for planning the syntheses in a more directed way. Unfortunately, no systematic studies were performed re-

garding speciation of S species under strongly alkaline reaction conditions especially with respect to the role of the amines displaying different charges, sizes and shapes. (For an S speciation in alkaline media see references [10, 11]). A few years ago we were able to isolate several compounds containing S_5^{2-}, S_6^{2-} and S_7^{2-} species [12 – 15]. Similarly, polysulfide species with compositions $[Sn(S_4)_3]^{2-}$ and $[Sn(S_6)(S_4)_2]^{2-}$ were isolated at relatively low temperatures during the synthesis of thiostannates [11]. These observations are clear hints for the coexistence of the polysulfide anions, and the successful isolation of such prototypes may encourage researchers to systematically study the S speciation in strongly alkaline medium by varying the reaction conditions.

The aim of the present contribution is not to recall the findings presented in the reviews mentioned above, but to focus on inorganic-organic hybrid thioantimonates(III) and thiostannates(IV). We use the term inorganic-organic hybrids for those thioantimonates and thiostannates containing either pure organic cations as structure director and charge compensating molecules, or transition metal complexes $(TML_x)^{n+}$ (L is an amine ligand) acting in the same manner. There are also examples where both types of cationic species are present. For the $(TML_x)^{n+}$-containing group of compounds one may distinguish between those where the transition metal cation is an integral part of the thiometallate network, and the group of compounds where cations and anionic networks are isolated from each other. After some general considerations concerning the thioantimonate and thiostannate chemistry we review synthetic and structural features of the two groups of compounds. As mentioned above only little is known about the formation mechanisms of thiometallates under solvothermal conditions. Several *in situ* X-ray scattering experiments were performed during the last years shedding light onto the crystallization processes occurring under real solvothermal conditions. The main results of these studies are reviewed below.

General Structural Features of Thioantimonates(III), Thiostannates(IV) and Thiostannates(II)

The thioantimonate(III) chemistry is very different from that of all other thiometallates due to the lone electron pair (LEP) of Sb(III) which often exhibits a pronounced stereo-activity [16, 17]. Therefore, Sb(III) shows very flexible coordination patterns with coordination numbers between 3 and 6, variable bond lengths and relatively flexible S–Sb–S angles. The most common primary building unit is the trigonal pyramidal $[SbS_3]^{3-}$ anion with three Sb–S bonds scattering in length in a narrow range between 2.3 and 2.5 Å. In many structures the coordination number around Sb(III) is enhanced to 4 yielding a $[SbS_4]$ moiety. Since the formal charge of the central Sb atom in this unit is still +III, the Sb–S bond lengths are enlarged, and typical patterns are two short/two long Sb–S bonds which are around 2.45 Å for the shorter and between about 2.6 and $\approx$ 2.8 Å for the longer bonds, *i. e.*, compared to the $[SbS_3]$ group in the $[SbS_4]$ unit all Sb–S bonds are longer. The long Sb–S bonds are always in *trans* position giving rise to S–Sb–S angles between 170 and 180°. In very rare cases $[SbS_5]$ is found as a primary building unit, and for this moiety the bond length pattern is unusual because there is only one Sb–S bond below 2.5 Å, two are between 2.6 and 2.7 Å, and another two range from $\approx$ 2.8 to about 3.0 Å [see *e. g.* ref. 18]. The occurrence of such a variety of primary building units is unique in the field of thiometallate chemistry. The structural diversity of thioantimonates(III) results from these different primary building units. Their connection *via* corner- and/or edge-sharing leads to the next complex building blocks like $[Sb_2S_4]$ (edge-sharing of $[SbS_3]$), $[Sb_2S_5]$ (corner-sharing of $[SbS_3]$), *trans*- or *cis*-$[Sb_2S_6]$ groups (edge-sharing of two $[SbS_4]$ units) or so-called $[Sb_3S_4]$ semi-cubes (edge- and corner-sharing of two $[SbS_4]$ units and one $[SbS_3]$ unit).

A special feature of most thioantimonate(III) compounds is the occurrence of long Sb–S separations with distances up to about 3.6 Å (see discussion below). Hence, the coordination geometry of the Sb(III) atoms is often expanded, and in several structures distorted $[SbS_6]$ octahedra may be identified considering the S atoms at longer distances.

Hydrogen bonding interactions are very important despite the weakness of S···H bonds. Often the ammonium group points towards the inorganic network in a way enabling optimal interactions. Therefore it can be assumed that the organic cations exert a structure-directing effect.

The structural chemistry of thiostannates is less rich than that of the thioantimonates, and the most common polyhedra for Sn(IV) are $[SnS_4]$ tetrahedra and $[SnS_5]$ trigonal bi-pyramids. These primary units often condense forming $[Sn_2S_6]^{4-}$ bi-tetrahedra and/or $[Sn_3S_4]$ semi-cubes (Fig. 1).

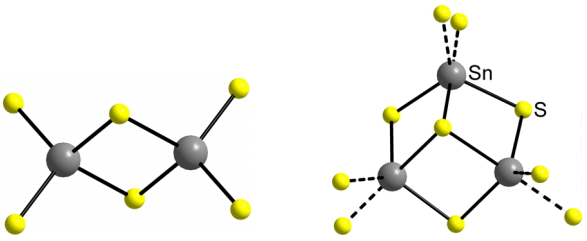

Fig. 1 (color online). Condensed polyhedra in thiostannates; left: $[Sn_2S_6]^{4-}$ unit with Sn atoms in a tetrahedral environment; right: $[Sn_3S_4]$ semi-cube with trigonal-bipyramidal coordination of Sn atoms.

For the relatively rare Sn(II) species the $[SnS_3]$ pyramid is often observed. The presence of a $[SnS_3]$ unit is an indication for Sn^{2+}. The existence of Sn in a pyramidal environment of S atoms is quite rare, with examples including the well-known Ottemannite $Sn(SnS_3)$ [19], but also $(Me_4N)(tb_3)Sn$ [20], $(AsPh_4)(Ph_3S_3)Sn$ [21] and $(PPh_4)(Ph_3S_3)Sn$ [22] (for abbrevations see Table 1). In some cases Sn(II) also occurs in an octahedral environment as *e. g.* in $SnCl_2(SC(NH_2)_2)$ [23], $Sn(S_2CN(C_2H_5)_2)_2$ [24] and $(Et_4N)_4Sn_2(WS_4)_4$ [25].

In contrast to Sb(III), neither for Sn(II) nor for Sn(IV) the tendency to form weak so-called secondary bonds is observed making a decision about the structural dimensionality of the inorganic network much easier. In the oxidation state +II there is also a LEP at the tin atom but it seems that it is less active than the LEP of Sb(III). Under the basic conditions of the solvothermal syntheses it can be assumed that the Sn(IV)S_x species in solution like $[SnS_4]^{4-}$ carry a larger negative charge than the dissolved Sb(III)S_x units. The larger negative charge must be compensated by appropriate positively charged cations. Maybe this is the reason why thiostannates(IV) with protonated mono- or diamines are rare. In addition there is a large tendency of the tetrahedral $[SnS_4]^{4-}$ anion to condensate forming the $[Sn_2S_6]^{4-}$ building unit. As a consequence this is the most common thiostannate(IV) anion.

Approaches to a Structural Classification for Thioantimonates(III)

Only very few hybrid thioantimonates(III) contain well isolated small thioantimonate(III) anions and charge-compensating protonated amine molecules or transition metal cations. Examples are the *cis*-$[Sb_2S_4]^{2-}$ unit in $(maH)_2Sb_2S_4$ [26] where the anion is composed of two edge-sharing $[SbS_3]$ pyramids, and

Table 1. List of the abbreviation used in this paper.

Abbreviation	Chemical name	Chemical formula
1,2-dach	1,2-diaminocyclohexane	$C_6H_{14}N_2$
1,2-dap	1,2-diaminopropane	$C_3H_{10}N_2$
1,3-dap	1,3-diaminopropane	$C_3H_{10}N_2$
1,3-dape	1,3-diaminopentane	$C_5H_{14}N_2$
1,4-dab	1,4-diaminobutane	$C_4H_{12}N_2$
1,4-dach	1,4-diaminocyclohexane	$C_6H_{14}N_2$
1,6-dah	1,6-diaminohexane	$C_6H_{16}N_2$
1a-2p	1-amino-2-propanol	C_3H_9NO
2-mpd	2-methylpropane-1,2-diamine	$C_2H_{10}N_2$
4,4′-epip	4,4′-ethylenedipiperazinium	$C_{10}H_{22}N_4$
aep	1-(2-aminoethyl)-piperazine	$C_6H_{15}N_3$
amp	3-aminomethylpiperazine	$C_6H_7N_2$
ap-en	*N*,*N*′-bis(3-aminopropyl)-ethylenediamine	$C_8H_{22}N_4$
$AsPh_4$	tetraphenylarsonium	$C_{24}H_{20}As$
baep	1,4-bis(2-aminoethy)piperazine	$C_8H_{20}N_4$
Bu_4N^+	tetrabutylammonium	$(C_4H_9)_4N^+$
$BuNH_3^+$	tributylammonium	$(C_4H_9)_3NH^+$
cha	cyclohexylamine	$C_6H_{13}N$
$C_3N_2H_6$	1-*N*-methylimidazole	$C_3N_2H_6$
$Cl_3SnBu\text{-}SnCl_3$	1,4-bis(trichlorostannyl)butane	$Cl_3Sn(CH_2)_4SnCl_3$
cyclam	1,4,8,11-tetraazacyclotetradecane	$C_{10}H_{24}N_4$
DABCO	triethylenediamine, 1,4-diazabicyclo[2.2.2]octane	$C_6H_{12}N_2$
DBN	1,5-diazabicyclo[4.3.0]non-5-ene	$C_7H_{12}N_2$
DBU	1,8-diazabicyclo[5.4.0]-undec-7-ene	$C_9H_{16}N_2$ $C_9H_{16}N_2$
dda	dodecylamine	$C_{12}H_{25}NH_3$
deen	*N*,*N*-diethylethylenediamine	$C_6H_{16}N_2$
depn	3-dimethylpropanediamine	$C_5H_{14}N_2$
dien	diethylenetriamine	$C_4H_{13}N_3$
dma	dimethylamine	C_2H_7N
dmen	*N*,*N*-dimethylethylenediamine	$C_4H_{12}N_2$
ea	ethylamine	C_2H_7N
en	ethylenediamine	$C_2H_8N_2$
Et_4N^+	tetraethylammonium	$(C_2H_5)_4N^+$
etam	ethanolamine	C_2H_7NO
*i*pa	*iso*-propylamine	C_3H_9N
ma	methylamine	CH_5N
mba	methylbutylamine	$C_5H_{13}N$
mdap	*N*-methyl-1,3-diaminopropane	$C_4H_{13}N_2$
Me_3NH^+	trimethylammonium	$(CH_3)_3NH^+$
Me_4N^+	tetramethylammonium	$(CH_3)_4N^+$
*n*ba	butylamine	$C_4H_{11}N$
*n*pa	propylamine	C_3H_9N
pea	pentylamine	$C_5H_{13}N$
Ph_3S_3	tris(phenylthiolato)	$C_{18}H_{15}S_3$
phen	1,10-phenanthroline	$C_{12}H_8N_2$
pip	piperazine	$C_4H_{10}N_2$
PPh_4	tetraphenylphosphonium	$C_{24}H_{20}P$
Pr_3NH^+	tripropylammonium	$(C_3H_7)_3NH^+$
Pr_4N^+	tetrapropylammonium	$(C_3H_7)_4N^+$
pyr	pyrrolidine	C_4H_9N
tb_3	tris(thiobenzoato)	$C_{21}H_{15}O_3S_3$
tepa	tetraethylenepentamine	$C_8H_{23}N_5$
THF	tetrahydrofuran	C_4H_8O
tren	tris(2-aminoethyl-)amine	$C_6H_{18}N_4$
trien	triethylenetetramine	$C_6H_{18}N_4$

the discrete $[Sb_2S_5]^{4-}$ anion constructed by vertex-linking of two $[SbS_3]$ units as in $[Fe(en)_3]_2Sb_2S_5 \cdot 0.55\,H_2O$ [27] or $[Mn(en)_3]Sb_2S_5$ [28]. Table 1 gives an overview of the abbreviations of the organic compounds used in this review.

It appeares that under basic conditions small thioantimonate(III) anions have a pronounced tendency to condensate forming larger structural aggregates like chains, layers or three-dimensional networks, and that the isolation of few small anions may be viewed as a "snapshot" of the condensation reactions occurring during reaction progress. It is notable that $(maH)_2Sb_2S_4$ could only be obtained as a minority phase (5 % yield) using a mixture of Mn, Sb, S in methylamine solution heated at 145 °C for 5 d. A similar observation was reported for $[Fe(en)_3]_2Sb_2S_5 \cdot 0.55H_2O$ which appeared as the minor phase besides $[Fe(en)_3]Sb_4S_7$. Interestingly, $[Mn(en)_3]Sb_2S_5$ was reported as a phase-pure material, but we note that the synthesis was performed in pure en solution at the relatively high temperature of 180 °C which may provide suitable conditions for the isolation of small thioantimonate(III) anions. For these three compounds the structural classification is unambiguous, *i. e.*, they contain discrete thioantimonate(III) anions.

The classification of thioantimonates(III) with extended structures can be achieved applying different approaches based on structural dimensionality of the anion, on the Sb : S ratio, or on the organic or complex cation present. The first approach based on the dimensionality is not straightforward because Sb–S distances scatter over a wide range from 2.3 to about 3.6 Å which is the sum of the van der Waals radii [29]. Because an interatomic distance alone is not a good criterion to decide whether there is a bond or not, one can either try to extract the valence of a Sb–S bond applying the bond valence method [16, 17] or using theoretical calculations on a higher level. For the first approach Liebau and coworkers showed that bond valences of about 0.1 were obtained for Sb–S distances as long as 3.5 Å. But considering other parameters like the S–Sb–S bonding angles this is not generally applicable to other Sb–S separations as mentioned in [16, 17]. Theoretical calculations based for instance on DFT have not been performed due to the low structural symmetry and very large number of atoms in the unit cell together with pronounced hydrogen bonding interactions making such calculations very challenging. Nevertheless, to be consistent in the determination of the dimensionality of an anionic network we use a cut-off of about 3 Å for significant Sb–S bonding interactions.

A possible approach for the classification of thioantimonates(III) is the usage of the Sb : S ratio in the inorganic network. Thus all thioantimonates(III) can be sorted *e. g.* according to the increase in S content, but there are several examples of compounds with an identical Sb : S ratio but a different chemical formula and different structural dimensionality. On the other hand, for one and the same Sb : S ratio and an identical chemical formula different structural dimensionalities of the anionic networks have been observed. Some examples are given to shortly highlight the problem. For Sb : S = 1 : 2 the anions with compositions $[SbS_2]^-$ [30, 31], $[Sb_2S_4]^{2-}$ [26, 32, 33], $[Sb_3S_6]^{3-}$ [34], and $[Sb_4S_8]^{4-}$ [27, 35 – 37] were reported. In the $[SbS_2]^-$ and $[Sb_2S_4]^{2-}$ anions the $[SbS_3]$ trigonal pyramids and $[SbS_4]$ units are joined forming one-dimensional chains or two-dimensional sheets whereas the latter two anions may occur as isolated ring anions [34 – 36] or as short chains [27]. Once the structure of these species is known some conclusions can be drawn if only Sb-S-Sb connectivity and no bonding interactions to TM^{n+} and/or no S–S bridges are present. An isolated ring with composition $[Sb_2S_4]^{2-}$ should be not very stable due to the unfavorable strain of bonds, and the occurrence of larger rings like a $[Sb_5S_{10}]^{5-}$ anion is also not very likely due to the conformational flexibility and the relatively large negative charge located on the ring. However, one cannot exclude that such new thioantimonate(III) motifs are stabilized under more stringent conditions. We note that the structural diversity of $[Sb_4S_8]^{4-}$ is enhanced if bonding interactions between the thioantimonate anion and TM^{n+} centers occurs [37]. Further details concerning these results will be discussed below.

The anion with composition $[Sb_4S_7]^{2-}$ (Sb : S ratio = 1 : 1.75) is the most common one among all thioantimonate(III) anions, and until now about 40 different compounds containing this anion have been reported (see Table 2). In our opinion it is the most appropriate example to demonstrate the structural diversity of thioantimonate anions with a given Sb : S ratio concerning the connection of $[SbS_x]$ units and the network dimensionality [38, 39, 42, 44, 48, 50 – 53, 56 – 61]. In a recently published paper we have already summarized the thioantimonates(III) with the $[Sb_4S_7]^{2-}$ anion [45], and therefore only some selected aspects are discussed in the present review. Considering solely inorganic-organic hybrids, very few

Table 2. Selected structural parameters in thioantimonates containing $[Sb_4S_7]^{2-}$ anions (Dim. = dimensionality).

		Dim.	a (Å)	b (Å)	c (Å)	α (deg)	β (deg)	γ (deg)	V (Å^3)
$P\bar{1}$	$(eaH)_2Sb_4S_7$ [38]	2	7.015	11.867	13.324	63.789	78.629	87.597	973
	$(npaH)_2Sb_4S_7$ [39, 40]	2	7.012	11.930	14.267	114.06	98.43	92.61	1071
	$(nbaH)_2Sb_4S_7$ [39, 41]	2	7.038	11.95	15.501	67.90	77.30	87.28	1178
	$(peaH)_2Sb_4S_7$ [39]	2	7.015	11.917	16.743	109.18	99.75	92.82	1294
	$(ipaH)_2Sb_4S_7$ [39]	2	7.042	11.92	14.128	114.32	99.42	92.33	1059
	$(1a\text{-}2pH)_2Sb_4S_7$ [42]	2	7.010	11.950	14.570	113.43	97.86	92.26	1103
	$(trenH_2)Sb_4S_7$ [43]	1	5.935	9.114	19.636	98.99	98.41	94.49	1032
	$(1,4\text{-}dabH_2)Sb_4S_7$ [39]	2	6.017	8.975	16.549	89.74	86.329	84.60	888
	$(1,6\text{-}dahH_2)Sb_4S_7$ [44]	2	6.983	11.875	13.659	115.25	100.17	92.57	999
	$[Ni(tren)Sb_4S_7]$ [45]	1	8.086	9.514	14.309	85.83	75.14	83.12	1056
	$[Zn(trien)Sb_4S_7]$ [45]	1	8.3935	10.756	12.132	91.14	95.31	99.88	1074
	$[Mn(trien)Sb_4S_7]$ [45]	1	8.3202	10.957	12.131	91.39	95.12	99.26	1086
$P2_1/n$	$[Ni(1,2\text{-}dap)_3]Sb_4S_7$ [46, 47]	2	10.809	15.795	16.115	90	90.75	90	2751
	$[Co(1,2\text{-}dap)_3]Sb_4S_7$ [47]	2	10.814	15.705	16.046	90	90.542	90	2725
	$[Zn(tren)Sb_4S_7]$ [48]	1	7.978	10.625	25.901	90	90.75	90	2195
	$[Mn(tren)Sb_4S_7]$ [48]	1	8.008	10.626	25.991	90	90.71	90	2211
	$[Co(tren)Sb_4S_7]$ [48]	1	7.962	10.541	25.897	90	90.90	90	2173
	$[Fe(tren)Sb_4S_7]$ [48]	1	8.003	10.562	25.955	90	90.809	90	2193
	$[Ni(dien)(tren)]Sb_4S_7$ [45]	2	12.919	16.217	13.037	90	97.441	90	2708
	$[Cr(tren)Sb_4S_7]$ [49]	1	7.976	10.519	25.880	90	90.864	90	2171
$P2_1/c$	$[Ni(dien)_2]Sb_4S_7\cdot H_2O$ [50]	2	9.603	16.137	17.272	90	91.68	90	2675
	$[Mn(dien)_2]Sb_4S_7\cdot 0.5H_2O$ [51]	2	9.722	16.113	17.339	90	91.88	90	2715
	$[Mn(en)_3]Sb_4S_7$ [52]	1	10.003	14.224	17.397	90	101.89	90	2422
	$[Ni(en)_3]Sb_4S_7$ [33]	1	9.93	14.21	17.242	90	102.55	90	2375
	$[Co(en)_3]Sb_4S_7$ [43]	1	9.932	14.218	17.278	90	102.45	90	2383
	$[Fe(dien)_2]Sb_4S_7\cdot H_2O$ [45]	2	9.692	16.106	17.348	90	91.67	90	2707
	$[Co(dien)_2]Sb_4S_7\cdot 0.5H_2O$ [45]	2	9.638	16.111	17.293	90	91.762	90	2684
	$[Mg(en)_3]Sb_4S_7$ [53]	1	9.927	14.254	17.259	90	102.611	90	2383
$C2/c$	$[Co(cyclam)]_x(cyclamH_2)_{1-x}Sb_4S_7$ [54]	3	13.600	11.919	15.431	90	102.56	90	2441
	$[Ni(cyclam)]Sb_4S_7$ [54]	3	13.778	11.869	15.386	90	102.77	90	2454
	$(cyclamH_2)Sb_4S_7$ [54]	3	13.713	11.886	15.437	90	102.71	90	2454
Others	$(pipH_2)Sb_4S_7$ [55] - *Ama*2	2	9.950	28.513	5.903	90	90	90	1674
	$(1a\text{-}2pH)_2Sb_4S_7$ [42] - *Abm*2	1	19.632	9.941	11.373	90	90	90	2220

compounds exhibit a true three-dimensional network. These include $(cyclamH_2)Sb_4S_7$, $[Ni(cyclam)]Sb_4S_7$, and $[Co(cyclam,)]_x(cyclamH_2)_{1-x}Sb_4S_7$ ($0.08 \leq x \leq 0.74$) [54]. This observation is somewhat surprising because the cyclam molecule is relative large, and a general rule states that network dimensionality is reduced with increasing size of the charge-compensating counterion.

Compounds with layered $[Sb_4S_7]^{2-}$ anions were observed in *e. g.* $[Fe(dien)_2]Sb_4S_7 \cdot H_2O$, $[Co(dien)_2]Sb_4S_7 \cdot 0.5\ H_2O$, $[Ni(dien)(tren)]Sb_4S_7$, $[M(trien)Sb_4S_7]$ (M = Zn, Mn) [45], $[Ni(1,2\text{-}dap)_3]Sb_4S_7$ [46], $[M(1,2\text{-}dap)_3]Sb_4S_7$ (M = Ni, Co) [47], $(amine)_2Sb_4S_7$ (amine = *n*paH, *n*baH, peaH, *i*paH) [39, 40], $(1,6\text{-}dahH_2)Sb_4S_7$ [44], $(eaH)_2Sb_4S_7$ [38], and $(1a\text{-}2pH)_2Sb_4S_7$ [42] (see also Table 2).

One-dimensional $[Sb_4S_7]^{2-}$ chain anions were found in the compounds $[Co(en)_3]Sb_4S_7$, $(trenH_2)Sb_4S_7$ [43], $[Ni(en_3)]Sb_4S_7$ [33], $[Mg(en)_3]Sb_4S_7$ [53], $(1a\text{-}2pH)_2Sb_4S_7$ which is a polymorph of the above mentioned compound with a two-dimensional $[Sb_4S_7]^{2-}$ anion [42], $(pipH_2)Sb_4S_7$ [55], $[Cr(tren)Sb_4S_7]$ with Cr in the rather unusual +II oxidation state [49], $[M(tren)Sb_4S_7]$ with M = Mn, Fe, Co, and Zn [48], *etc.* (see Table 2). In many thioantimonates with a $[Sb_4S_7]^{2-}$ chain anion, layers are generated by weak Sb–S contacts at longer separations around 3 Å.

The high flexibility and variable connectivity of $[SbS_3]$ pyramids and $[SbS_4]$ moieties in one-dimensional $[Sb_4S_7]^{2-}$ anions is briefly demonstrated with four different examples. In the structure of $[Co(en)_3]Sb_4S_7$ undulated chains are observed constructed from alternating $[Sb_3S_4]$ semi-cubes and $[SbS_3]$ pyramids sharing common corners (Fig. 2, left). The structure of $(1,4\text{-}dabH_2)Sb_4S_7$ contains $[SbS_3]$ and $[SbS_4]$ building units which share corners and edges yielding Sb_2S_2, Sb_3S_3 and Sb_4S_4 heterocycles as secondary building blocks. These rings are finally con-

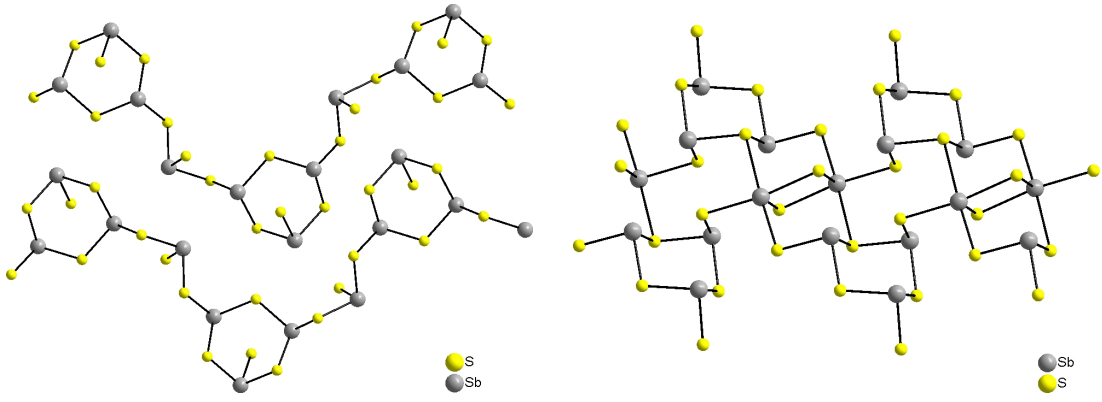

Fig. 2 (color online). The $[Sb_4S_7]^{2-}$ chain anion in $[Co(en)_3]Sb_4S_7$ (left) and in $(1,4\text{-dabH}_2)Sb_4S_7$ (right).

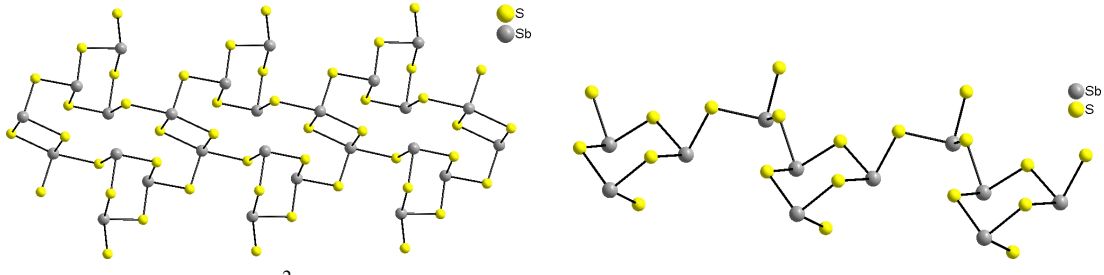

Fig. 3 (color online). The $[Sb_4S_7]^{2-}$ chain anion in $(trenH_2)Sb_4S_7$ (left) and in $(pipH_2)Sb_4S_7$ (right).

densed forming the one-dimensional $[Sb_4S_7]^{2-}$ anion (Fig. 2, right).

$[SbS_3]$ pyramids and $[SbS_4]$ moieties are also the primary building units in the structure of $(trenH_2)Sb_4S_7$, but these units are connected in a way that Sb_2S_2, Sb_3S_3 and large 16-membered Sb_8S_8 rings are generated (Fig. 3, left). Finally, the anion in $(pipH_2)Sb_4S_7$ is composed solely of $[SbS_3]$ units which are vertex-sharing to form alternating Sb_3S_3 rings and $[SbS_3]$ pyramids (Fig. 3, right).

Whereas for the Sb : S ratio of 1 : 1.75 only one composition is known, thioantimonates(III) with a Sb : S ratio of 1 : 1.67 display five different compositions including $[Sb_3S_5]^-$ [55, 62, 63], $[Sb_6S_{10}]^{2-}$ [64 – 69], $[Sb_9S_{15}]^-$ [67] and $[Sb_{12}S_{20}]^{4-}$ [70]. For instance, in the layered anions of (*trans*-1,4-dachH)Sb_3S_5 and (*trans*-1,2-dachH)$Sb_3S_5 \cdot H_2O$ the primary building units are condensed forming Sb_2S_2, Sb_4S_4 and Sb_5S_5 rings as the secondary building blocks [63]. The influence of the structure-directing cations on the network topology is small despite the very different arrangements of the protonated amine molecules in the two compounds shown in Figs. 4 and 5.

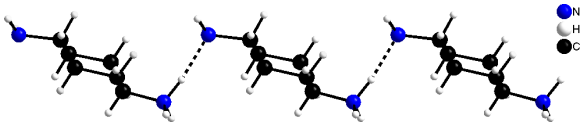

Fig. 4 (color online). The hydrogen-bonded *trans*-1,4-dachH cations in (*trans*-1,4-dachH)Sb_3S_5.

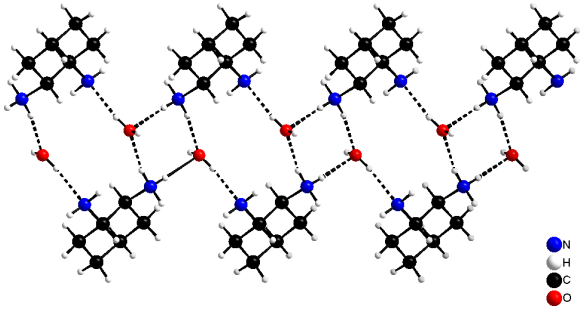

Fig. 5 (color online). The hydrogen bond network of *trans*-1,2-dachH cations and H_2O molecules in (*trans*-1,2-dachH)$Sb_3S_5 \cdot H_2O$.

For the thioantimonate anion $[Sb_3S_5]^-$ one-dimensional chains are observed in $(Pr_4N)Sb_3S_5$ [55] while $(PPh_4)_2Sb_6S_{10}$ contains the $[Sb_6S_{10}]^{2-}$ anion [64]. Interestingly, in both compounds a Sb_5S_5

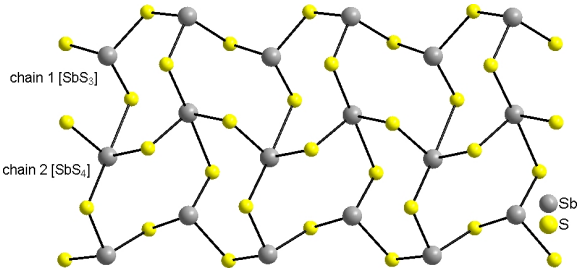

Fig. 6 (color online). The $[Sb_9S_{15}]^{3-}$ chain anion constructed by connection of $[SbS_3]$ and $[SbS_4]$ units [67].

ring constructed by corner-linking of $[SbS_3]$ trigonal pyramids is the main structural motif. The rings are condensed to form the chain anions. The topology of the anion in $[M(dien)_2]Sb_6S_{10} \cdot 0.5H_2O$ (M = Fe, Ni, Co) [65, 69] is relatively complex and may be described as chains generated by linking the $[SbS_3]$ and $[SbS_4]$ moieties to form Sb_2S_2, Sb_4S_4, and Sb_5S_5 heterocycles. The chains are then joined by condensation of the rings in the order Sb_4S_4-Sb_5S_5-Sb_2S_2-Sb_5S_5-Sb_4S_4 into large 32-membered $Sb_{16}S_{16}$ rings [65]. The layered $[Sb_6S_{10}]^{2-}$ anion in $(cyclamH_2)Sb_6S_{10}$ represents different structural motifs constructed by condensation of Sb_2S_2, Sb_4S_4 and Sb_7S_7 heterocycles [71].

A one-dimensional thioantimonate(III) anion is present in $(aepH_2)Sb_6S_{10}$ [67], which is characterized by Sb_3S_3 rings and $[Sb_3S_4]$ semi-cubes. In many other thioantimonates(III) weak Sb–S bonding interactions (Sb–S distances above 3 Å) increase the structural dimensionality, and in the present compound a three-dimensional thioantimonate(III) network is also generated.

There is only one example for the $[Sb_9S_{15}]^{3-}$ chain anion [67] which exhibits a very unusual linkage of the $[SbS_3]$ and $[SbS_4]$ primary building blocks. Two chains are composed exclusively of alternating $[SbS_3]$ pyramids by vertex-linkage, and a third chain is constructed solely by corner-sharing of $[SbS_4]$ units. The latter chain is embedded into the two chains composed of the $[SbS_3]$ pyramids (Fig. 6).

Finally, a one-dimensional $[Sb_{12}S_{20}]^{4-}$ chain anion is found in $[(maH)_{1.03}K_{2.97}]Sb_{12}S_{20} \cdot 1.34H_2O$ displaying a central Sb_4S_4 ring bound to six Sb_3S_3 groups forming the next hierarchical building block. These blocks are connected *via* S atoms, and larger Sb_8S_8 heterorings are formed [70].

For the Sb : S ratio of 1 : 1.60 only the $[Sb_{10}S_{16}]^{2-}$ anion has been reported so far with compositions $(aepH_2)Sb_{10}S_{16}$ [68], $(deenH_2)Sb_{10}S_{16} \cdot H_2O$ [46], and $(1,2\text{-}dapH_2)Sb_{10}S_{16}$ [72]. The thioantimonate(III) $(aepH_2)Sb_{10}S_{16}$ was synthesized from a mixture of Sb, $FeCl_3$ and S (mmolar ratio = 1 : 1 : 3) heated in 4 mL of 50 % aqueous tren at 200 °C for 7 d. All attempts to prepare the compound without $FeCl_3$ were not successful. In addition, the tren molecule is transformed under the reaction conditions producing the 2-piperazine-*N*-ethylamine cation. The crystal structure (Fig. 7) contains a large $Sb_{31}S_{31}$ ring with a double-ellipsoidal shape composed of vertex-linked $[SbS_3]$ pyramids and $[SbS_4]$ units. The two ellipsoidal parts of the ring are separated by a 'bottleneck'. The dimensions of the pores measure about 8.9×9.3 Å. The structure-directing cation is located above/below the ellipsoidal pores.

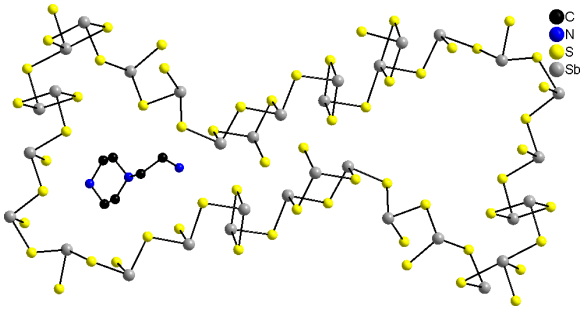

Fig. 7 (color online). The large $Sb_{31}S_{31}$ ring in the thioantimonate(III) ion of $(aepH_2)Sb_{10}S_{16}$. One cation is displayed showing the structure-directing effect.

The layers are two atoms thick and exhibit a wave-like fashion with the cations located at the inflection points of the layers (Fig. 8). A different network topology is observed in $(deenH_2)Sb_{10}S_{16} \cdot H_2O$ with a large 60-membered $Sb_{30}S_{30}$ ring. The compound was synthesized using Zn (1.1 mmol), Sb (1 mmol) and S (2.2 mmol) in 5 mL of a 50 % aqueous solution of *N*,*N*-diethylethylenediamine heated at 140 °C for 6 d. The authors have mentioned that the yield decreased significantly when no Zn was added to the educt mixture.

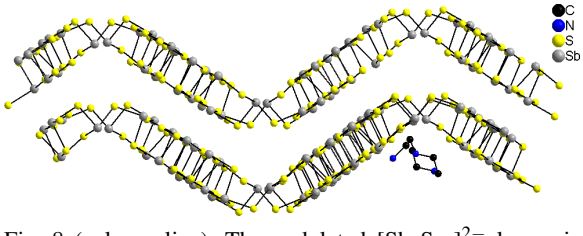

Fig. 8 (color online). The undulated $[Sb_6S_{10}]^{2-}$ layers in $(aepH_2)Sb_{10}S_{16}$. The structure-directing cations are located at the inflection points of the layers.

Table 3. Selected structural data of compounds with the $[Sb_8S_{13}]^{2-}$ anion (SG = space group), Dim. = dimensionality).

Compound	Dim. / SG	a (Å)	b (Å)	c (Å)	α (deg)	β (deg)	γ (deg)	V
$(maH)_2Sb_8S_{13}$ [74]	3 / $P\bar{1}$	15.866	11.581	8.295	71.46	75.71	82.25	1398
$(pyrH)_2Sb_8S_{13}\cdot 0.15H_2O$ [75]	2 / $P\bar{1}$	6.929	16.747	17.976	94.84	95.41	125.28	1670
$[Ni(en)_3]Sb_8S_{13}$ [69]	2 / $P\bar{1}$	9.041	12.376	16.549	100.372	94.579	110.34	1687
$(ipaH)_2Sb_8S_{13}$ [73]	2 / $P\bar{1}$	7.012	13.794	17.216	94.45	96.49	101.21	1614
$(1,2\text{-}dapH)_2Sb_8S_{13}$ [73]	2 / $P\bar{1}$	6.992	13.705	18.105	100.15	96.22	101.09	1658
$[(maH)_{0.5}(NH_4)_{1.5}]Sb_8S_{13}$ [74]	2 / $P2_1/m$	7.193	25.770	15.999	90	96.856	90	2945
$(dienH_2)Sb_8S_{13}\cdot 1.5H_2O$ [73]	2 / $P2_1/m$	7.190	25.900	15.979	90	97.39	90	2951
$(ampH_2)Sb_8S_{13}\cdot 2.5H_2O$ [73]	2 / $P2_1/m$	7.208	25.741	15.937	90	96.96	90	2935
$(dmenH_2)Sb_8S_{13}\cdot H_2O$ [46]	2 / $P2_1/c$	9.143	23.515	13.871	90	105.0	90	2881
$(depnH_2)Sb_8S_{13}\cdot H_2O$ [78]	2 / $P2_1/c$	9.237	24.05	13.912	90	106.06	90	2970
$(enH)_2Sb_8S_{13}$ [76]	1 / $Cmc2_1$	22.874	10.058	11.338	90	90	90	2609
$(1,3\text{-}dapH_2)Sb_8S_{13}$ [73]	2 / $I4_1md$	22.590	22.590	22.461	90	90	90	11461
$(etamH_2)Sb_8S_{13}$ [79]	2 / $P2_1/m$	7.167	25.899	16.044	90	96.85	90	2957

The only known composition for the Sb : S ratio of 1 : 1.625 is the $[Sb_8S_{13}]^{2-}$ anion present in the compounds $(ipaH)_2Sb_8S_{13}$, $(1,2\text{-}dapH)_2Sb_8S_{13}$, $(1,3\text{-}dapH_2)Sb_8S_{13}$, $(dienH_2)Sb_8S_{13}\cdot 1.5H_2O$, $(ampH_2)Sb_8S_{13}\cdot 2.5H_2O$ [73], $(maH)_2Sb_8S_{13}$ [74], $(pyrH)_2Sb_8S_{13}\cdot 0.15H_2O$ [75], $(enH_2)Sb_8S_{13}$ [76], $[(maH)_{0.5}(NH_4)_{1.5}]Sb_8S_{13}\cdot 2.8H_2O$ [77], $(dmenH_2)Sb_8S_{13}\cdot H_2O$ [46], $[Ni(en)_3]Sb_8S_{13}$ [69], $(depnH_2)Sb_8S_{13}\cdot H_2O$ [78], and $(etamH_2)Sb_8S_{13}$ [79] (see Table 3). The structures of thioantimonates(III) with the $[Sb_8S_{13}]^{2-}$ anion range from a three-dimensional network [74] (Fig. 9) to a one-dimensional chain observed for $(enH_2)Sb_8S_{13}$ [76]. The formation of a three-dimensional network with the relatively small $[maH]^+$ cation is in line with the general relation between cation size and network dimensionality. But this simple relation does not hold strictly, as the only one-dimensional thioantimonate anion is observed for the $[enH_2]^{2+}$ cation which is smaller than *e. g.* the $[Ni(en)_3]^{2+}$ cation. Hence, other factors seem to play also an important role in determining the network dimensionality. The layered $[Sb_8S_{13}]^{2-}$ anions are characterized by large pores of different sizes reflecting the structure-directing effects of the different ammonium or transition metal cations. A large 44-membered $Sb_{22}S_{22}$ ring with dimensions 7×17 Å is observed in $[Ni(en)_3]Sb_8S_{13}$ [69], whereas a more round-shaped $Sb_{18}S_{18}$ pore with diameter 11.9×11.2 Å occurs in $(pyrH)_2Sb_8S_{13}$ [75] (see Fig. 10). More ellipsoidal 24-membered $Sb_{12}S_{12}$ rings (dimensions: 8.7×14.6 Å) are the main structural motif in the two compounds $(ampH_2)Sb_8S_{13}$ and $(dienH_2)Sb_8S_{13}$ [73] (see Fig. 11). The number of atoms contained in the heterocycles is not directly related to the dimensions of the pore sizes as is evidenced by the $Sb_{19}S_{19}$ ring in $(1,3\text{-}dapH_2)Sb_8S_{13}$ [73] shown in Fig. 12. The central 38-membered ring measures only 9.9×7.8 Å which is caused by the special arrangement of the primary and secondary building units forming a type of pockets at the periphery of the ring.

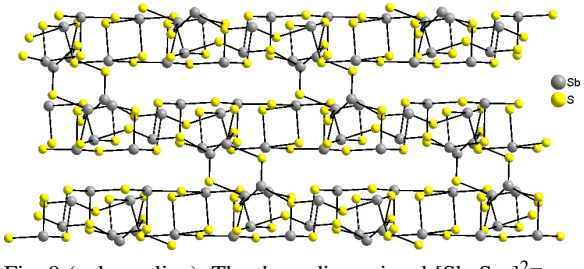

Fig. 9 (color online). The three-dimensional $[Sb_8S_{13}]^{2-}$ anion in $(maH)_2Sb_8S_{13}$ [74].

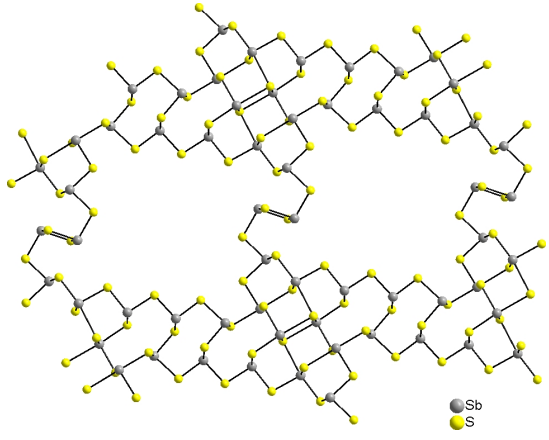

Fig. 10 (color online). The layered $[Sb_8S_{13}]^{2-}$ anion of $(pyrH)_2Sb_8S_{13}\cdot 0.15H_2O$ with large round $Sb_{18}S_{18}$ pores [75].

In all compounds containing $[Sb_8S_{13}]^{2-}$ anions the structure-directing protonated amine molecules

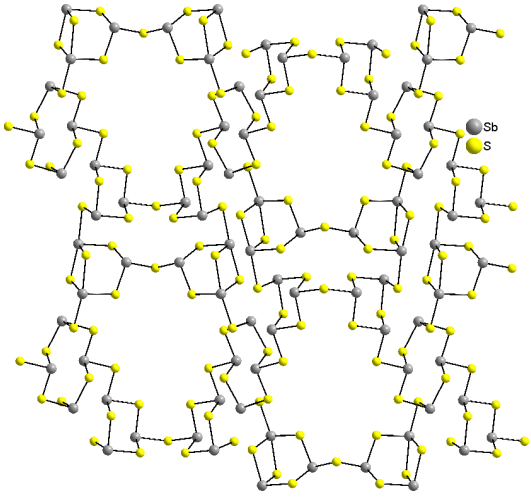

Fig. 11 (color online). The layered $[Sb_8S_{13}]^{2-}$ anion in $(ampH_2)Sb_8S_{13} \cdot 2.5H_2O$ with ellipsoidal 24-membered rings.

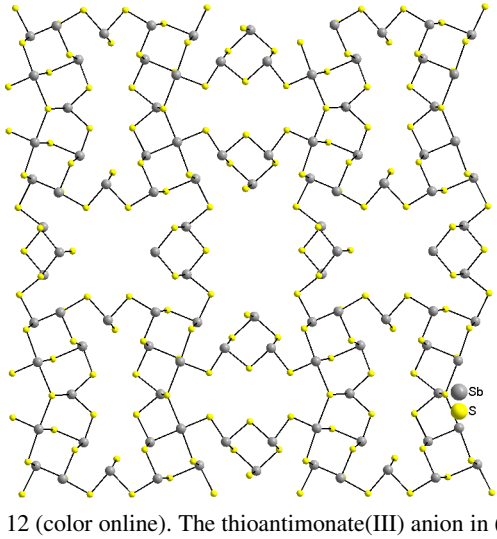

Fig. 12 (color online). The thioantimonate(III) anion in $(1,3\text{-}dapH_2)Sb_8S_{13}$ with central $Sb_{19}S_{19}$ ring [73].

are located above resp. below the heterocycles with the largest dimensions. Therefore, these compounds are examples demonstrating the influence on network topology and connectivity of the primary as well as secondary building units.

There are also some thioantimonate(III) compounds which do not fit in any of the groups presented above. One of these compounds is an oxo-thioantimonate with composition $(trenH_3)Sb_9S_{14}O$ [80] featuring the unusual $[SbS_2O]$ unit. The compound was synthesized using Sb_2O_3 (0.5 mmol) and S (3 mmol) in 4 mL 50 % aqueous tren solution heated to 150 °C for 7 d. The primary building units $[SbS_3]$ and $[SbS_2O]$ share common corners to form 20-membered heterorings with pore diameters of 7.7×8.3 Å. The protonated tren molecule acts as a tetradentate ligand around the O atom of the $[SbS_2O]$ group. The $[Sb_9S_{14}O]^{3-}$ anion is an example demonstrating the problem of the assignment of the dimensionality. Considering only Sb–S bond lengths up to about 2.5 Å the anion is one-dimensional. If Sb–S separations up to about 3.4 Å are considered as weak bonding interactions a three-dimensional network can be identified.

A three-dimensional network with one-dimensional circular channels is observed in $[M(en)_3]Sb_{12}S_{19}$ (M = Co, Ni) [69, 81] displaying a low Sb : S ratio of 1 : 1.583. The compound was synthesized from a mixture of CoS, Sb_2S_3 and S in en solution at 170 °C. $[SbS_3]$ and $[SbS_4]$ units share corners and edges to form Sb_2S_2, Sb_3S_7 and Sb_6S_{12} secondary building blocks which are joined into a three-dimensional network.

Structural Classification Approaches for Thiostannates

There are at least three different possibilities of charge compensation of anionic thiostannate networks. The simplest way is represented by metal cations surrounding the network leading to purely inorganic compounds which are not considered in the present review. The second possibility is charge compensation by organic molecules, protonated amine molecules or even transition metal complexes. The third option is represented by the integration of cationic transition metal complexes into the thiostannate network, an approach which is still less explored.

Thiostannates with organic molecules or protonated amine molecules acting as charge-compensating cations

The first layered thiostannates synthesized under solvothermal conditions applying alkylammonium cations were reported in 1989 [82 – 84]. The authors used the notation "R-$M'M$S-n" for the new thiometallates where the organic molecule R is acting as structure director and charge-compensating cation. M' represents a 3d or 4d metal cation and M = Ge, Sn, Sb and In are the network atoms. The different structure types are distinguished by the notation "n". The syntheses of the thiostannates are carried out under solvothermal conditions using metal sulfides or metals and sulfur and the corresponding amine solutions

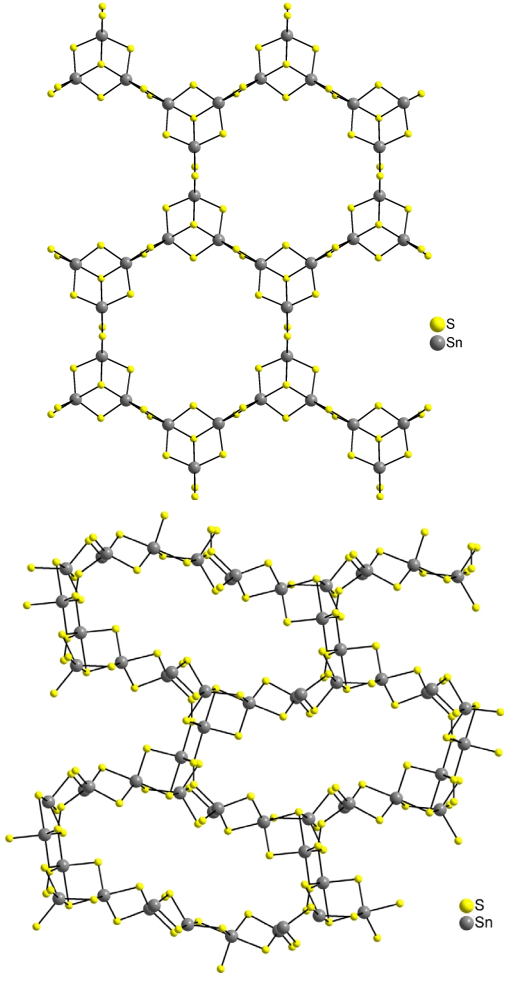

Fig. 13 (color online). Anionic layers of the R-SnS-n material, top: the $[Sn_3S_7]^{2-}$ anion with hexagonal pores, bottom: the $[Sn_4S_9]^{2-}$ anion with elliptical pores. The organic molecules have been omitted for clarity.

or alkylammonium salts. In most cases lamellar structures are formed, while three-dimensional framework structures are quite rare, and some of the products are the purely inorganic thiostannates $K_2Sn_2S_5$ [85] and $Na_4Sn_3S_8$ [86]. To the best of our knowledge a three-dimensional hybrid thiostannate network was never observed.

The two well-known structure types R-SnS-1 and R-SnS-3 consist of two-dimensional $[Sn_3S_7]^{2-}$ resp. $[Sn_4S_9]^{2-}$ layers with $[Sn_3S_4]$ semi-cubes as the main structural motif (see Fig. 13) which are connected *via* Sn–μ-S–Sn bonds to form the layers. The charge-compensating cations are located between the layers below/above the pores. Typical values for the inter-layer distances range from 8 to 9 Å for R-SnS-1 and up to 14 Å for R-SnS-3 [87].

The members of this thiostannate family have been well characterized, and many interesting experiments were conducted yielding promising results. The readers of the present article should consult some preceding articles for further information [2, 10, 87, 88], as the main interest of the present review article is focussed on other thiostannate compounds.

Table 4 gives an overview of thiostannates with organic molecules as charge-compensating cations.

Thiostannates with transition metal complexes acting as charge-compensating cations

The integration of transition metal (*TM*) cations into the thiostannate network should lead to significant alterations of the physico-chemical properties and enhance the structural diversity and variety. Unfortunately, solvothermal syntheses applying transition metals and structure-directing amines very often yield separated TM^{n+} complexes without any bonding to the anionic network, and discrete thiostannate anions. We note that thiostannate chemistry was extended very recently by the application of lanthanoid complexes Ln^{3+} as charge-compensating cations [103, 104]. In these compounds the Ln^{3+}-centered complexes have no bonds to the thiostannate anions like in many TM^{n+} containing compounds. In Table 5 thiostannates with transition metal complexes are compiled with some selected structural details and synthesis conditions.

Integration of transition metal complex cations into thiostannate networks

A few years ago we published the thiostannate compounds $[Ni(en)_3]_2Sn_2S_6$ and $[Ni(dap)_3]_2Sn_2S_6 \cdot 2H_2O$ consisting of isolated Ni^{2+} complexes and the $[Sn_2S_6]^{4-}$ anion. In this publication we also presented the new compound $[\{Co(tren)\}_2Sn_2S_6]$ [108] in which Co^{2+} has bonds to the N atoms of the amine and to the thiostannate anion (see Fig. 14).

The latter compound was prepared according to the idea presented below. During the last years several other compounds were synthesized applying multidentate amines like *e. g.* tren, trien or tepa leading to similar structural motifs (see Table 6). As discussed above such multidentate amines leave one or two binding positions of the TM^{n+} cations free for bonding to S atoms of the thiostannate anion. An interesting observation made also in the field of

Table 4. Overview of inorganic hybrid thiostannates with some experimental details, selected structure information and special remarks concerning possible applications and structural details (SG = space group).

Compounds	Cell parameters a (Å), b (Å), c (Å), α (deg), β (deg), γ (deg); SG	Starting materials	Synthesis conditions	Remarks
$R_2Sn_3S_7$ resp. "R-SnS-1" with R = NH_4^+, Me_4N^+, Et_4N^+, Pr_3NH^+, $BuNH_3^+$, ... [82, 83, 84, 89 – 93] $R_2Sn_4S_9$ resp. "R-SnS-3" with R = Pr_4N^+, Bu_4N^+ [91, 94]	The synthesis conditions and cell parameters can be found in the literature or other review articles [2, 10, 85, 88].			application in fields of catalysis, absorbers, molecule sensors and ion exchangers
$(DABCOH)_2Sn_3S_7$ [95]	22.281, 13.336, 17.188, 105.53; $C2/c$	Sn, S, $(NH_4)_2S$, H_2O, DABCO	2 h to 150 °C, 72 h 150 °C, in 20 h to r. t. or under stirring conditions in 24 h at 150 °C	pH value dependence of the formation of the crystals
$(chaH)_4Sn_2S_6$ [11]	26.861, 7.466, 20.109, 111.14; $C2/c$	Sn, S, cha, H_2O	2 d 150 °C, with 8 $K \cdot h^{-1}$ to r. t.	
$(trenH)_2Sn_2S_6 \cdot 2H_2O$ [96]	7.7499, 9.7054, 10.908, 89.22, 75.27, 67.4; $P\bar{1}$	Co, Sn, S, tren	7 d, 140 °C	discrete $[Sn_2S_6]^{4-}$ anions
$(dda)_4Sn_2S_6 \cdot 2H_2O$ [97]	7.533, 10.162, 21.688, 101.22, 90.76, 101.82; $P\bar{1}$	$SnCl_4 \cdot 5H_2O$, H_2O, $Na_2 \cdot 9H_2O$, dda in EtOH	45 d, r. t.	
$^1_\infty[SnS_2 \cdot en]$ [98, 99]	15.317, 10.443, 12.754, 93.62; $C2/c$	Sn, S, en, H_2O or $Bu(SnCl_3)_2$, S, en	150 °C or 5 d, 180 °C	1D structure, the organic part is connected with the Sn atoms forming $[SnS_4N_2]$ octahedra
$(enH_2)(enH)_2Sn_2S_6$ [100]	8.7638, 10.729, 12.222, 74.85, 73.00, 88.98; $P\bar{1}$	Sn, S, en in MeOH	3 d, 160 °C	$[Sn_2S_6]^{4-}$ anions and single as well as double protonated amine molecules
$(enH)_4Sn_2S_6 \cdot en$ [99]	9.877, 9.934, 15.423, 72.63, 86.22, 81.38; $P\bar{1}$	Sn, S, en	5 d, 180 °C	
$(pipH)_2(4,4'\text{-epip}H_2)Sn_5S_{12}$ [101]	10.342, 10.483, 10.716, 68.10, 70.82, 79.71; $P\bar{1}$	SnS_2, DABCO, H_2O	200 °C	polythio-stannate anion; the synthesis with DABCO yields pipH and 4,4′-epipH_2 between the inorganic layers
$(Pr_4N)(Me_3NH)Sn_4S_9$ [94]	14.832, 18.612, 15.039, 96.90; $P2_1/n$	SnS_2, Pr_4NOH, S, H_2O	72 h, 150 °C	*in situ* formation of Me_3NH^+ from Pr_4N^+
$(DBNH)_2Sn_3S_6$ [102]	9.5822, 13.1199, 19.9506, 97.192; $P2_1/n$	Sn, S, DBN	20 d, 170 °C or 5 to 27 d, 140 °C	mixed-valent thiostannate

Table 5. Overview of transition metal complex-containing thiostannates together with selected structural details and synthesis conditions (SG = space group).

Compounds	Cell parameters a (Å), b (Å), c (Å), α (deg), β (deg), γ (deg); SG	Starting materials	Synthesis conditions	Remarks
$[Mn(en)_3]_2Sn_2S_6 \cdot 2H_2O$ [105]	10.129, 15.746, 11.524, 102.36; $P2_1/c$	Mn, Sn, S, en, H_2O	5 d, 180 °C	$[Sn_2S_6]^{4-}$, $[MnN_6]$ octahedra
$[Mn(dien)_2]_2Sn_2S_6$ [105]	12.4812, 9.376, 17.7617, 121.752; $P2_1/c$	Mn, Sn, S, dien, H_2O	10 d, 150 °C	$[Sn_2S_6]^{4-}$, $[MnN_6]$ octahedra
$[Ni(en)_3]_2Sn_2S_6$ [106]	11.5212, 18.631, 15.2368; *Pbca*	$NiCl_2 \cdot 6H_2O$, $SnCl_4 \cdot 5H_2O$, S, en resp. dien	4 h to 180 °C, 4 d, 180 °C	$[Sn_2S_6]^{4-}$, $[NiN_6]$ octahedra
$[Ni(dien)_2]_2Sn_2S_6$ [106]	9.9168, 14.392, 12.0589, 91.906; $P2_1/n$			
$[Mn(en)_3]_2Sn_2S_6$ [107]	15.138, 10.6533, 23.586, 118.42; $C2/c$	$MnCl_2$ / $CoCl_2 \cdot 6H_2O$ / $ZnCl_2$, $SnCl_4 \cdot 5H_2O$, S, en	4 d, 180 °C	$[Sn_2S_6]^{4-}$, $[TMN_6]$ octahedra
$[Co(en)_3]_2Sn_2S_6$ [107]	15.640, 11.564, 18.742; *Pbca*			
$[Zn(en)_3]_2Sn_2S_6$ [107]	15.452, 11.524, 18.619; *Pbca*			
$[Ni(en)_3]_2Sn_2S_6$ [108]	15.227, 11.530, 18.701; *Pbca*	Ni, Sn, S, en, H_2O	7 d, 170 °C	$[Sn_2S_6]^{4-}$, $[NiN_6]$ octahedra
$[Ni(1,2\text{-dap})_3]_2Sn_2S_6 \cdot 2H_2O$ [108]	9.9046, 10.527, 11.319, 72.13, 85.19, 63.63; $P\bar{1}$	Ni, Sn, S, 1,2-dap	7 d, 140 °C	$[Sn_2S_6]^{4-}$, $[NiN_6]$ octahedra
$[Nd_2(en)_6(\mu\text{-}OH)_2]Sn_2S_6$ [103]	10.1757, 11.3870, 15.018, 97.869; $P2_1/n$	$LnCl_3$, $SnCl_4 \cdot 5H_2O$, S, en resp. dien	7 d, 160 °C	$[Sn_2S_6]^{4-}$, binuclear $[Ln_2(en)_6(\mu_2\text{-}OH)_2]^{4+}$ complex
$[Gd_2(en)_6(\mu\text{-}OH)_2]Sn_2S_6$ [103]	10.1053, 13.575, 14.9237, 98.346; $P2_1/n$			
$[Gd(dien)_3]_2Sn_2S_6Cl$ [103]	11.6623, 15.1681, 14.1849, 95.696; $P2_1/n$			
$[Dy_2(en)_6(\mu\text{-}OH)_2]Sn_2S_6$ [104]	10.0725, 11.3533, 14.904, 98.608°; $P2_1/n$	Dy_2O_3 / Er_2O_3, $SnCl_4$, S, en	5 d, 180 °C	$[Sn_2S_6]^{4-}$, binuclear $[Ln_2(en)_6(\mu_2\text{-}OH)_2]^{4+}$ complex
$[Er_2(en)_6(\mu\text{-}OH)_2]Sn_2S_6$ [104]	10.0644, 11.3287, 14.854, 99.009; $P2_1/n$			

Table 6. Overview of thiostannates having bonds to transition metal cations, and thiostannates containing a transition metal cation in the network. Selected structural data and synthesis conditions are also summarized (SG = space group).

Compounds	Cell parameters a (Å), b (Å), c (Å), α (deg), β (deg), γ (deg); SG	Starting materials	Synthesis conditions	Remarks
$[\{Co(tren)\}_2Sn_2S_6]$ [108]	12.228, 9.7528, 23.285, 102.90; $C2/c$	Co, Sn, S, tren, H_2O	6 d, 140 °C	$[Sn_2S_6]^{4-}$ anions connected with $[Co(tren)]^{2+}$ complexes
$[\{Mn(tepa)\}_2(\mu_2\text{-}Sn_2S_6)]$ [119]	12.5326, 13.7091, 13.9894; $P2_12_12_1$	$SnCl_4 \cdot 5H_2O$, $MnCl_2 \cdot 6H_2O$, S, tepa, H_2O	10 d, 157 °C	$[Sn_2S_6]^{4-}$ anions connected with $[Mn(tepa)]^{2+}$ complexes
$[\{Co(tepa)\}_2Sn_2S_6]$ [120]	25.973, 25.973, 9.8942; $I4_1/a$	$CoCl_2 \cdot 6H_2O$ / Fe / $NiCl_2 \cdot 6H_2O$, $SnCl_2 \cdot 2H_2O$, S, tepa, H_2O	25 h, 160 °C	$[Sn_2S_6]^{4-}$ anions connected with $[TM(tepa)]^{2+}$ complexes
$[\{Fe(tepa)\}_2Sn_2S_6]$ [120]	25.964, 25.964, 9.9936; $I4_1/a$			
$[\{Ni(tepa)\}_2Sn_2S_6]$ [120]	9.1425, 13.1394, 13.075, 93.002; $P2_1/n$			
$[\{Mn(1,2\text{-dach})_2(H_2O)\}_2\ Sn_2S_6]$ [109]	23.750, 15.5655, 12.1072, 113.532; $C2/c$	Mn, Sn, S, 1,2-dach, H_2O	98 h, 130 °C	$[Sn_2S_6]^{4-}$ anion connected with $[Mn(1,2\text{-dach})_2\ H_2O]^{2+}$ complex
$[\{Mn(1,2\text{-dach})_2\}Sn_2S_6] \cdot 2$ 1,2-dach [109]	7.3019, 11.1798, 13.2837, 76.877, 74.719, 82.972; $P\bar{1}$			$[\{Mn(1,2\text{-dach})_2\}\ Sn_2S_6]$ chains and isolated amine molecules
$[\{Mn(trien)\}_2SnS_4] \cdot 4H_2O$ [110]	10.8446, 20.9740, 13.2746, 113.487; $P2_1/c$	Sn, Mn, S, trien	480 h, 140 °C	chain structure $[\{Mn(trien)\}_2SnS_4]$, $[SnS_4]^{4-}$ anion in μ_3-bridging mode connecting the $[Mn_2S_2N_8]$ di-octahedra.
$[\{Mn(en)_2\}_2(\mu\text{-en})\ (\mu Sn_2S_6)]_\infty$ [111]	9.0097, 9.7735, 10.8421, 60.379, 67.235, 70.250; $P\bar{1}$	1. $SnCl_4 \cdot 5H_2O$, S, en, 2. $MnCl_2 \cdot 6H_2O$, en	2 d, 160 °C and 7 d, 160 °C	two-step-synthesis, $[\{Mn(en)_2\}_2(\mu\text{-en})\ (\mu\text{-}Sn_2S_6)]_\infty$ (hains with bridging en molecules
$(DBUH)CuSnS_3$ [113]	9.2541, 8.6190, 18.135, 92.803; $P2_1/n$	Sn, Cu, S, 1,4-dab resp. DBU	120 h, 170 °C, cooling to 25 °C in 30 h	$[CuSnS_3]^-$ chain, protonated organic amines acting as charge compensating cations
$(1,4\text{-dabH}_2)Cu_2SnS_4$ [113]	14.5392, 14.5392, 11.4776; $P4_2/n$		120 h, 150 °C	$[Cu_2SnS_4]^{2-}$ chain surrounded by charge-compensating protonated amine molecules
$(1,4\text{-dabH}_2)Ag_2SnS_4$ [114]	14.7847, 14.7847, 11.9087; $P4_2/n$	Ag, Sn, S, 1,4-dab	145 h, 150 °C	$[Ag_2SnS_4]^{2-}$ chain surrounded by charge-compensating protonated amine molecules
$(1,4\text{-dabH})_2MnSnS_4$ [112]	22.8124, 24.7887, 6.4153; $Fdd2$	Sn, Mn, S, 1,4-dab	120 h, 150 °C	anionic chain of alternating $[SnS_4]$ and $[MnS_4]$ tetrahedra

Table 6 (continued).

Compounds	Cell parameters a (Å), b (Å), c (Å), α (deg), β (deg), γ (deg); SG	Starting materials	Synthesis conditions	Remarks
$(enH_2)HgSnS_4$ [118]	13.863, 6.640, 23.198, 106.168; *C2/c*	HgI_2, SnS_2, en, pyridine, $HSCH_2CH(SH)CH_2OH$	7 d, 160 °C	$[HgSnS_4]^{2-}_{\infty}$ columns separated by $(enH_2)^{2+}$ columns
$(enH_2)Ag_2SnS_4$ [117]	11.115, 6.7618, 15.0663, 105.562; *C2/c*	Sn, $AgNO_3$, S, en in EtOH / 2,3-dimercapto-1-propanol	5 d, 120 °C	chiral 2D structure with $[Ag_2SnS_4]^{2-}$ layers
$(DBNH)_2Cu_6Sn_2S_8$ [102]	21.3017, 6.6837, 19.9480; *I4m2*	Sn, Cu, S, DBN	27 d, 140 °C, cooling to 25 °C in 30 h	$[CuS_3]$ triangles and $[SnS_4]$ tetrahedra forming different six-membered Cu_2SnS_3 heterorings yielding an undulated layered structure
$(dienH_2)Cu_2Sn_2S_6$ [115]	7.8793, 7.8793, 24.9955; *I4m2*	Sn, Cu, S, dien	120 h, 170 °C, cooling to 25 °C in 30 h	layered $[Cu_2Sn_2S_6]^{2-}$ anion composed of $[CuS_4]$ and $[SnS_4]$ tetrahedra and protonated amine molecules between the layers

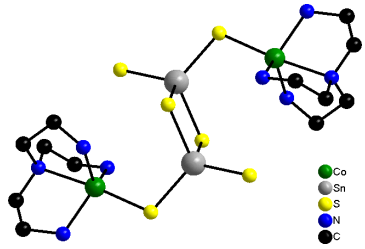

Fig. 14 (color online). The $[\{Co(tren)\}_2Sn_2S_6]$ molecule showing the environment of the Co^{2+} cation in the complex connected with the $[Sn_2S_6]^{4-}$ anion.

thioantimonate(III) chemistry is the different behavior of Mn^{2+} compared to that of Co^{2+} or Ni^{2+}. Even when identical synthesis conditions are applied Co^{2+} / Ni^{2+} prefer coordination to N atoms of the amine ligands, whereas Mn^{2+} forms bonds to S atoms as well as to N atoms without any preference even when bidentate amines are used. Selected examples are $[\{Mn(1,2\text{-dach})_2(H_2O)\}_2Sn_2S_6]$, $[\{Mn(1,2\text{-dach})_2\}Sn_2S_6] \cdot 2$ 1,2-dach [109], $[Mn(trien)]_2SnS_4 \cdot 4H_2O$ [110], and $[\{Mn(en)_2\}_2(\mu\text{-en})(\mu\text{-}Sn_2S_6)]_\infty$ [111]).

Despite many synthetic efforts the attempted integration of TM^{n+} into thiostannate frameworks was not successful, and the first thiostannate compound (1,4-dabH$_2$)MnSnS$_4$ [112] with integrated Mn^{2+} cations in anionic thiostannate chains and charge compensating ions was reported only recently.

In contrast to the early transition metal cations the elements Cu and Ag prefer bonds to sulfur instead of nitrogen or oxygen, and therefore an incorporation into the thiostannate framework is more likely than the formation of $[Cu(amine)_x]^{y-}$ or $[Ag(amine)_x]^{y-}$ complexes. The compounds (DBUH)-CuSnS$_3$ [113], (DBNH)$_2$Cu$_6$Sn$_2$S$_8$ [102], (1,4-dabH)-$_2$Cu$_2$SnS$_4$ [113] and the isostructural compound (1,4-dabH)$_2$Ag$_2$SnS$_4$ [114] were the first examples confirming the chalcophilic character of the two elements. In (DBUH)CuSnS$_3$ one-dimensional

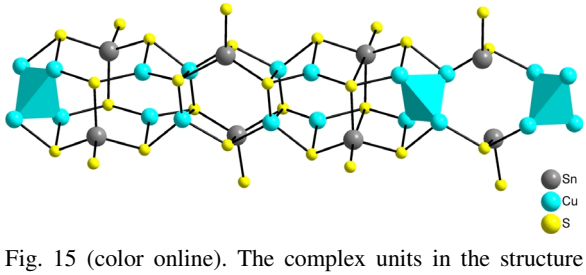

Fig. 15 (color online). The complex units in the structure of (1,4-dabH)$_2$Cu$_2$SnS$_4$; the $[CuS_4]$ tetrahedra are shown as polyhedra. The protonated amine molecules are not shown.

$[CuSnS_3]^-$ chains are surrounded by protonated amine molecules, and in $(1,4\text{-dabH})_2Cu_2SnS_4$ the chains consist of $[Cu_2SnS_4]^{2-}$ anions (Fig. 15).

The structure of $(DBNH)_2Cu_6Sn_2S_8$ exhibits undulated anionic layers separated by protonated amine molecules. The layers may be described as distorted graphene 6^3 layers, and such a structural motif was never found in thiostannates before (Fig. 16).

The integration of Cu^+ into the networks or layers yields new materials with interesting properties, one promising example being $(dienH_2)Cu_2Sn_2S_6$ [115], a layered thiostannate with photoconductive properties. The layers consist of $[CuS_4]$ and $[SnS_4]$ tetrahedra (Fig. 17).

In $(NH_4)_2Ag_6Sn_3S_{10}$ [116] cationic $[Ag_6SnS_4]^{2+}$ chains are separated by $[SnS_3]^{2-}$ zigzag chains, and the resulting 1D channels are filled with NH_4^+ cations (Fig. 18).

A chiral two-dimensional structure was observed for $(enH_2)Ag_2SnS_4$ [117] with $[Ag_2SnS_4]^{2-}$ layers

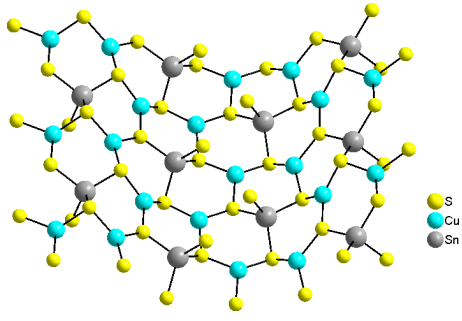

Fig. 16 (color online). Different heterorings are condensed in $(DBNH)_2Cu_6Sn_2S_8$ yielding anionic layers.

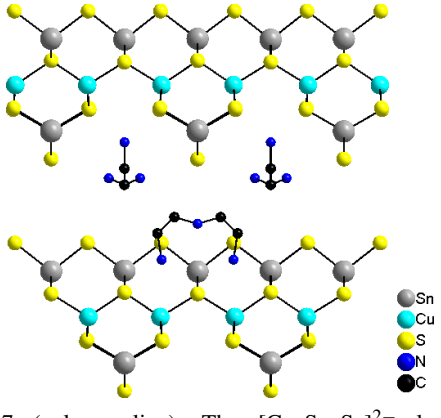

Fig. 17 (color online). The $[Cu_2Sn_2S_6]^{2-}$ layers in $(dienH_2)Cu_2Sn_2S_6$ with the protonated amine molecules in the interlayer galleries. The hydrogen atoms have been omitted for clarity.

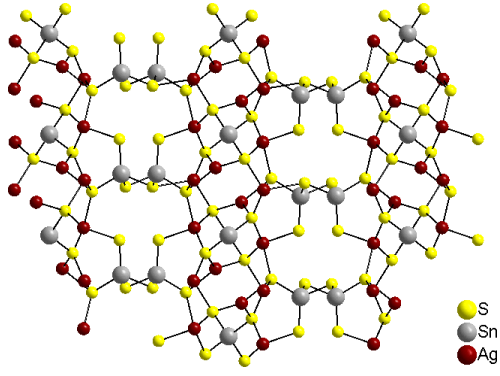

Fig. 18 (color online). View along [010] of $(NH_4)_2Ag_6Sn_3S_{10}$ with 1D channels. The cationic $[Ag_6SnS_4]^{2+}$ layers are separated by $[SnS_3]^{2-}$ zigzag chains. The ammonium ions have been omitted for clarity.

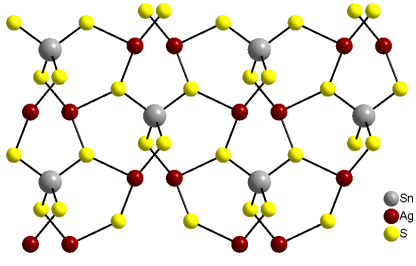

Fig. 19 (color online). Anionic layers in $(enH_2)Ag_2SnS_4$ with $[SnS_4]$ tetrahedra and $[AgS_3]$ pyramids.

consisting of $[SnS_4]$ tetrahedra and $[AgS_3]$ pyramids (Fig. 19).

In $(enH_2)HgSnS_4$ columns of $[HgSnS_4]_\infty^{2-}$ anions composed of $[SnS_4]$ tetrahedra, and $[HgS_3]$ units are separated by $(enH_2)^{2+}$ columns [118]. An overview of thiostannates with transition metal cations bound to thiostannate anions and thiostannates with integrated transition metals is given in Table 6.

Synthetic Aspects of Thioantimonate(III) Chemistry

For the synthesis of thioantimonates the main Sb sources are elemental Sb or Sb_2S_3, but there are also some examples where other starting materials like $SbCl_3$ were used. Under basic conditions a ring-opening nucleophilic attack by the base may produce in the first step reactive S species according to the equation $S_8 + R\text{-}NH_2 \rightarrow {}^-S\text{-}S_6\text{-}S\text{-}{}^+NH_2\text{-}R$ [11]. It can be assumed that cleavage of S–S bonds occurs through electron transfer from metal to S atoms thus producing several further intermediate species like S_6^{2-}, S_4^{2-}, S_2^{2-}, *etc*. The different S species then solubilize the

Table 7. Synthesis conditions of the Ni-Sb-S-dien system.

Product	Ni / Sb / S – Educt (mmol)	Solvent (mL) / Yield	T (°C)	Time (d)	Ni / Sb / S – Product
$[Ni(dien)_2]_2Sb_4S_8$ [35]	1 / 1 / 3	3 / 100 %	145	11	1 / 2 / 4
$[Ni(dien)_2]_3Sb_{12}S_{21}\cdot H_2O$ [50]	1 / 1 / 2	10 / 50 %	140	7	1 / 4 / 7
$[Ni(dien)_2]_9Sb_{22}S_{42}\cdot 0.5H_2O$ [18]	1 / 1 / 3	3 / 80 %	140	7	1 / 2.44 / 4.66
$[Ni(dien)_2]Sb_4S_7\cdot H_2O$ [50]	1 / 1 / 3	2 / 50 %	140	5	1 / 4 / 7
$[Ni(dien)_2]_2Sb_4S_9$ [121]	1 / 1 / 3	2 / 50 %	140	10	1 / 2 / 4.5
$[Ni(dien)_2]_3[Sb_3S_6]_2$ [34]	1 / 1 / 3	2 / 50 %	140	4	1 / 2 / 4
$[Ni(dien)_2]Sb_6S_{10}\cdot 0.5H_2O$ [65]	1 / 1 / 3	10 / 10 %	140		1 / 6 / 10

metals applied forming different stable metal polysulfides and sulfides which participate in the product formation.

Aqueous mixtures of amines are used as both the solvent and the structure-directing systems, and their concentration covers a wide range. Transition metals are supplied as elements or as salts. The solvothermal syntheses are mainly performed in Teflon-lined steel autoclaves or in sealed glass ampoules.

According to our experiences one can roughly distinguish between syntheses where small changes of the reaction conditions lead to crystallization of different compounds even if most other reaction parameters and the amine supplied are held constant, and those leading to more robust products, where even different amines or applying relatively large temperature ranges lead to very similar results. Some examples can serve to highlight these differences. In the system Ni–Sb-S-dien six compounds could be crystallized and characterized by slightly varying the synthesis conditions (Table 7).

In the compound $[Ni(dien)_2]_2Sb_4S_8$ [35], the $[Sb_4S_8]^{4-}$ ring composed of four corner-sharing $[SbS_3]$ pyramids could be isolated for the first time. The compound crystallized from a mixture of Ni : Sb : S = 1 : 1 : 3 mmol in 3 mL of a concentrated dien solution heated to 145 °C for 11 d. Within the ring the Sb–S bond lengths are between 2.429 and 2.492 Å whereas the bonds to terminal S atoms are significantly shorter (2.315 – 2.337 Å) indicating a partial back-bonding. Despite many different variations of the synthesis conditions the smaller ring with composition $[Sb_3S_6]^{3-}$ [34] could not be obtained applying these educts and ratios. The first mixed-valent Sb(III)/Sb(V) hybrid compound, $[Ni(dien)_2]_2Sb_4S_9$ [121], was synthesized applying again the ratio Ni : Sb : S = 1 : 1 : 3 mmol but using 2 mL of a 50 : 50 H_2O/dien mixture heated at 140 °C for 10 d [121]. The presence of both Sb oxidation states was verified by ^{121}Sb Mössbauer spectroscopy. The crystal structure is characterized by a one-dimensional undulated chain made up by corner-sharing [Sb(III)S_3] pyramids where [Sb(V)S_4] tetrahedra are bound to the chain by one corner. The Sb(V)–S bonds are significantly shorter than the Sb(III)–S bonds. In contrast to many other thioantimonates(III) the Sb atoms do not have contacts to S atoms at longer distances.

The compound $[Ni(dien)_2]_9Sb_{22}S_{42}\cdot 0.5H_2O$ [18] was crystallized from a mixture Ni : Sb : S = 1 : 1 : 3 mmol with 3 mL 80 % dien solution heated for 10 d at 140 °C. Several structural features are unusual in this compound. Firstly, the five crystallographically independent $[Ni(dien)_2]^{2+}$ complexes adopt the three different isomeric forms *s-fac*, *mer* and *u-fac*. Secondly, the primary building units are $[SbS_3]$, $[SbS_4]$, and $[SbS_5]$, *i. e.* this compound is one of the rare examples where these moieties are present simultaneously. Thirdly, the primary units are joined to form a very large ellipsoidal $Sb_{30}S_{30}$ heteroring with dimensions of about 7.3 × 12.5 Å which are condensed to form layers. The Ni^{2+} complexes act as structure directors being located above and below the large rings. Like for many other thioantimonates(III) most Sb centers complete their coordination environment by S atoms located at distances up to 3.6 Å.

Another layered thioantimonate with composition $[Ni(dien)_2]Sb_6S_{10}\cdot 0.5H_2O$ was obtained from a slurry of Ni : Sb : S = 1 : 1 : 3 mmol in 10 mL of 50 % dien solution heated for 6 d at 150 °C [65, 122]. This compound features $[SbS_3]$ and $[SbS_4]$ as primary building units which are joined to form the layered $[Sb_6S_{10}]^{2-}$ anion. The main structural motif is a 32-membered $Sb_{16}S_{16}$ ring which is 'templated' by the Ni^{2+} complexes above and below. The $[Ni(dien)_2]^{2+}$ cations adopt the *mer*- and *s-fac*-configurations. Most Sb atoms enlarge their coordination environment by contacts to S atoms located at longer distances. Considering these long Sb–S contacts the large ring is divided into several smaller rings. We note that this compound can also be obtained by heating a mixture of Sb_2S_3 and $NiSO_4\cdot 7H_2O$ in 3 mL 50 % aqueous dien solution (molar ratio Ni : Sb : S : dien = 2 : 1 : 3 : 7)

for 3.5 d at 165 °C [69]. A differently layered anion with composition $[Sb_4S_7]^{2-}$ was synthesized from a mixture of Ni : Sb : S = 1 : 1 : 3 mmol in 2 mL 50 % aqueous dien solution heated for 5 d at 140 °C. The unique $[Ni(dien)_2]^{2+}$ complex adopts the *mer*-configuration. The $[Sb_4S_7]^{2-}$ anion is composed of $[SbS_3]$ trigonal pyramids and $[SbS_4]$ units displaying the typical Sb–S bond lengths and S–Sb–S angles. Two $[SbS_4]$ units are joined by a common edge forming a *trans*-$[Sb_2S_6]$ moiety displaying a central Sb_2S_2 ring, and two $[SbS_3]$ pyramids share a corner yielding a $[Sb_2S_5]$ group. Interconnection of the *trans*-$[Sb_2S_6]$ and $[Sb_2S_5]$ units generates Sb_8S_8 rings which are condensed along two crystallographic axes. The condensation of the 16-membered rings yields smaller Sb_4S_4 rings, and the final layered anion may be described as a net composed of Sb_2S_2, Sb_4S_4, and Sb_8S_8 rings. Again the $[Ni(dien)_2]^{2+}$ complex exerts a structure-directing effect and is located above/below the largest ring. Another compound with composition $[Ni(dien)_2]_3Sb_{12}S_{21}\cdot H_2O$ containing a three-dimensional anionic network was obtained from a slurry with composition Ni : Sb : S = 1 : 1 : 2 in 10 mL of a 50 % aqueous solution heated for 7 d at 140 °C. The structure is built of *cis*-$[Sb_2S_6]$ units made up by edge-sharing $[SbS_4]$ groups, $[Sb_2S_5]$ units formed by corner-sharing $[SbS_3]$ pyramids, Sb_3S_3 rings built by two $[SbS_3]$ and one $[SbS_4]$ moiety, and Sb_4S_4 rings composed of two $[SbS_3]$ and two $[SbS_4]$ units. A two-dimensional network is generated by condensation of the secondary building blocks in the sequence Sb_4S_4-Sb_3S_3-Sb_2S_5-Sb_3S_3-Sb_4S_4. Further interconnection into the third dimension is achieved by S atoms of the Sb_4S_4 rings containing the *cis*-$[Sb_2S_6]$ moiety. The connectivity scheme generates Sb_xS_x rings with x = 2, 3, 4, 8 and 32, *i. e.* the largest ring contains 64 atoms with dimensions of about 7.6 × 13.5 Å. The $[Ni(dien)_2]^{2+}$ complexes adopting the *u-fac*- and *s-fac*-configuration are located above/below the large rings and also in the plane of these rings. Taking into account the longer Sb–S distances the connectvity scheme becomes more complex due to the higher coordination numbers of some Sb centers.

In the study of the latter two compounds we investigated whether the redox reaction Ni → Ni^{2+} plays an important role for product formation. Therefore, the syntheses were performed with *mer*-$[Ni(dien)_2]Cl_2\cdot H_2O$ as Ni source instead of elemental Ni keeping the Ni : Sb : S ratio, the reaction time and the temperature constant and varying the amine concentration. Interestingly, both compounds could be obtained with this Ni source indicating that the oxidation of Ni plays no crucial role. Furthermore, higher amine concentrations favor the crystallization of the three-dimensional compound, whereas the layered material is obtained with smaller amounts of the amine. Another interesting finding was that the configuration of the Ni complex is retained in the layered compound, whereas in $[Ni(dien)_2]_3Sb_{12}S_{21}\cdot H_2O$ the *u-fac*- and *s-fac*-forms were observed like in the compound synthesized with Ni. The change from the *mer*- to the *u-fac*- and *s-fac*-forms implies Ni–N bond breaking and rearrangement during the synthesis.

Table 8. Synthesis conditions of $[Mn(L)MnSb_2S_5]$ compounds.

Product	Mn/Sb/S Educt (mmol)	Solvent (mL) / Yield	*T* (°C)	Time (d)
$[\{Mn(ma)_2\}MnSb_2S_5]$ [124]	2 / 2 / 5	3 / 40 %	130	5
$[Mn(1,3\text{-dap})MnSb_2S_5]$ [124]	2 / 2 / 5	3 / 40 %	130	5
$[\{Mn(ea)_2\}MnSb_2S_5]$ [125]	1 / 1 / 1	10 / 70 %	125	6
$[\{Mn(en)_2\}MnSb_2S_5]$ [123]	1 / 1 / 2.5	10 / 50 %	130	5
$[Mn(dien)MnSb_2S_5]$ [126]	2 / 2 / 5	5 / 50 %	120	5
$[Mn(mdap)MnSb_2S_5]$ [126]	2 / 2 / 5	5 / 50 %	120	5
$[\{Mn(tren)_2\}MnSb_2S_5]$ [127]	1 / 1 / 2.5	5 / 95 %	140	7
$[Mn(1,3\text{-dape})MnSb_2S_5]$ [128]	1 / 1 / 3	3 / 100 %	170	14
$[Mn(en)_3]_2MnSb_2S_5$ [28]	3 / 3 / 9	8 / 100 %	180	7
$[Mn(phen)MnSb_2S_5]$ [129]	1 / 1 / 3	78 mg phen 0.2 mL en 5 mL H_2O / 38 %	150	5

Whereas the first example highlights that small variations of the synthesis conditions lead to the crystallization of thioantimonate(III) structures with different composition, distinct interconnection of the primary and secondary building units and different structural dimensionality, the second example shows that an identical network topology can be obtained with very different amines, differing educt ratios, reaction temperatures, and reaction times. The syntheses were performed applying the elements Mn, Sb und S with methylamine, ethylamine, 1,3-diaminopropane, diethylenetriamine, *N*-methyl-1,3-diaminopropane, or 1,3-diaminopentane solutions. The synthesis conditions together with some further details are illustrated in Table 8. We note that by applying ethylenediamine a compound with composition $[\{Mn(en)_2\}MnSb_2S_5]$ was obtained with the same chemical composition of the inorganic network but displaying a different topology compared to the other $[Mn(L)MnSb_2S_5]$ compounds mentioned in Table 8. $[\{Mn(en)_2\}MnSb_2S_5]$ could only be prepared as a mixture with $[Mn(en)_3]Sb_4S_7$ as a second phase [123]. This exper-

	ma	ea	dien	1,3-dap	mdap	dape
Average Sb–S, Å	2.454	2.444	2.446	2.448	2.450	2.450
⟨Mn(2)–S⟩, Å	2.637	2.634	2.637	2.634	2.639	2.622
⟨Mn(1)–S⟩, Å	2.643	2.614	2.604	2.595	2.593	2.593
Mn(1)–S(2), Å	2.866	2.927	3.038	3.074	3.185	2.986
⟨Mn(1)–N⟩, Å	2.238	2.238	2.254	2.214	2.234	2.211
N–Mn(1)–N, deg	98.7	95.1	77.6	89.9	89.4	87.78
D1 (Mn2–Mn2), Å	8.716	8.760	9.153	9.079	9.138	8.965
D2 (Sb1–Sb1), Å	7.696	7.700	7.522	7.527	7.513	7.495
Ratio D1/D2	1.133	1.138	1.217	1.206	1.216	1.196

Table 9. Selected distances and angles for the $[Mn(L)MnSb_2S_5]$ compounds.

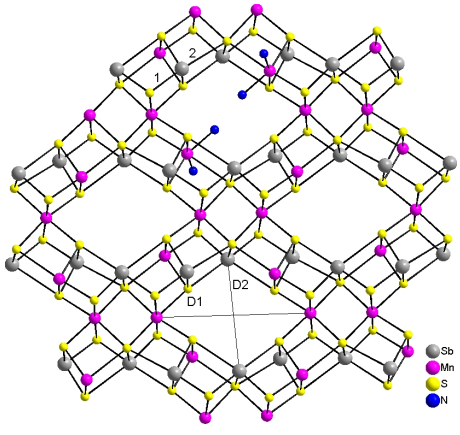

Fig. 20 (color online). The layer in the compounds $[Mn(L)MnSb_2S_5]$ showing two different heterocubane units. D1 and D2 are the diameters of the ellipsoidal holes. Note that only selected N atoms are displayed, and C atoms have been omitted for clarity.

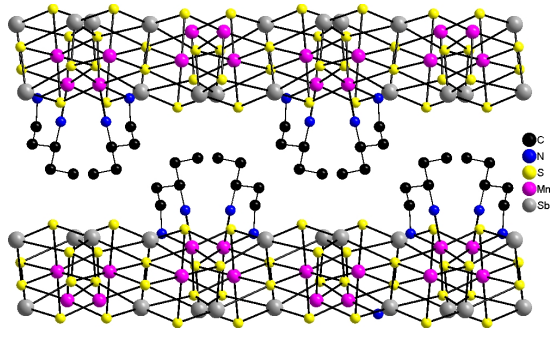

Fig. 21 (color online). Stacking of the $[Mn(L)MnSb_2S_5]$ layers showing the "key-into-lock" principle of the amine molecules.

imental finding is also different from the results of the syntheses of the other $[Mn(L)MnSb_2S_5]$ compounds where by-products consist of binary sulfides.

Comparing the synthesis parameters in Table 8, no obvious relationship between the educt ratios, the amine concentration, reaction time, or reaction temperature can be extracted. One may speculate that under the synthesis conditions chosen the $[Mn(L)MnSb_2S_5]$ network is more stable than competing Mn(II) thioantimonate(III) phases. Indeed the compound $[Mn(dien)_2]Sb_4S_7 \cdot 0.5H_2O$ could only be synthesized using $MnSb_2S_4$ in 3 mL conc. dien solution at 130 °C and 14 d reaction time [51].

The main structural motif of the compounds $[Mn(L)MnSb_2S_5]$ is a distorted heterocubane unit $MnSb_2S_4$ composed of $[MnS_6]$ and $[MnN_2S_4]$ octahedra and two $[SbS_3]$ trigonal pyramids (Fig. 20). One edge of the cube is a relatively long Sb–S bond and another one a long Mn–S bond. The interconnection of the cubanes generates a second heterocubane unit denoted as 2 in Fig. 20. The final layered structure is achieved by condensation of the two different types of cubanes *via* common corners, edges and faces. Within the layer ellipsoidal holes with different diameters are observed (Table 9). The layers are stacked onto each other generating channels running along one of the crystallographic directions. One N atom of the ligands points into the hole, the remaining part of the ligands being oriented perpendicular to the layers separating the sheets from each other.

A special feature of successive layers is the "key into lock" stacking with the hydrophobic part of ligands filling the space between the layers (see Fig. 21 as an example).

The interlayer interactions are of van der Waals type but weak hydrogen bonding interactions may also stabilize the framework. Analyzing the geometric parameters of the different members of the $[Mn(L)MnSb_2S_5]$ structure family several conclusions can be drawn. First, the short Sb–S bonds, the average Mn(1)–N and the average Mn(2)–S bonds show no systematic alterations within the series (see Table 9). Secondly, significant differences can be identified for the long Mn(1)–S(2) bond and the N–Mn(1)–N angles in the $[MnN_2S_4]$ octahedra. The long Mn(1)–S(2) distances

range from 2.866 Å (L = ma) to 3.185 Å (L = mdap). The elongation of this bond is accompanied by a reduction of the average Mn(1)–S bond length to the other three S atoms. The angles N–Mn(1)–N are significantly larger than 90° for L = ma and ea (Table 9), near 90° for L = 1,3-dap, mdap and dape where six-membered MnN_2C_3 rings are present, and deviates strongly for L = dien where a five-membered MnN_2C_2 ring occurs (Table 9). It is still not clear why one of the Mn–S bonds exhibits such a significant lengthening. One may speculate that the S atom involved in this bond has bonding interactions to three Mn and two Sb cations, whereas the other unique S atoms are only involved in bonding to two Mn and one Sb or to two Mn and two Sb cations. Different sterical, spatial and electronic requirements of the ligands may also play a role for the weakening of one Mn–S bond. A more detailed analysis of all Mn–S and Mn–N bond lengths and the corresponding angles suggests that the long Mn–S bond may be viewed as the weakest link in the network allowing the crystal structure to relax and to reduce an internal "strain" exerted by the amine ligands. The two diameters D1 and D2 of the ellipsoidal holes in the layers give an impression of the shapes caused by the different amines. The ratio D1/D2 reveals that for all bidentate ligands the shape of the hole deviates more strongly from an ideal round pore (Table 9).

From a synthetic point of view the occurrence of two different $[MnL_6]$ (L = ligand) octahedra is surprising. The amine concentration is very large compared to the S concentration, and one would assume that the formation of $[MnN_6]$ octahedra is preferred. In contrast to this assumption, Mn^{2+} has a pronounced tendency to form bonds to S atoms.

Recently, the rigid ligand phen could be integrated into the $Mn_2Sb_2S_5$ network yielding $[Mn(phen)MnSb_2S_5]$ [129]. The synthesis was performed with Mn : Sb : S = 1 : 1 : 3 mmol heated in a mixture of phen/en in water for 5 d at 150 °C. The role of en was not discussed by the authors but one can assume that it supplies the high pH value necessary for the formation of the reactive S species in solution. In the structure the Mn(1)–S bond lengths scatter in the much more narrow range 2.551 to 2.624 Å than for the other compounds presented above.

The structural family of compounds containing heterocubane units composed of Mn, Sb and S atoms was recently extended with the compound $[Mn(trien)Mn_2Sb_2S_6]$ composed of $[Mn_4Sb_2S_6]$ double-cubanes. The material was synthesized using Mn : Sb : S in a 1 : 1 : 2.5 mmol ratio heated in a mixture of 2 mL triethylenetetramine and 3 mL H_2O for 7 d at 140 °C. In the structure one unique $[SbS_3]$ trigonal pyramid, one unique $[MnS_6]$ and one independent $[MnS_4N_2]$ octahedron are joined to form the $[Mn_4Sb_2S_6]$ double-cubane (Fig. 22). The $[MnS_6]$ octahedron shares one edge with the $[SbS_3]$ group and two edges with two symmetry-related $[MnS_4N_2]$ octahedra. The two symmetry-related $[MnS_4N_2]$ octahedra have a common edge, and each is joined to the $[SbS_3]$ unit and one $[MnS_6]$ octahedron *via* edge-sharing. The double-cubane units are connected into linear rods by the $[MnS_6]$ octahedra which have a common edge with one $[SbS_3]$ pyramid and one $[MnS_4N_2]$ octahedron. The rods are joined into layers by the tetradentate ligand acting in a bidentate fashion to Mn^{2+} cations of neighboring rods (Fig. 22).

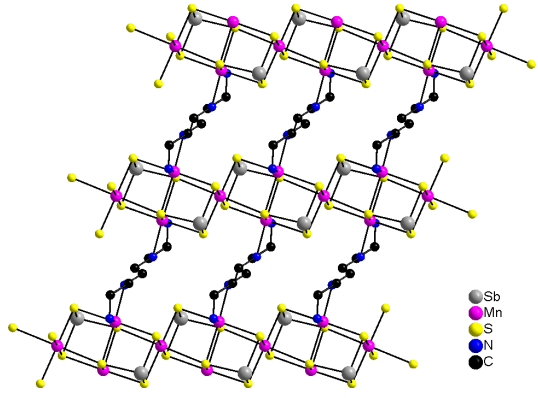

Fig. 22 (color online). The double-cubane units in $[Mn(trien)Mn_2Sb_2S_6]$ forming rods which are joined by the amine molecules thus forming layers. The H atoms are not shown.

We note that the changes of the bonding interactions in the $[Mn(L)MnSb_2S_5]$ compounds are significantly reflected in the magnetic properties of the different compounds as discussed in [130].

Synthetic Aspects of Thiostannate Chemistry

Thiostannates are synthesized from different Sn sources as starting materials. In most cases elemental Sn is used, but also $SnCl_4 \cdot 5H_2O$ [103, 106, 107, 111, 119], $SnCl_4$ [97, 104], SnS_2 [94, 101, 118], $SnCl_2 \cdot 2H_2O$ [119, 120], and even Sn-organic compounds like for example $Cl_3SnBu\text{-}SnCl_3$ [99] were applied.

The variety of different tin sources in diverse oxidation states indicates the complexity of the reactions occurring in the slurries under solvothermal conditions.

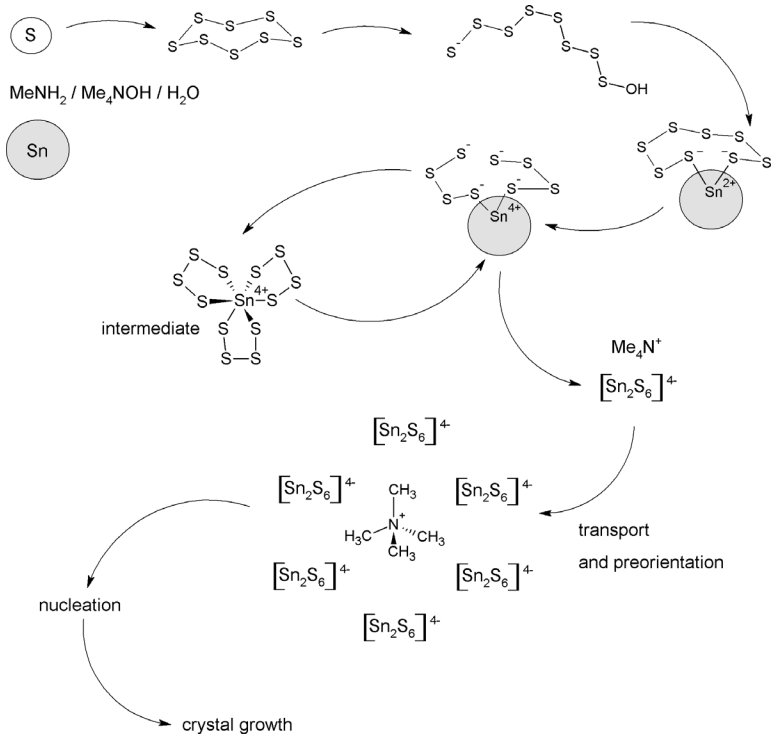

Fig. 23. Scheme of the formation of R-SnS-1 materials from Sn and S under solvothermal conditions with organic molecules as structure directors for the example $(Me_4N)_2Sn_3S_7$ [11].

The influence of the starting material onto product formation is still not well understood, and no systematic investigations have been performed to gain more information about the relation of the Sn source and the crystallized material. During the optimization of the synthesis of some thiostannates we applied different reactants as *e. g.* $Sn(Ph)_4$ for the preparation of $(1,4\text{-dabH}_2)Cu_2SnS_4$ [113] or SnS_2 for the synthesis of $(dienH_2)Cu_2Sn_2S_6$ [115]. In both cases the desired compounds were formed, but applying $Sn(Ph)_4$ resp. SnS_2 gave materials with poor crystallinity, and the best results were obtained applying elemental Sn.

The formation of thiostannates under hydrothermal conditions was investigated with energy-dispersive X-ray diffraction [131]. The authors proposed that after dissolution of the solid reactants the thiostannate anions are formed, and elemental Sn is oxidized to Sn(IV), followed by the condensation of the anions and the formation of the anionic layers which are at the early stages disordered. Characterizing the species in solution by means of ^{119}Sn NMR and UV/Vis spectroscopy led to the identification of several species [11]. In the quenched reaction intermediates the dominating anion $[Sn_2S_6]^{4-}$, the polysulfides $[Sn(S_4)_3]^{2-}$ and $[Sn(S_4)_2(S_6)]^{2-}$, or $[S_2O_3]^{2-}$ could be identified. According to these results the following reactions may proceed in the mother liquor [11]:

$$Sn + S_8 \rightarrow Sn^{2+} + {S_8}^{2-}$$

$$Sn^{2+} + {S_8}^{2-} \rightarrow Sn^{4+} + {S_6}^{2-} + {S_2}^{2-}$$

$$Sn^{2+} + {S_8}^{2-} \rightarrow Sn^{4+} + 2{S_4}^{2-}$$

$$Sn^{4+} + 3{S_4}^{2-} \rightarrow [Sn(S_4)_3]^{2-}$$

$$Sn^{4+} + 2{S_4}^{2-} + {S_6}^{2-} \rightarrow [Sn(S_4)_2(S_6)]^{2-}$$

$$Sn + {S_2}^{2-} \rightarrow Sn^{2+} + 2S^{2-}$$

$$2Sn^{4+} + 6S^{2-} \rightarrow [Sn_2S_6]^{4-}$$

Based on the results obtained with the X-ray scattering experiments and those obtained by analyzing the solutions a reaction mechanism was proposed as depicted in Fig. 23.

According to the proposed scheme the amine reacts with sulfur forming polysulfide species attached to elemental Sn. Several intermediates are then formed, and the alkylammonium ions act as structure-directing molecules leading to the nucleation and finally to crystal growth.

The reaction mechanism just presented is applicable to using sulfur as starting material, but as shown in Tables 4 – 6 there are also examples where SnS_2 (*e. g.* for $(pipH)_2(4,4'\text{-epipH}_2)Sn_5S_{12}$ [101]), $Na_2S \cdot 9H_2O$ (for $(dda)_4Sn_2S_6 \cdot 2H_2O$ [97]), $HSCH_2CH(SH)CH_2OH$ (for $(enH_2)HgSnS_4$ [118]) or additional $(NH_4)_2S$ (for $(DABCOH)_2Sn_3S_7$ [95]) were used as sources. Hence it is not sure whether all these reactions include all the different steps schematically shown in Fig. 23, and more investigations are needed for a better understanding of the formation of thiostannate compounds.

The amine molecule acts as solvent, structure-directing medium, and charge-compensating cation, and is responsible for the formation of the reactive polysulfides. The amines are applied in different concentrations mainly diluted with water, and only few examples were reported for using mixtures of amines with other solvents like methanol ($(enH_2)(enH)_2Sn_2S_6$ [100]) or ethanol ($(dda)_4Sn_2S_6 \cdot 2H_2O$ [97], $(enH_2)Ag_2SnS_4$ [117]). Therefore, the thiostannate chemistry using defined mixtures of different solvents is not well explored, and one can assume that a systematic variation of this reaction parameter should lead to the formation of new compounds.

According to the synthetic conditions compiled in Tables 4 and 5, the transition metals are supplied as elements or as chlorides (see Tables 5 and 6), and only a few experiments were carried out with other starting materials, *e. g.* $AgNO_3$ for the preparation of $(enH_2)Ag_2SnS_4$ [117] or HgI_2 for the synthesis of $(enH_2)HgSnS_4$ [118]. No further details were reported concerning the choice of the educts, and therefore one can only speculate why these starting materials were selected, and/or that the thiostannates were obtained with these materials after some explorative experiments.

Integration of Transition Metal Cations into Thioantimonate(III) Networks

Whereas for the incorporation of Mn^{2+} into the inorganic thioantimonate(III) frameworks no special synthetic efforts are needed, the integration of TM^{n+} like Fe, Co, Ni, or Zn requires synthetic "tricks". Normally, cations like Fe^{2+}, Co^{2+}, Ni^{2+} or Zn^{2+} form stable complexes when mono-, bi-, or tridentate amines are used. In such cases the TM^{n+} ions are coordinatively saturated, and no bond formation to the thioantimonate(III) network is observed. On the basis of structural considerations one must use a tetradentate ligand which cannot satisfy the coordination requirements of the complex cations which prefer octahedral or trigonal-bipyramidal environments. Hence at least one site is left free at the TM^{n+} for bonding to S atoms of the inorganic network. With this idea in mind we enforced the incorporation of transition metal cations into the inorganic networks using the tetradentate amine tren. The first examples were the layered compound $[Co(tren)Sb_2S_4]$ and the chain compound $[Ni(tren)Sb_2S_4]$ [132]. Both compounds were prepared using elemental Co resp. Ni, Sb, and S in the molar ratio 1 : 1 : 3 in 10 mL of a 50 % aqueous tren solution heated at 140 °C. In the structure of the former compound the Co^{2+} cation is coordinated by four N atoms of the ligand and by one S atom of the thioantimonate anion yielding a trigonal-bipyramidal coordination geometry. The $[Co(tren)]^{2+}$ complex is located above/below a 20-membered $Sb_{10}S_{10}$ ring. Two $[SbS_4]$ units share a common edge to form an Sb_2S_2 ring. Four such Sb_2S_2 rings are at the corners of a two-dimensional square net, and further interconnection of the rings by $[SbS_3]$ pyramids generates the $Sb_{10}S_{10}$ ring with pore diameters of 10×8.4 Å.

In contrast, the Ni^{2+} cation adopts an octahedral environment with four N atoms of the tren ligand and two S atoms of the thioantimonate(III) network to form a chain structure. The $[Sb_2S_4]^{2-}$ anion in the Ni compound is formed by corner-sharing with $[SbS_3]$ pyramids. The mode of connectivity between the anions and the $[Ni(tren)]^{2+}$ complexes generates $NiSb_2S_3$ rings in twist conformation with an unusually large Ni–S–Sb angle of 121.7°. The different coordination behavior of Co^{2+} and Ni^{2+} can be rationalized on the basis of the electronic configuration of the two cations. For the Co^{2+} cation with the d^7 configuration the energy difference between an octahedral and a trigonal-bipyramidal environment should be very small and the geometrical requirements of the tren ligand enforce the formation of the five-fold coordination. For Ni^{2+} with the d^8 electronic configuration the octahedral surrounding is energetically favorable compared to the trigonal-bipyramidal environment.

In the meantime several other transition metal-containing compounds were synthesized using this synthetic approach. The compound $[Fe(tren)FeSbS_4]$ was prepared with $FeCl_3 : Sb : S$ in a 1 : 1 : 3 mmol ratio in 8 mL 50 % aqueous tren solution heated for 5 d at 170 °C. In the structure Fe^{2+} and Fe^{3+} coexist in different environments. The Fe^{2+} cation is surrounded by the four N atoms of the tetradentate ligand and by one S atom of the $[FeSbS_4]^{2-}$ chain anion yielding a dis-

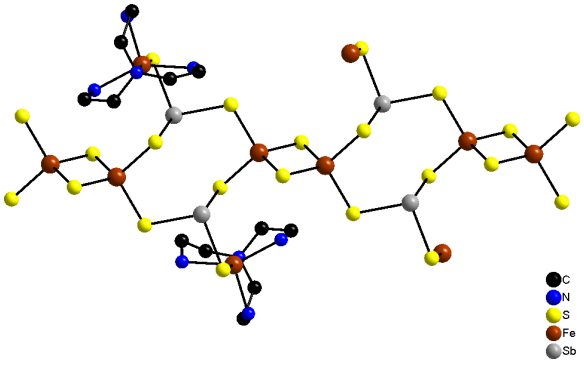

Fig. 24 (color online). Interconnection of the different building units in the structure of [Fe(tren)FeSbS$_4$]. The amine ligands around the Fe^{2+} cations are only shown for two ions with H atoms omitted.

torted trigonal bipyramidal coordination polyhedron. The Fe^{3+} cation is in a tetrahedral environment of four S atoms, and two symmetry-related [FeS_4] tetrahedra share a common edge thus forming a [Fe_2S_6] bitetrahedron (Fig. 24). The [Fe_2S_6] units and the [SbS_3] pyramids are vertex-linked generating a central 8-membered $Fe_2Sb_2S_4$ ring. The rings and the bitetrahedra alternate along the chain structure [133].

The isostructural compounds [M(tren)Sb_4S_7] with M = Mn, Fe, Co, and Zn feature a one-dimensional $[Sb_4S_7]^{2-}$ anion with the $[M(\text{tren})]^{2+}$ cations bound to the thioantimonate backbone *via* one S atom, *i. e.* in all compounds the M^{2+} cations are in a trigonal bipyramidal polyhedron. The synthesis of the compounds with M = Mn, Co was performed applying the elements as starting materials whereas the Fe compound was obtained using $FeCl_3$ [48]. The $[Sb_4S_7]^{2-}$ anion is constructed by a [Sb_3S_4] semi-cube composed of two [SbS_3] pyramids and one [SbS_4] moiety by corner- and edge-sharing. These semicubes are connected into the final anion by [SbS_3] units (Fig. 25). Longer Sb–S contacts connect the chains to form layers. Interest-

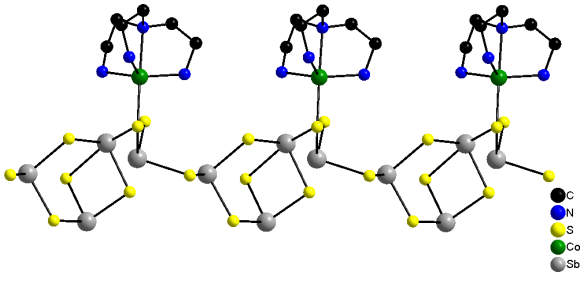

Fig. 25 (color online). The chain structure in the compounds [M(tren)Sb_4S_7]. H atoms are not displayed.

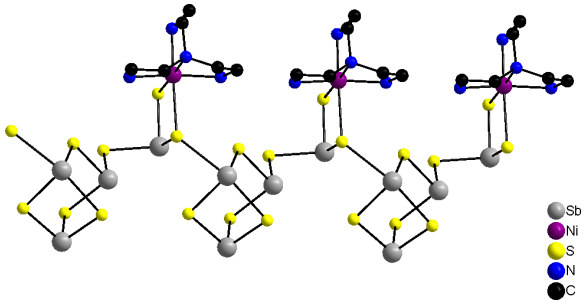

Fig. 26 (color online). The chain structure in [Ni(tren)Sb_4S_7] with the Ni^{2+} cation in a distorted octahedral environment (compare Fig. 25).

ingly, the optical band gap of the compounds vary from 2.04 eV for M = Fe to 3.11 eV for M = Mn. Using appropriate mixtures of transition metal cations the band gap can be tuned to about 1.1 eV.

The compound [Ni(tren)Sb_4S_7] is not isostructural to the other [M(tren)Sb_4S_7] examples (see above) because the Ni^{2+} cation adopts a distorted octahedral environment of four N and two S atoms (Fig. 26). Whereas in the former compounds the [SbS_3] group joining the [Sb_3S_4] semi-cubes has one bond to the M^{2+} cation, in the Ni^{2+}-containing material the [SbS_3] pyramid has two bonds to Ni^{2+}. This connectivity pattern generates a small $NiSbS_2$ ring with one long Ni–S bond of 2.782 Å as compared to the other Ni–S bond which may be caused by steric reasons [45].

Applying the amine trien, which is an isomer of tren, the two thioantimonates [M(trien)Sb_4S_7] (M = Zn, Mn) were obtained upon heating mixtures of M : Sb : S in a 1 : 1 : 2.5 mmol ratio in 40 % aqueous trien solution

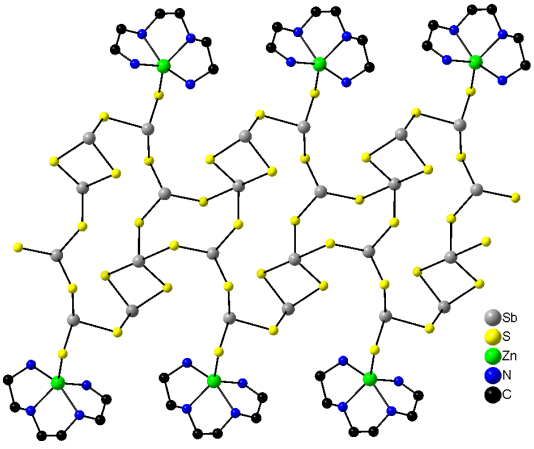

Fig. 27 (color online). The chain anion [M(trien)Sb_4S_7] with the metal complexes located at the periphery of the thioantimonate chain.

for 7 d at 140 °C. The structure of the $[Sb_4S_7]^{2-}$ anion is unique and is composed of $[Sb_2S_5]$ assemblies generated by vertex-linking of two $[SbS_3]$ pyramids and edge-sharing of one $[SbS_3]$ unit with a $[SbS_4]$ moiety. The two $[Sb_2S_5]$ units share a common S atom forming the next hierarchical block of composition $[Sb_4S_9]$. Neighboring $[Sb_4S_9]$ units are related by a center of inversion creating a $[Sb_8S_{16}]$ building block which may be regarded as the main structural motif. Two of the terminal S atoms of the $[Sb_8S_{16}]$ assembly have bonds to the $[M(\text{trien})]^{2+}$ cations, and the remaining four terminal S atoms connect the $[Sb_8S_{16}]$ groups into the final $[Sb_4S_7]^{2-}$ chain anion (Fig. 27) [45].

There are only three examples where transition metal cations have been incorporated into the thioantimonate network without enforcement by a suitable ligand as discussed above. The first compound $[Co(en)_3]CoSb_4S_8$ was obtained applying the unusual starting materials $CoBr_2$ and Na_3SbS_3 (ratio: 0.4 : 0.32 mmol) in an en/H_2O mixture heated to 130 °C for 3 d. In the structure isolated $[Co(en)_3]^{2+}$ cations and non-centrosymmetric $[CoSb_4S_8]^{2-}$ layers coexist. The layer is constructed of $[SbS_2]$ chains composed of corner-sharing $[SbS_3]$ pyramids. Four terminal S atoms of two neighboring chains have bonds to Co^{2+} leading to $[CoS_4]$ tetrahedra which thereby connect the chains to give the $[CoSb_4S_8]^{2-}$ layer. Within the layer small 6-membered $CoSb_2S_3$ and larger 20-membered $Co_2Sb_2S_{10}$ rings are embedded. The isolated cation is located above and below the large rings [134]. The second compound with composition $[Fe(dien)_2]Fe_2Sb_4S_{10}$ was synthesized using $FeCl_3$, Sb and S (ratio: 1 : 1 : 3 mmol) in 8 mL of a 50 % aqueous dien solution heated at 170 °C for 5 d. The structure is composed of the octahedral $[Fe(dien)_2]^{2+}$ cation in *s-fac*-configuration and the one-dimensional $[Fe_2Sb_4S_{10}]^{2-}$ anion. The chain anion is constructed by the interconnection of two $[SbS_3]$ pyramids and one $[FeS_4]$ tetrahedron with Fe^{3+} as central cation. Two $[FeS_4]$ tetrahedra are related by a center of inversion to form a $[Fe_2S_6]$ bitetrahedron by sharing a common edge. Vertex-linking of two $[SbS_3]$ pyramids generates a $[Sb_2S_5]$ moiety as a secondary building block which shares two S atoms with the bitetrahedron thus yielding the next hierarchical structural motif containing a 7-membered $Fe_2Sb_2S_3$ ring. A Sb_4S_4 ring in chair conformation is formed around a center of inversion relating to the $[Sb_2S_5]$ moieties. The one-dimensional chain may be viewed as a condensation product of the Sb_4S_4 rings and the $[Fe_2S_6]$ bitetrahedra. Because a Fe^{3+} salt was used as starting compound a redox reaction must have occurred under the synthetic conditions generating the Fe^{2+} cations.

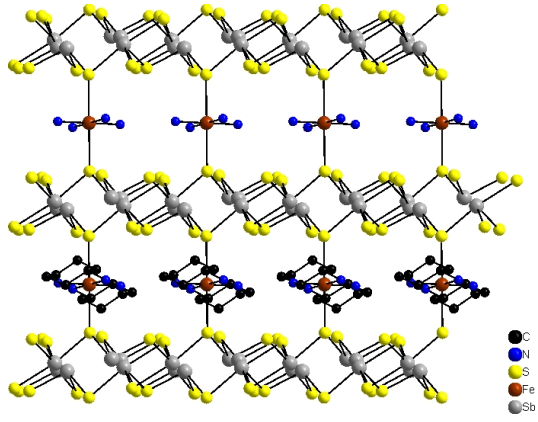

Fig. 28 (color online). Pillaring of the $[Sb_6S_{10}]^{2-}$ layers *via* the Fe^{2+}-centered cations in $[Fe(\textit{trans}\text{-}1,2\text{-dach})_2Sb_6S_{10}]$.

The last example, $[Fe(\textit{trans}\text{-}1,2\text{-dach})_2Sb_6S_{10}]$, represents the rare case of a layered thioantimonate(III) anion with bridging transition metal complexes yielding a three-dimensional network (Fig. 28). The compound was prepared using $FeSO_4 \cdot 7H_2O$ (0.25 mmol), Sb (1 mmol) and S (3 mmol) in a 50 % (±)-*trans*-1,2-diaminocyclohexane solution (4 mL). The slurry was heated for 7 d at 150 °C. The $[Sb_6S_{10}]^{2-}$ anion contains two $[SbS_3]$ trigonal pyramids and one $[SbS_4]$ unit. Two symmetry-related SbS_4 groups are edge-sharing to form a $[Sb_2S_6]$ moiety, and two symmetry-related $[SbS_3]$ units form a $[Sb_2S_4]$ building block by sharing common edges. The $[Sb_2S_6]$ moiety and the $[Sb_2S_4]$ building block are vertex-linked to another $[SbS_3]$ unit producing the anion layer. The anion contains several rings, namely Sb_2S_2, Sb_6S_6 and $Sb_{10}S_{10}$ (approximate diameters: 3.15 and 10 Å). The layers are bridged by the $[Fe(C_6H_{14}N_2)_2]^{2+}$ cations with a remarkably long Fe–S bond of 2.770 Å which may be caused by a pronounced Jahn-Teller distortion [135]. The connection mode generates large tunnels which are in part occupied by the ligand molecules. Neglecting the amine molecules, the potential solvent area amounts to 36.5 %. The presence of Fe^{2+} in the high-spin state was verified by Mössbauer spectroscopy.

Thioantimonate(III) Anions Acting as Ligands

Above we have noted that only few compounds with small thioantimonate(III) ions could be isolated and structurally characterized, which may

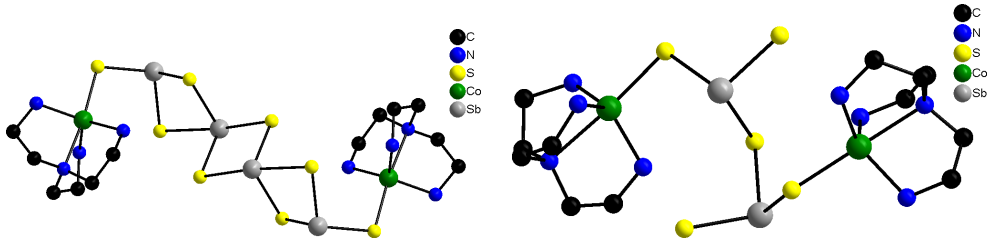

Fig. 29 (color online). The $[Sb_4S_8]^{4-}$ ligand in $[\{Co(tren)\}_2Sb_4S_8]$ joining two Co^{2+} cations (left) and the $[Sb_2S_5]^{4-}$ anion in $[\{Co(tren)\}_2Sb_2S_5]$ connecting two $[Co(tren)]^{2+}$ complexes (right). H atoms have been omitted for clarity.

be due to the pronounced tendency towards condensation of such small anions. In the presence of transition metal cations several complexes with thioantimonate(III) anions acting as ligands could be synthesized. These include $[Cr(en)_2SbS_3]$ [136], $[\{Co(tren)\}_2Sb_4S_8]$ and $[\{Co(tren)\}_2Sb_2S_5]$ [137], $[\{Mn(tren)\}_4Mn_2Sb_4S_{12}]$ [138], $[\{Zn(tren)\}_2Sb_4S_8] \cdot 0.75H_2O$ [37], $[\{Mn(tren)\}_2Sb_2S_5]$ and $[\{Mn(tren)\}_2Mn_2Sb_4S_{10}]$ [127], $[Cr(tren)SbS_3] \cdot H_2O$ [139], $[\{Co(tren)_2\}CoSb_2S_6] \cdot H_2O$ [140], $[La(dien)_2(\mu_4\text{-}Sb_2S_5)(\mu_3\text{-}SO_4)]_n$ [141], and $[Cr(trien)SbS_3]$ [142].

The smallest anion $[SbS_3]^{3-}$ acts as a bidentate ligand in $[Cr(en)_2SbS_3]$, $[Cr(tren)SbS_3] \cdot H_2O$ and $[Cr(trien)SbS_3]$. An $[Sb_4S_8]^{4-}$ ligand composed of two $[SbS_3]$ and two $[SbS_4]$ units joins two $[M(tren)]^{2+}$ complexes (M = Co, Zn) with its two terminal S atoms (Fig. 29, left). The transition metal cations are fivefold coordinated by four N atoms and one S atom in a distorted trigonal-bipyramidal fashion. The Co compound was prepared using a mixture of Co : Sb : S = 1 : 1 : 3 mmol in 3 mL of a 95 % tren solution heated for 4 d at 140 °C. Using identical synthesis conditions but increasing the reaction time to 12 d, $[\{Co(tren)\}_2Sb_2S_5]$ was obtained as a phase-pure product. At intermediate reaction times both compounds could be identified in the X-ray powder patterns. This is another example demonstrating the influence of the reaction time on product formation.

The structure of $[\{Co(tren)\}_2Sb_2S_5]$ consists of an $[Sb_2S_5]^{4-}$ anion (Fig. 29, right) composed of two edge-linked $[SbS_3]$ pyramids acting as a bidentate ligand to the $[Co(tren)]^{2+}$ cations. We note that the layered compound $[Co(tren)Sb_2S_4]$ was synthesized applying the identical ratio of the starting materials and the same reaction temperature but using 10 mL of a 50 % aqueous tren solution (see above). A different binding mode of the $[Sb_2S_5]^{4-}$ anion is observed in $[\{Mn(tren)\}_2Sb_2S_5]$ (Fig. 30). The $[Sb_2S_5]^{4-}$ unit connects two $[Mn(tren)]^{2+}$ cations in a tetradendate

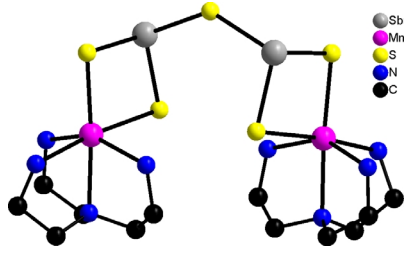

Fig. 30 (color online). The $[Sb_2S_5]^{4-}$ anion connecting two $[Mn(tren)]^{2+}$ complexes in $[\{Mn(tren)\}_2Sb_2S_5]$. H atoms have been omitted for clarity.

manner, and as a consequence the Mn^{2+} ions are in a distorted octahedral environment of two S and four N atoms. The compound crystallized from a mixture of Mn : Sb : S = 1.1 : 2.5 mmol heated in 5 mL of a 95 % tren solution for 7 d at 140 °C.

During thermal decomposition amine molecules are emitted from $[\{Mn(tren)\}_2Sb_2S_5]$ which is thus transformed into the amine-poorer compound $[\{Mn(tren)\}_2Mn_2Sb_4S_{10}]$ showing a more complex interconnection of different building units (Fig. 31) such as $[SbS_3]$ trigonal pyramids and $[MnS_4]$ tetrahedra. The peripheral Mn^{2+} cations are again in an octahedral coordination of four N and two S atoms. Some special features of the structure are five 4-membered and two 6-membered heterocycles. With the organic ligands not considered, the structure may be viewed as an $[Mn_2Sb_4S_{10}]$ core acting as a complex tetradentate ligand which is bound to two further Mn^{2+} cations.

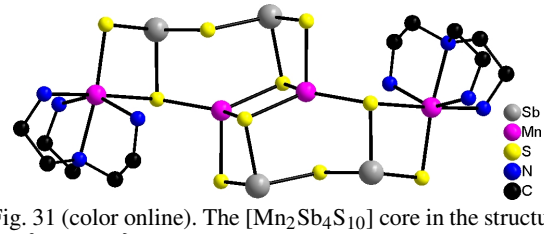

Fig. 31 (color online). The $[Mn_2Sb_4S_{10}]$ core in the structure of $[\{Mn(tren)\}_2Mn_2Sb_4S_{10}]$ acting as a tetradentate ligand.

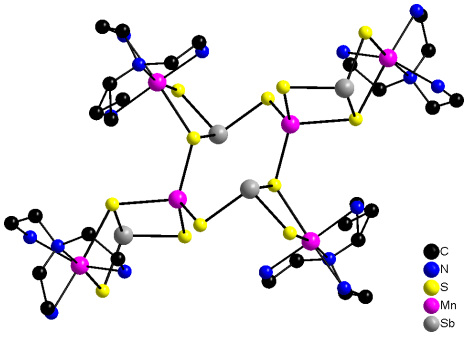

Fig. 32 (color online). The central core $[Mn_2Sb_4S_{12}]$ in the structure of $[\{Mn(tren)\}_4Mn_2Sb_4S_{12}]$ joining four $[Mn(tren)]^{2+}$ cations located at the periphery of the structure. H atoms have been omitted for clarity.

Heating this compound in a tren solution at 140 °C the amine-richer sample crystallized after 12 d. From a synthetic point of view two results are remarkable. First, an amine-rich thioantimonate was decomposed by a thermal treatment in inert atmosphere yielding a new amine-poorer compound with a hitherto never observed heterometallic core. Second, the amine-richer starting material was obtained by treating the decomposition product in an amine solution. Changing the reaction conditions (Mn : Sb : S = 1 : 1 : 2.5 mmol) and using a more diluted tren solution (70 %) a different compound with composition $[\{Mn(tren)\}_4Mn_2Sb_4S_{12}]$ crystallized after 7 d at 140 °C. The structure of this compound is characterized by an unusual $[Mn_2Sb_4S_{12}]$ core formed by $[SbS_3]$ groups and $[MnS_4]$ tetrahedra. Considering the core as an octadentate ligand, four $[Mn(tren)]^{2+}$ complexes are bound to it. A central 8-membered $Mn_2Sb_2S_4$ ring can be viewed as the main structural motif (Fig. 32).

Another unusual ligand was synthesized using the elements Co, Sb, and S (1 : 1 : 3 mmol ratio) heated in a mixture of 0.4 mL tren, 2.6 mL dien and

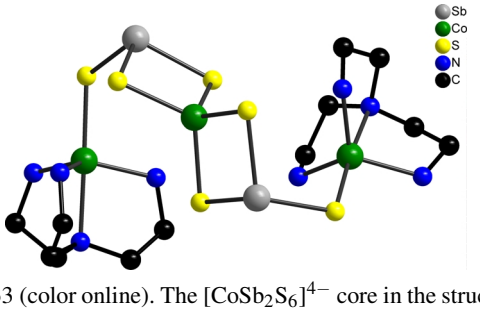

Fig. 33 (color online). The $[CoSb_2S_6]^{4-}$ core in the structure of $[\{Co(tren)_2\}CoSb_2S_6] \cdot H_2O$.

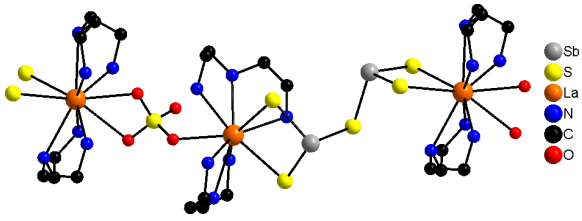

Fig. 34 (color online). The polymeric chain in $[La(dien)_2(\mu_4\text{-}Sb_2S_5)(\mu_3\text{-}SO_4)]_n$ showing the connection of the La^{3+}-centered complexes by $[Sb_2S_5]^{4-}$ and SO_4^{2-} anions. H atoms are not shown.

1 mL water for several days at 110 °C. The compound $[\{Co(tren)_2\}CoSb_2S_6] \cdot H_2O$ contains a $[CoS_4]$ tetrahedron sharing two edges with two $[SbS_3]$ pyramids (Fig. 33) to form the $[CoSb_2S_6]^{4-}$ core. Both terminal S atoms have a bond to a $[Co(tren)]^{2+}$ complex [140].

We note that an increase of the reaction temperature to about 140 °C leads to the crystallization of a different compound with composition $[Co(dien)_2][Co(tren)SbS_4]_2 \cdot 0.5H_2O$ containing the $[SbS_4]^{3-}$ anion.

Recently we started to explore the thioantimonate(III) chemistry of lanthanoide cations (Ln^{3+}). In contrast to transition metal cations, the Ln^{3+} ions prefer larger coordination numbers between 7 and 10, and one can expect new structural motifs and dimensionalities of the thioantimonate networks containing Ln^{3+} cations. The main disadvantage working with lanthanoides is their pronounced oxophilic character. Water must therefore be avoided in the solvothermal syntheses. The one-dimensional polymeric compound with composition $[La(dien)_2(\mu_4\text{-}Sb_2S_5)(\mu_3\text{-}SO_4)]_n$ was isolated heating $La(OH)_3$, Sb, and S (0.5 : 1 : 3 mmol ratio) in 100 % dien (3 mL) for 7 to 10 d at 150 °C. The two independent La^{3+} cations are nine- $[LaN_6OS_2]$ and ten-coordinated $[LaN_6O_2S_2]$ and are joined by a μ_3-bridging SO_4^{2-} anion and a μ_4-acting $[Sb_2S_5]^{4-}$ anion (Fig. 34).

The Effect of Reaction Time on the Product Formation of Thioantimonates(III)

The effect of the reaction time on the product formation was not systematically studied until now. Most thioantimonates(III) were synthesized with reaction times ranging between about 3 and 10 d. However, one can assume that the thioantimonates(III) formed under the specific solvothermal conditions may in many cases be only kinetically stable, and that compounds with more stable structures can be expected

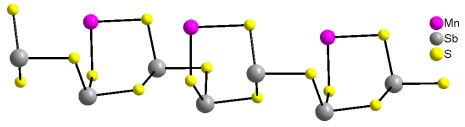

Fig. 35 (color online). The chain structure in [Mn(tren)-Sb_2S_4] form I. The ligand molecules are not shown.

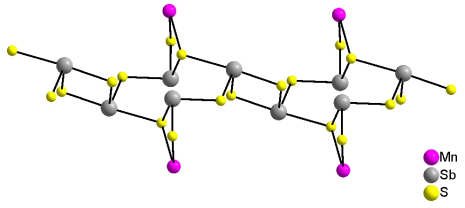

Fig. 36 (color online). The chain structure in [Mn(tren)-Sb_2S_4] form II. The ligand molecules are not shown.

according to Ostwald's rule. There is one example where the influence of the reaction time on the product formation was investigated. The two compounds [Mn(tren)Sb_2S_4] (I = short reaction times, II = long reaction times) were prepared heating a mixture of Mn (1 mmol), Sb (2 mmol) and S (4 mmol) in 5 mL of a 50 % aqueous tren solution at 140 °C. Compound I crystallized if the reaction time was shorter than 13 d, compound II occurred after 13 d. The experiment was extended up to 33 d, and the reaction was quenched every day. The X-ray powder patterns of the reaction products gave no hints for the coexistence of the two samples. In further experiments crystals of II were used as seeds in a synthesis, and after 7 d only crystals of II were observed. Furthermore, from syntheses performed in Teflon liners which were formerly used for the preparation of II only this compound could be isolated. These observations are clear hints that II is more stable than I.

The structures of the two modifications (Figs. 35 and 36), both with the $[Mn(tren)]^{2+}$ complexes having two bonds to the thioantimonate(III) $[Sb_2S_4]^{2-}$ backbones, are very different. In the structure of I only $[SbS_3]$ trigonal pyramids are present, whereas in the structure of II $[SbS_3]$ and $[SbS_4]$ moieties coexist. The Sb–S bonds in the $[SbS_4]$ units show the typical pattern of two shorter and two longer bonds.

The Effect of Reaction Parameters on the Product Formation of Thiostannates

The effect of the reaction time on the product formation can be nicely demonstrated for the compound $[\{Ni(tepa)\}_2Sn_2S_6]$ (form I) [120]. The thiostannate

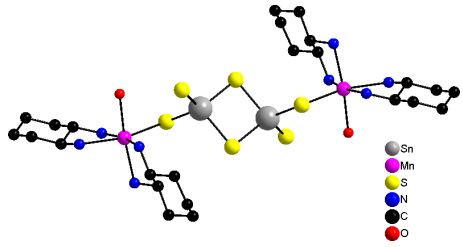

Fig. 37 (color online). The structure of $[\{Mn(1,2\text{-dach})_2(H_2O)\}_2Sn_2S_6]$. The hydrogen atoms have been omitted for clarity.

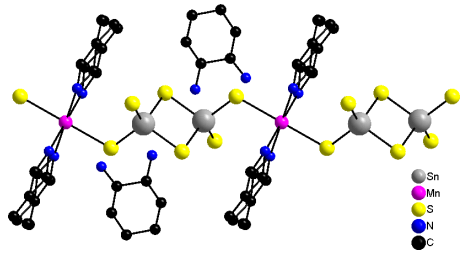

Fig. 38 (color online). Part of the structure of $[\{Mn(1,2\text{-dach})_2\}Sn_2S_6]\cdot 2$ 1,2-dach showing the one-dimensional coordination polymer and the protonated amine molecules around the chain. The hydrogen atoms have been omitted.

is obtained under solvothermal conditions applying $NiCl_2 \cdot 6H_2O$, $SnCl_2 \cdot 2H_2O$, S and tepa after 25 h at 160 °C. Extending the reaction time to several days a mixture of form I, and a second new form II of *ortho*-$[\{Ni(tepa)\}_2Sn_2S_6]$ appears. After 20 d of reaction time only form II could be identified [143].

The effect of the concentration of the amine on the product formation has also been demonstrated [109]. The thiostannates $[\{Mn(1,2\text{-dach})_2(H_2O)\}_2Sn_2S_6]$ (I) (Fig. 37) and $[\{Mn(1,2\text{-dach})_2\}Sn_2S_6]\cdot 2$ 1,2-dach (II) (Fig. 38) were synthesized under solvothermal conditions with 1,2-diaminocyclohexane solutions of different concentrations. Both structures feature $[Sn_2S_6]^{4-}$ anions which act as bidentate ligands and are bound to Mn^{2+} cations which are in an octahedral environment. Whereas in I an isolated complex is observed, a one-dimensional coordination polymer is formed in II with $[Sn_2S_6]^{4-}$ anions acting as linkers and Mn^{2+} complexes as nodes. Protonated amine molecules are located around the chains (Fig. 38).

Compound I crystallizes from diluted aqueous solutions of 1,2-diaminocyclohexane, and compound II from solutions with high amine concentrations or even from the pure amine. The variation of reaction conditions like the concentration of the amine leads to the crystallization of new compounds demonstrating the

great potential of the solvothermal method. But dilution experiments do not generally lead to the crystallization of new compounds, and often such experiments are just helpful to increase the yield of a desired thiometallate. New compounds can be prepared by changing this reaction parameter, as shown for the series of thioantimonates with $[Ni(dien)]^{2+}$ complexes [8, 35, 50, 121]. Solvothermal reactions are complex, and a simple explanation of the dilution effect cannot be given as yet. Indeed, a reduction of the amine concentration changes the pH value, but also several other parameters can be altered like the boiling point, redox potential, viscosity, supersaturation *etc*. Systematic experiments are required which may lead to the crystallization of new thiostannates, or generally to new thiometallates, by simply changing these reaction parameters.

Thioantimonates(III) Containing Polysulfide Fragments or Sb–Sb Bonds

It is somewhat surprising that only very few thioantimonate(III) compounds containing polysulfide fragments have been reported. As mentioned above, under basic conditions several polysulfide anions are formed which in principal can be integrated into thioantimonate networks. One can argue that the degradation of polysulfide anions is fast, and the reaction times are often long enough to leave only S^{2-} anions in the solution. There are few compounds with polysulfide anions larger than S_2^{2-}, namely $(PPh_4)_3Sb_3S_{25}$ (**1**), $(PPh_4)_2Sb_2S_{15}\cdot 2(C_3N_2H_6)$ (**2**) and $(PPh_4)_2Sb_2S_{15}$ (**3**) [13, 14]. The first two compounds were synthesized with a large excess of S (Sb : S = 1 : 8.5 mmol) in the presence of tetraphenylphosphonium bromide for 7 to 9 d heated at 125 °C. For the synthesis of **1** a 2 M solution of ammonia was added, whereas for **2** a 10 % aqueous solution of 1-*N*-methylimidazole was used. Both compounds could only be isolated as mixtures with $(PPh_4)_2S_7$ [144]. Compound **3** was obtained reacting $SbCl_3$ and S (1 : 9 mmol ratio) with

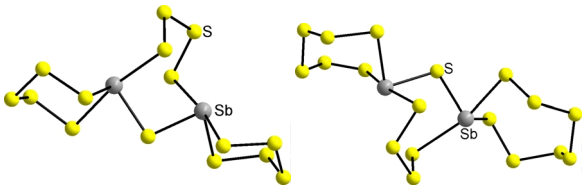

Fig. 39 (color online). The anions $[Sb_2S_{15}]^{2-}$ (left) and $[Sb_2S_{17}]^{2-}$ (right) observed in $(PPh_4)_2Sb_2S_{15}$ and $(PPh_4)_2Sb_2S_{17}$.

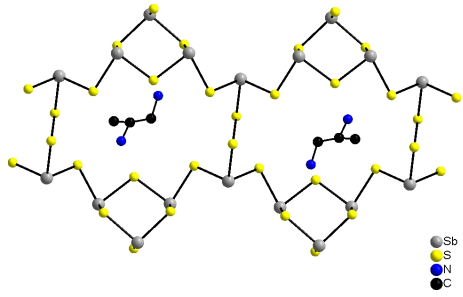

Fig. 40 (color online). The $[Sb_8S_{14}]^{2-}$ anion with the S_2^{2-} dumbbells. The protonated amine molecules are displayed demonstrating the structure-directing effect.

tetraphenylphosphonium bromide in 5 mL of a 2 M ammonia solution heated for 7 d at 130 °C. The two anions $[Sb_2S_{15}]^{2-}$ and $[Sb_2S_{17}]^{2-}$ are displayed in Fig. 39. In the structure of **1** two polysulfide anions $[Sb_2S_{16}]^{2-}$ and $[Sb_2S_{17}]^{2-}$ coexist. In all structures two Sb(III) centers are bridged by four different sulfide ligands yielding a tri-cyclic framework. The $[Sb_2S_{17}]^{2-}$ anion was also found in the compound $(PPh_4)_2Sb_2S_{17}$ [12].

Thioantimonate(III) compounds with the composition $[Sb_8S_{14}]^{2-}$ containing an S_2^{2-} dumbbell have also been reported ($(1,2\text{-dapH}_2)Sb_8S_{12}(S_2)$ [145]; $(dmaH_2)Sb_8S_{12}(S_2)$ [146]; $(2\text{-mpdH}_2)Sb_8S_{12}(S_2)$ [147]). All three compounds show an identical network topology, and an example is depicted in Fig. 40. Two chains formed by corner-sharing $[SbS_3]$ pyramids are joined by the S_2^{2-} anions yielding the two-dimensional layered $[Sb_8S_{14}]^{2-}$ anion. The synthesis conditions reported in the papers are very different, and only for the preparation of $(2\text{-mpdH}_2)[Sb_8S_{12}(S_2)]$ an appreciable excess of S was used [147].

Until now only one compound containing an Sb–Sb bond was synthesized under solvothermal conditions, namely $(ap\text{-}en)_{0.5}Sb_7S_{11}$ [148]. The sample was prepared applying a special procedure. Through the solution of the structure-directing amine *N*,*N*′-bis(3-aminopropyl)ethylenediamine a stream of H_2S gas was bubbled for 3 h prior to use. The amine was mixed with water (0.6 mL and 1.6 mL) and was added to Sb_2S_3 yielding a mixture with a molar ratio Sb_2S_3 : amine : water = 1 : 1 : 30. Heating the slurry for 7 d at 200 °C led to the crystallization of the compound in high yield. The primary building units are $[SbS_3]$ pyramids and $[SbS_4]$ moieties which are corner- and edge-linked to form secondary building blocks like Sb_2S_2, Sb_3S_3, Sb_4S_4 and $Sb_{10}S_{10}$ rings which are condensed generating a chain anion. The

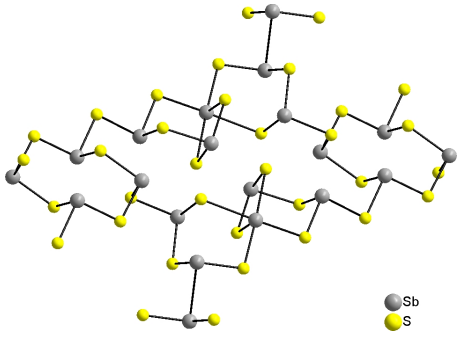

Fig. 41 (color online). Structure of the layered $[Sb_7S_{11}]^{2-}$ anion with Sb–Sb bonds.

chains are connected *via* Sb–Sb bonding yielding the layered $[Sb_7S_{11}]^{2-}$ anion (Fig. 41).

Thiostannates Containing Polysulfide Fragments or Thio-oxoanions

The structural variety of the thiostannates is caused by the coordination diversity of Sn and S, the tendency of S to build rings and chains, and the possibility of Sn to exist in the oxidation states +II and +IV. Different types of anions are formed as *e. g.* $[SnS_4]^{4-}$, $[Sn_2S_6]^{4-}$ and $[Sn_2S_7]^{4-}$, and also several polythiostannate anions

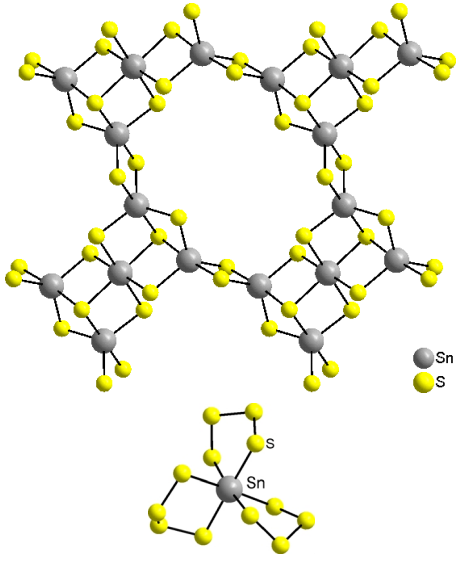

Fig. 42 (color online). Different types of polythiostannate anions; top: $[Sn_5S_{12}]^{4-}$ in $(pipH)_2(4,4'\text{-epip}H_2)Sn_5S_{12}$ with $[SnS_5]$ and $[SnS_6]$ polyhedra; bottom: $[Sn(S_4)_3]$ unit of $(PPh_4)_2Sn(S_4)_3$. The charge-compensating cations have been omitted.

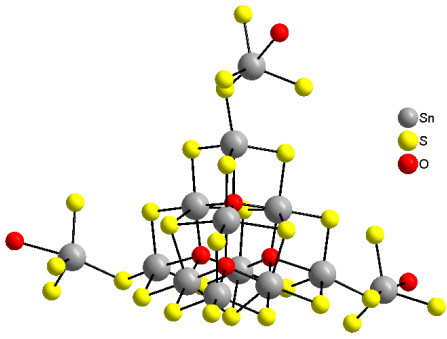

Fig. 43 (color online). Part of the structure of $(Me_3NH)_2Sn_5S_9O_2$ with $[Sn_{10}S_{20}O_4]^{8-}$ units. The cationic part is not displayed.

like $[Sn_5S_{12}]^{4-}$ in $(pipH)_2(4,4'\text{-epip}H_2)Sn_5S_{12}$ [101] with Sn in trigonal-bipyramidal and octahedral environment (Fig. 42, top) and S_x^{2-} ($x = 4, 5, 6, 9$) in $(Et_4N)_3(Sn(S_4)_2)_{0.4}(Sn(S_4)_2(S_6))_{0.6}$ [149] and $(PPh_4)_2Sn(S_4)_3$ [150] (Fig. 42, right) have been reported.

Until now only one compound has been reported with Sn having bonds to S and O atoms, namely $(Me_3NH)_2Sn_5S_9O_2$ [151] with a silicate-like structure consisting of $[Sn_{10}S_{20}O_4]^{8-}$ units (Fig. 43).

Synthetic and Structural Chemistry of Thiometallates with the Coinage Metals Cu and Ag

In the previous section we discussed special synthetic strategies for the incorporation of transition metal cations into thioantimonate(III) networks. Applying the calcophilic cations Cu^+ and Ag^+ in the solvothermal syntheses such synthetic 'tricks' are not required. A series of Cu(I)-thioantimonates(III) with general formula $(L)Cu_2SbS_3$ and L = *trans*-1,2-dach, dien, baep, en, 1,3-dap, and 1,4-dab [152, 153] (the en compound was also reported in ref. [154]) could be prepared under solvothermal conditions using different starting materials like Sb or Sb_2S_3, Cu or $CuCl_2 \cdot H_2O$, and S heated in the corresponding amine solution for 5 to 7 d at temperatures between 120 and 140 °C. All compounds crystallize in space group $P2_1/n$, and the network topology of the layered $[Cu_2SbS_3]^-$ anion is identical. The primary building units are one $[SbS_3]$ pyramid, one $[SbS_4]$ group, one $[CuS_3]$ triangle, and a distorted $[CuS_4]$ tetrahedron. A single layer is constructed by corner-sharing of these building units thus forming different types of heterocycles as shown in Fig. 44. The final double-layer is formed by Cu–S bonds between two individual layers.

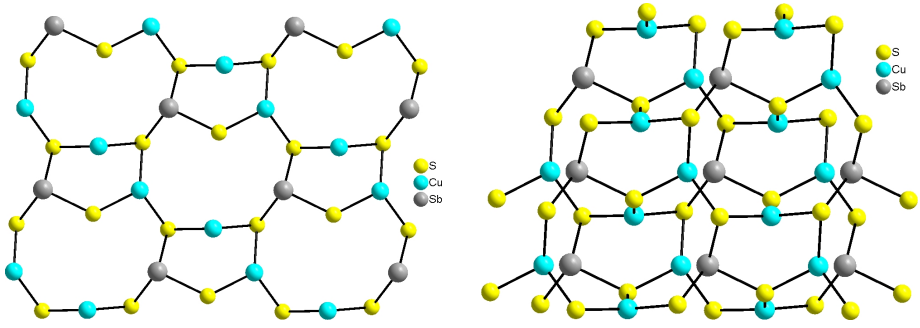

Fig. 44 (color online). A single layer (left) and a double-layer (right) of the $[Cu_2SbS_3]^-$ anion.

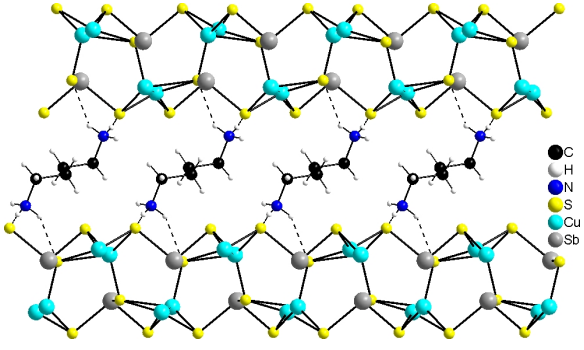

Fig. 45 (color online). The sandwich-like arrangement of the $[Cu_2SbS_3]^-$ layers and the structure-directing ammonium cations in the series of compounds $(L)Cu_2SbS_3$ (L = 1,4-dab as an example).

The structure-directing protonated amine molecules are located in the galleries of successive $[Cu_2SbS_3]^-$ layers (Fig. 45), and the interlayer separation depends on the chain lengths and orientation of the cations covering the range from 4.4 Å for L = en to 8.8 Å for L = baep. The ammonium head groups of the structure directors are always oriented in a way optimizing S···H bonding interactions.

Under identical reaction conditions a Cu(I)-thioantimonate(III) with a different composition $(L)Cu_3Sb_2S_5$ with L = dien could be synthesized. Applying L = trien a second compound with the same composition of the layered $[Cu_3Sb_2S_5]^-$ anion was obtained exhibiting a totally different topology. The structure of the $[Cu_3Sb_2S_5]^-$ anion with L = dien comprises one $[SbS_3]$ pyramid, one $[SbS_4]$ moiety, two $[CuS_3]$ triangles and one $[CuS_4]$ tetrahedron. These units are joined generating a complex undulated layer containing five different 6-membered rings, one 10-membered heterocycle and a 4-membered ring. Two such single layers yield a double-layer (Fig. 46). The shortest inter-layer separation measures 6.1 Å, and the cations are located within the galleries of successive layers.

The second compound with the $[Cu_3Sb_2S_5]^-$ anion contains two $[SbS_3]$ trigonal pyramids, two $[CuS_3]$ moieties, and one $[CuS_4]$ tetrahedron which are connected forming exclusively 6-membered Cu_2SbS_3 or $CuSb_2S_3$ rings (Fig. 47). The rings are condensed yielding a 6^3 net which may be regarded as a puckered graphene layer. Again the structure-directing cations are sandwiched by the $[Cu_3Sb_2S_5]^-$ layers with the shortest layer separation at about 6.4 Å. In all mentioned compounds relatively short Cu–Cu and in part Cu–Sb separations are observed which may indicate weak bonding interactions.

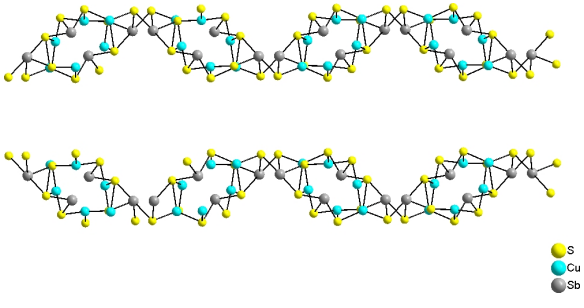

Fig. 46 (color online). The undulated layered $[Cu_3Sb_2S_5]^-$ anion in $(L)Cu_3Sb_2S_5$ with L = dien.

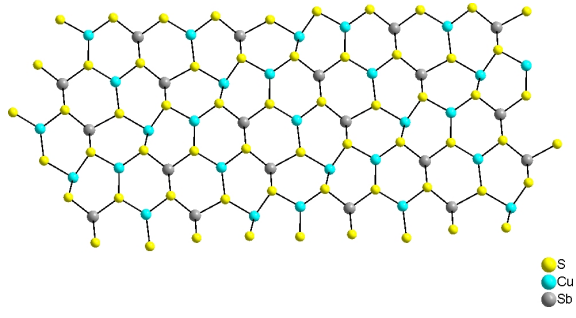

Fig. 47 (color online). The graphene-like layer anion in the compound $(L)Cu_3Sb_2S_5$ with L = trien.

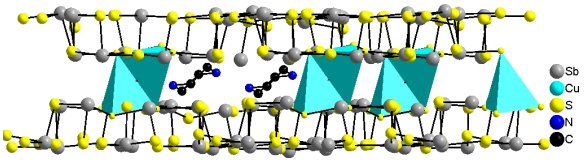

Fig. 48 (color online). Interconnection of the $[Sb_6S_{10}]^{2-}$ layers by $[CuS_4]$ tetrahedra in the compound $(pipH_2)_{0.5}CuSb_6S_{10}$.

Another Cu(I)-thioantimonate(III) with composition $(pipH_2)_{0.5}CuSb_6S_{10}$ could be prepared in the presence of triethylenetetramine applying a different synthesis strategy [155]. 0.9 mL of the amine was first treated with H_2S gas for 90 min and then mixed with 1.6 mL of water, followed by Sb_2S_3 and Cu_2S, and heated to 200 °C for 10 d. The layers with stoichiometry $[Sb_6S_{10}]^{2-}$ generated by $[SbS_3]$ pyramids and $[SbS_4]$ groups are pillared *via* severely distorted $[CuS_4]$ tetrahedra sharing a common edge (Fig. 48). The structure-directing molecule was decomposed under the synthesis conditions, and piperazine was identified in the cations.

Another interesting synthetic approach was also recently published [156]. The authors used *in situ* formed Ni^{2+} complex cations as structure-directing units and obtained the two new compounds $[Ni(1,2\text{-}dap)_2Cu_4Sb_2S_6]$ and $[Ni(dien)_2]CuSb_3S_6$. For the first compound a mixture of $CuCl_2 \cdot 2H_2O$, $NiCl_2 \cdot 6H_2O$, 1,2-propanediamine and S was used, and Sb, S, Cu, $NiCl_2 \cdot 6H_2O$ and diethylenetriamine for the second compound. A puckered anion layer $[Cu_4Sb_2S_6]^{2-}$ is formed therein by condensation of Cu_2SbS_3 rings in contrast to the $[Cu_3Sb_2S_5]^-$ anion where two types of rings, Cu_2SbS_3 and $CuSb_2S_3$, were observed. The layers are joined into a three-dimensional network by the $[Ni(1,2\text{-}dap)_2]^{2+}$ complexes. The layered structure of the $[CuSb_3S_6]^{2-}$ anion contains large 18-membered $Cu_2Sb_7S_9$ and six-membered $CuSb_2S_3$ heterorings.

With the Ag^+ cation thioantimonates(III) with the compositions $(1,4\text{-}dabH_2)Ag_3Sb_3S_7$, $(enH)_2Ag_5Sb_3S_8$ [157], $(enH)_2Ag_5Sb_3S_8$, $(enH)Ag_2SbS_3$ [158], and $(trienH_2)Ag_5Sb_3S_8$ [159] have been reported. The syntheses of these compounds were performed with $AgNO_3$ as Ag source and Sb or Sb_2S_3 as starting materials. The fusion of 5-membered Ag_2SbS_3 rings generates $[Ag_2SbS_3]^-$ chains in $(enH)Ag_2SbS_3$. The Ag^+ cations are in a nearly trigonal-planar environment of three S atoms. The individual chains are connected by Sb–S and Ag–S bonds to form the layered anion. Short Ag–Ag distances indicate $d^{10} - d^{10}$ bonding interactions [160]. The $[Ag_5Sb_3S_8]^{2-}$ anion features a bent $[AgS_2]$ moiety, $[AgS_3]$ triangles and $[AgS_4]$ tetrahedra besides $[SbS_3]$ pyramids. Vertex-linking of the primary building units generates 6-membered rings which are condensed to form a sheet. Because 1/8 of the rings contain two Sb and one Ag atom, the stoichiometry of the sheet corresponds to $[Ag_5Sb_3S_8]^{2-}$. Two individual sheets are linked by Ag–S bonds into a buckled double-layer anion (Fig. 49).

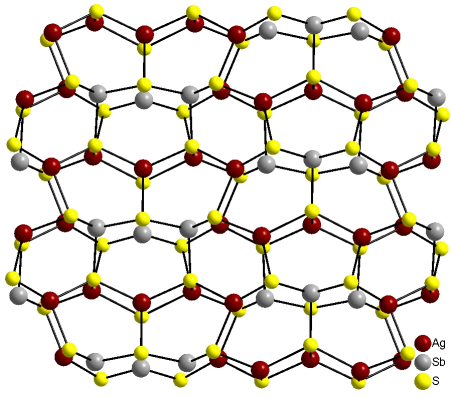

Fig. 49 (color online). The double-layer anion $[Ag_5Sb_3S_8]^{2-}$ generated by condensation of 6-membered rings.

Similar honeycomb-like layers of fused 6-membered rings were observed for $(enH)_2Ag_5Sb_3S_8$ [157] and $(trienH_2)Ag_5Sb_3S_8$ [159]. The main differences between the three compounds are found in the interatomic distances and in the arrangement of the protonated amine molecules residing in a sandwich-like fashion between the double-layers.

The structure of the layered $[Ag_3Sb_3S_7]^{2-}$ anion is unique and is composed of $[Sb_2S_4]$ chains formed by vertex-linking of $[SbS_3]$ pyramids and a $[Ag_3SbS_5]$ group composed of $[AgS_3]$, $[AgS_4]$ and $[SbS_3]$ units. The $[AgS_4]$ tetrahedron shares two edges with two $[AgS_3]$ triangles and one edge with the $[SbS_3]$ pyramid to form $[Ag_3SbS_5]$ moieties which are bridged by

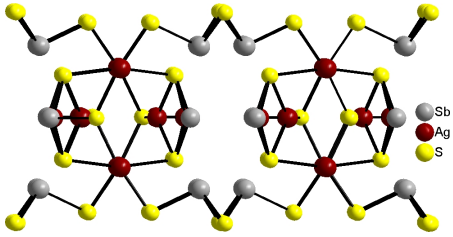

Fig. 50 (color online). The $[Ag_3SbS_5]$ moiety bridged by S atoms yielding the central chain of the $[Ag_3Sb_3S_7]^{2-}$ anion and the surrounding $[Sb_2S_4]$ chain.

an S atom yielding the central chain of the anion. Each central chain is connected to $[Sb_2S_4]$ chains forming the layered $[Ag_3Sb_3S_7]^{2-}$ anion (Fig. 50).

A special feature of the structure is the rare binding mode of one S atom having bonds to four Ag atoms and one Sb atom.

Synthetic and Structural Aspects of Thioantimonates(V)

Compared to the large number of thioantimonates(III), related compounds containing Sb(V) are still rare as summarized in Table 10. In most hybrid thioantimonate(V) structures the $[SbS_4]^{3-}$ anion and the counterions are isolated. There are few examples where bonding interactions between the $[SbS_4]^{3-}$ anions and transition or lanthanoide cations occur. These compounds are presented in Table 10 (marked with *). The $[SbS_4]^{3-}$ anion can act as monodentate ligand like in [Mn(tren)(trenH)]SbS_4 and [Mn(*trans*-1,2-dach)$_3$]$_2$[Mn(*trans*-1,2-dach)$_2$(SbS_4)$_2$] · $6H_2O$ [161], as a bidentate bridging ligand as observed in [Nd(en)$_3$(H_2O)(μ_2-SbS_4)] [162], or as a tridentate ligand like in [La(en)$_3$(μ_3-SbS_4)] [162]. In contrast to Sb(III)S_x moieties, the $[SbS_4]^{3-}$ tetrahedron has no tendency to further condensate like $[InS_4]^{5-}$ or $[GeS_4]^{4-}$ tetrahedra which form a large variety of more complex supertetrahedral clusters of types M_4S_{10}, $M_{10}S_{20}$, $M_{20}S_{35}$, and $M_{35}S_{56}$ (M = In, Ge) [3].

In situ Energy Dispersive X-Ray Scattering (EDXRD) Experiments Performed During the Solvothermal Syntheses of Thioantimonates and Thiostannates

The results discussed in the previous sections clearly demonstrate that no general rules can be formulated allowing a rational synthesis of new thiometallates. The processes leading to the formation and crystallization of such materials under solvothermal conditions are very complex and poorly understood. The understanding of the mechanism of the formation of the products is essential for more rational syntheses. In principal two approaches can be envisaged to acquire a deeper knowledge of the processes occurring under solvothermal conditions. In the first approach *ex situ* experiments can be conducted where the reactions are quenched after distinct reaction times and the reaction products isolated and characterized. There are several disadvantages of such experiments: a large number of syntheses must be performed to explore one reaction at one distinct temperature which is time consuming and also costly; quenching experiments are dangerous because one cannot be sure that the reaction processes occurring at elevated temperatures are really frozen during the quenching procedure. *In situ* experiments are more suitable because crystallization processes and reaction kinetics can be studied without disturbing the reacting system. In several contributions it has been demonstrated that *in situ* EDXRD using synchrotron radiation is a powerful method [102, 131, 167 – 178]. The *in situ* approach allows continuous monitoring of the syntheses, and much more data are obtained for one reaction in comparison to *ex situ* experiments. An important advantage of the *in situ* technique is the possibility of observing the formation of intermediate phases and their transformation into the final products. Using the high-energy and brilliant synchrotron radiation, EDXRD allows monitoring reactions at short time scales, and under special conditions X-ray powder patterns can be collected within a few seconds.

Table 10. Thioantimonates(V).

	Ref.
[Sm(en)$_4$]SbS_4 · 0.5en	[163]
[Sm(en)$_3$(H_2O)(μ-SbS_4)]*	[163]
[La(en)$_3$(μ_3-SbS_4)]*	[162]
[Nd(en)$_3$(H_2O)(μ_2-SbS_4)]*	[162]
[Eu(en)$_4$]SbS_4 · 0.5en	[162]
[Dy(en)$_4$]SbS_4 · 0.5en	[162]
[Yb(en)$_4$]SbS_4 · 0.5en	[162]
[Ni(*trans*-1,2-dach)$_3$]$_3$(SbS_4)$_2$ · $4H_2O$	[163]
[Co(*trans*-1,2-dach)$_3$]$_3$(SbS_4)$_2$ · $4H_2O$	[164]
[Co(dien)$_2$][Co(tren)SbS_4]$_2$ · $4H_2O$*	[164]
[Ni(en)$_3$](enH)SbS_4	[28]
[Ni(tren)SbS_4](paH)*	[165]
[Mn(tren)(trenH)]SbS_4	[161]
[Mn(*trans*-1,2-dach)$_3$]$_2$[Mn(*trans*-1,2-dach)$_2$(SbS_4)$_2$]·$6H_2O$*	[161]
[Ce(dien)$_2$(μ_3-SbS_4)]$_n$*	[141]
(trenH$_3$)SbS_4	[166]

For such *in situ* EDXRD experiments of solvothermal syntheses special reaction cells are required which were developed in our laboratory a few years ago [171]. In the following some selected results of *in situ* EDXRD studies are discussed. It is beyond the scope of this review to present all details of the investigations, and the reader should consult the references for more information.

The results of the *in situ* EDXRD study of the crystallization of [Mn(1,3-dap)$MnSb_2S_5$] (see above) performed under solvothermal conditions have demonstrated that the induction time is significantly reduced with increasing reaction temperature. At $T > 105$ °C all

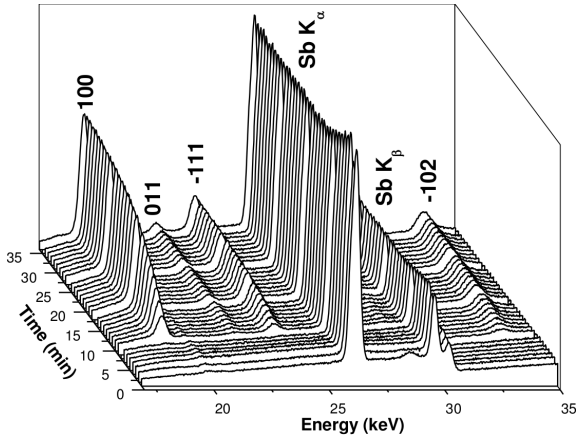

Fig. 51. Time-resolved powder pattern recorded at 110 °C for the formation of [Mn(1,3-dap)$MnSb_2S_5$] (see text). For the most intense reflections the indices are given, and the Sb fluorescence lines are marked. (Reprinted with permission from [171].)

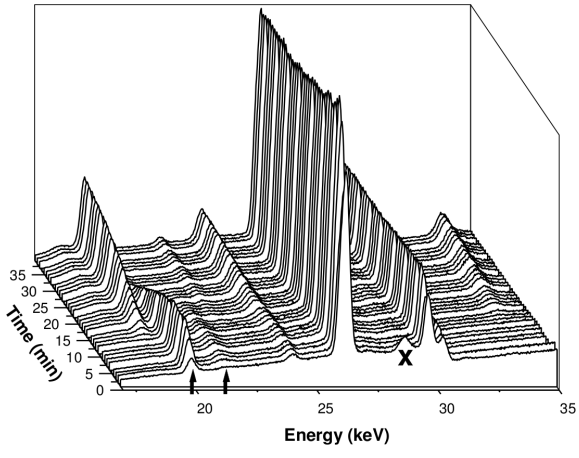

Fig. 52. The sequence of powder patterns recorded at 150 °C showing the occurrence of the two crystalline intermediates in which the most intense lines of the first (cross) and second (arrows) intermediate are marked (*c.f.* Fig. 51). (Reprinted with permission from [171].)

product reflections grow simultaneously, and the reaction is finished within several hours (Fig. 51).

At lower temperatures two crystalline intermediates are detected (Fig. 52) of which the first one decays within a very short time. The intensities of the reflections of the second crystalline intermediate first grow and then start to decay as the product growth starts.

A detailed analysis of the extent of reaction α suggests that a small fraction of the intermediate is either dissolved or converted into an amorphous state, followed by fast crystallization of the product (Fig. 53).

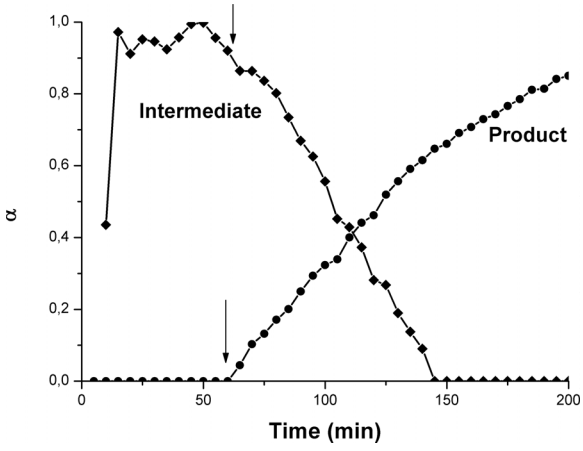

Fig. 53. Extent of reaction α for the second crystalline intermediate and the product at T = 105 °C (*c.f.* Figs. 51, 52). (Reprinted with permission from [171].)

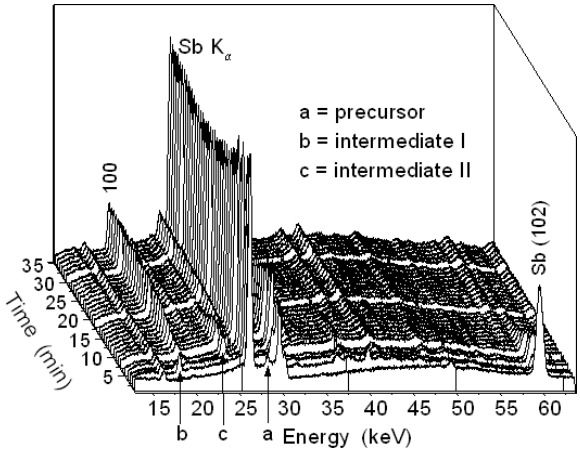

Fig. 54. Time-resolved diffraction pattern of [Mn(dien)-$MnSb_2S_5$] at T = 130 °C. The three crystalline intermediates are marked with a, b, and c. (Reprinted with permission from [172].)

The evaluation of the crystallization kinetics shows that similar mechanisms dominate at temperatures between 105 and 125 °C. A good agreement is obtained with a first-order reaction and/or phase boundary-controlled mechanisms. At later stages of the reaction the mechanism seems to change, suggesting consecutive and/or parallel kinetics as the reaction proceeds. At 130 °C and $\alpha > 0.75$ a three-dimensional diffusion-controlled process dominates.

Very different behaviors were observed for L = mdap and dien. Performing the synthesis with mdap down to the lowest temperature no crystalline intermediates could be detected. The evaluation of the

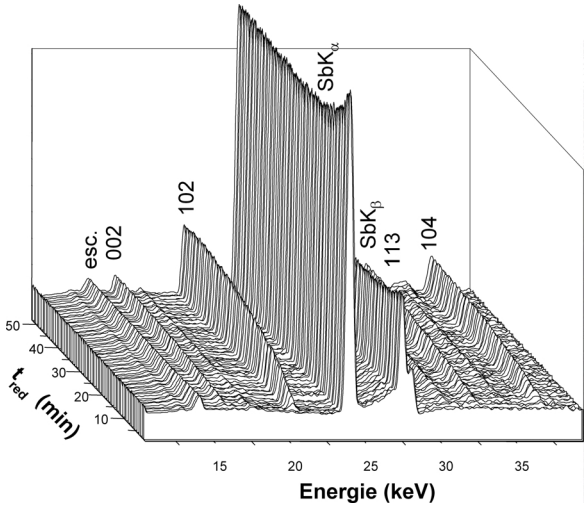

Fig. 55. Powder patterns recorded at a reaction temperature of 120 °C for the formation of [Co(tren)Sb_2S_4]. Reflection indices and Sb K fluorescences are marked. (Reprinted with permission from [173].)

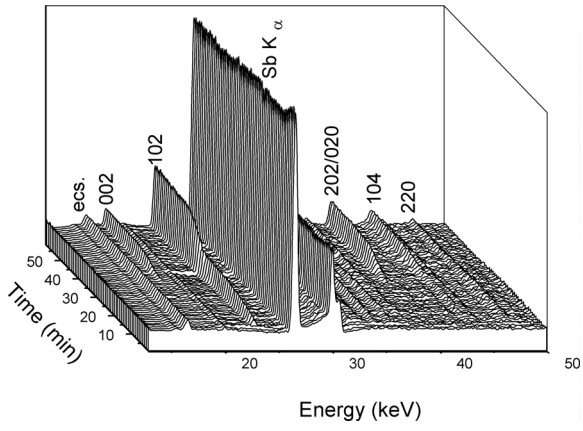

Fig. 56. The evolution of the reflection intensities recorded at 120 °C demonstrating the different growth behavior compared to that displayed in Fig. 55, see text. (Reprinted with permission from [173].)

crystallization kinetics suggest that up to α = 0.8 the reaction is dominated by nucleation, and that a diffusion-controlled mechanism dominates at later stages.

In contrast, applying dien at least three crystalline phases occur (Fig. 54) before the product starts to grow.

The crystallization seems to be diffusion-controlled and faster than for the 1,3-dap and mdap compounds. Conversion experiments were performed heating the compounds with L = 1,3-dap or mdap in a dien solution. The *in situ* EDXRD patterns show a conversion to the dien product, and the analysis of the data revealed that the two educts are dissolved followed by crystallization of the dien-containing material. The activation energy for the crystallization of the mdap-containing sample was estimated to about 65(5) kJ/mol, and to 73(3) kJ/mol for L = dien. The results of these studies have demonstrated that even for compounds with very similar network topologies the crystallization mechanisms differ significantly.

In a further study we combined *in situ* EDXRD with *in situ* X-ray absorption fine structure spectroscopy (EXAFS). The formation of [Co(tren)Sb_2S_4] (see above) was investigated at different reaction temperatures and using different Co sources. In most reactions all product reflections grow simultaneously suggesting that after *in situ* formation of the layered material these layers adopt the three-dimensional long-range ordering within a very short time period (see Fig. 55). The analysis of the crystallization kinetics suggests a change of the crystallization mechanism as the reaction progresses. At the early stages of the reaction diffusion seems to play the most important role, whereas at later stages a more complex behavior is observed. At the end of the reaction a second Co-free phase is formed which coexists with [Co(tren)Sb_2S_4]. The results of the studies suggest that the second phase is not formed by decomposition of [Co(tren)Sb_2S_4] but rather due to the very low Co^{2+} concentration in the solution.

In some reactions a very different behavior was observed. After the induction period first only one intense reflection could be detected and after a distinct time all other reflections of the product phase grew simultaneously (Fig. 56).

This unusual behavior indicates that first layers are formed which show no three-dimensional long-range order, and at later stages this ordering occurs. The *in situ* EXAFS experiments performed at the Sb *K*-edge provided evidence that independent of the reaction time, the Sb : S ratio, and the amine applied only the two species [SbS_3] and [SbS_4] coexist in solution in an approximate 50 : 50 ratio. Furthermore, the changes in the spectra give clear hints that an amorphous phase is formed at intermediate stages.

The results of the experiments are schematically summarized in Fig. 57. After dissolution of the starting materials the dissolved species condense forming layers which are directly organized in a three-dimensional long-range order (pathway 4 in Fig. 57) or which form

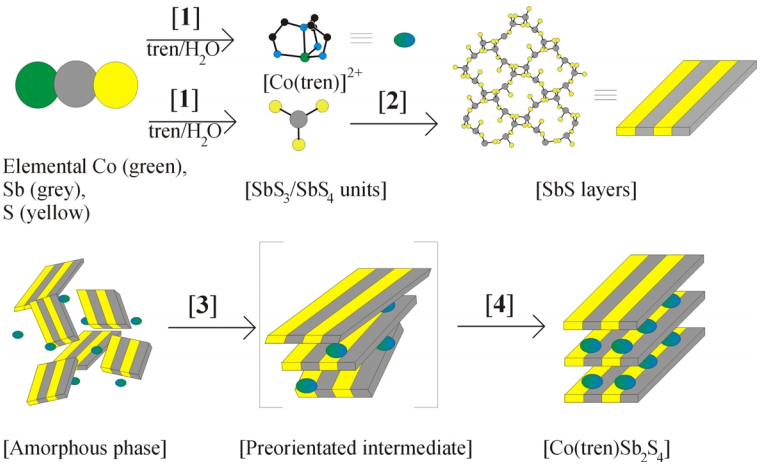

Fig. 57 (color online). Reaction scheme for the formation of $[Co(tren)Sb_2S_4]$. (Reprinted with permission from [173].)

the intermediate (pathway 3 in Fig. 57) leading to the unusual growth behavior.

In several experiments a soluble Co salt was used as starting material. In all reactions only one reaction pathway could be observed, and in all powder patterns the reflections of the product started to grow simultaneously. We concluded from these experiments that elemental Co adhered at the surface of the magnetic stirrer stick, and dissolution of Co was somewhat arbitrary.

Solvothermal reactions are influenced by a large number of different parameters which are not well understood in detail. Several efforts were undertaken to improve the knowledge and to shed light on heterogeneous multicomponent reactions.

The layered compound $(Me_4N)_2Sn_3S_7$ was investigated as case study, and the ion exchange capability with alkali and earth alkali metal cations [93], the tuning of the optical band gap by partial substitution of S with Se [179] or the influence of microgravity onto the self-assembly of the layered structure [92] were studied.

However, all these investigations gave only details about the properties of a compound, and no conclusions could be drawn concerning the formation mechanisms and crystallization kinetics. Such information can only be acquired using *in situ* methods like *in situ* energy dispersive X-ray diffraction (*in situ* EDXRD) [131]. According to a first study using this technique the thiostannate anions produced by dissolving Sn and S in aqueous Me_4NOH solution form anionic layers by condensation, and after some time the three-dimensional orientation of the layered anions is achieved (Fig. 58).

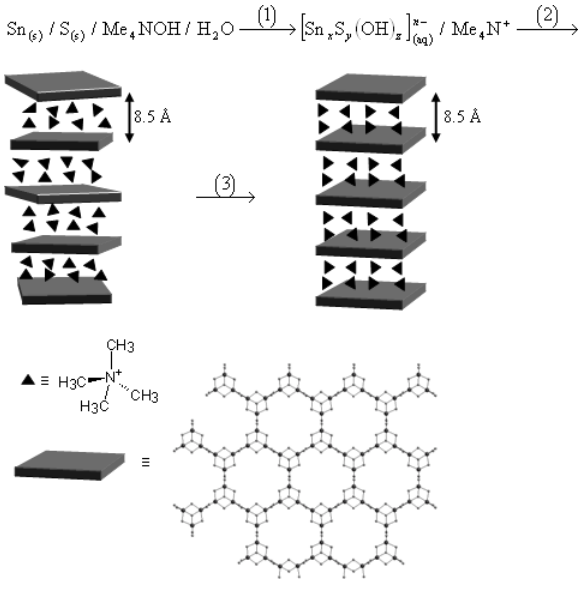

Fig. 58. Scheme of the postulated mechanism of the formation of $(Me_4N)_2Sn_3S_7$: (1) solid reactants are dissolved and form thiostannate anions and methylammonium cations; (2) condensation and preorientation of the layers followed by three-dimensional ordering of the layers (3). (Reprinted with permission from [131].)

As mentioned above we applied *in situ* EDXRD investigations very successfully for monitoring solvothermal syntheses of thiometallates and other compounds [102, 171 – 173]. The great potential of this method was recently demonstrated studying the solvothermal synthesis using Sn, Cu, S, and DBN [102]. The two thiostannates $(DBNH)_2Sn_3S_6$ and $(DBNH)_2Cu_6Sn_2S_8$ coexist under the chosen reaction conditions, and interestingly $(DBNH)_2Sn_3S_6$ is a

Cu-free mixed-valent product with Sn(II) and Sn(IV). In order to obtain crystals of $(DBNH)_2Cu_6Sn_2S_8$ with a sufficient quality for a single-crystal structure determination the reaction time must be extended from 5 d up to 27 d. However, longer reaction times are not always an advantage because binary sulfides may be more stable than the complex thiostannate compounds.

To understand the complex reactions occurring under the solvothermal conditions and to optimize the synthesis conditions leading to crystallization of only one of the two compounds mentioned above, many *ex situ* experiments and also time-resolved *in situ* EDXRD investigations were undertaken. First the influence of the reaction temperature onto the product formation was investigated. The results have demonstrated that the induction time, which is the time until the first crystallites are observed, decreases with increasing reaction temperature, *i. e.*, the formation of the compounds is much faster at elevated temperatures. In further studies the influence of Cu on product formation, especially on the crystallization of the mixed-valent compound, was followed *in situ*. It is quite remarkable that in this case the induction time decreases drastically, and the Cu-free mixed-valent compound is formed after a very short time. In the presence of Cu in the reaction mixture, the nucleation and crystallization of $(DBNH)_2Cu_6Sn_2S_8$ is preferred, and the growth of $(DBNH)_2Sn_3S_6$ is significantly retarded.

Conclusions

During the last decade a large number of hybrid inorganic-organic thioantimonates and thiostannates have been synthesized under mild solvothermal conditions in the temperature range between 100 and 200 °C. As the synthesis parameters can be greatly varied, it can be expected that many more thiometallates will be reported in the future. The flexible coordination behavior of Sb(III) and the strong condensation tendency of the primary $[SbS_x]$ ($x = 3-5$) units allows to generate networks with structural dimensionalities ranging from isolated thioantimonate anions to three-dimensional networks. Interestingly, the tetrahedral $[SbS_4]^{3-}$ anion with Sb(V) exhibits no condensation tendency, and its structural chemistry is less diverse than that of thioantimonates(III). In many thioantimonates(III) the structure-directing effect of the protonated amine molecules or transition metal complexes is obvious. These molecules lead to the formation of large pores in the networks and become located mainly above/below these pores. Another striking feature of the thioantimonate and thiostannate chemistry is the occurrence of extended S···H hydrogen bonding interactions. In most crystals the structure-directing molecules are oriented with respect to the anionic networks optimizing these interactions.

The coordination preference of transition metals can be used for the synthesis of networks with different topologies and different connection modes of the primary thiometallate units. In most syntheses a sulfur excess is supplied, but the polysulfide species which are present in the reaction solution are seldom found in the structures of the thiometallates. In contrast to the lighter homologous element As, antimony has no pronounced tendency for homologous bond formation, and only one compound with a Sb–Sb bond was reported until now.

In the presence of suitable multidentate amines and transition metal cations thioantimonates and thiostannates can act as ligands forming compounds of different complexity. The structural chemistry of thiostannates is dominated by the $[SnS_4]^{4-}/[Sn_2S_6]^{4-}$ anions, and in contrast to Sb(III) the Sn(IV)/Sn(II) cations show no tendency to extend the coordination geometry.

Analyzing the synthesis conditions of the relatively large number of thioantimonate and thiostannate compounds no general rules can be formulated which may lead to more rational syntheses. The number of reaction parameters is too large, and there have been only very few systematic studies exploring the influence of temperature, time, starting materials, concentration of amine *etc*. The results of several *in situ* X-ray diffraction studies performed under real solvothermal conditions gave some insights into the crystallization kinetics and stability of thiometallates, but many more such studies are needed before general trends or rules can be formulated.

Acknowledgements

The authors thank the State of Schleswig-Holstein and the Deutsche Forschungsgemeinschaft (DFG) for financial support. The authors gratefully acknowledge the contributions of the members of the group working in thiometallate chemistry.

[1] W. S. Sheldrick, M. Wachhold, *Coord. Chem. Rev.* **1998**, *176*, 211 – 322.
[2] W. S. Sheldrick, *J. Chem. Soc., Dalton Trans.* **2000**, 3041 – 3052.
[3] X. Bu, N. Zheng, P. Feng, *Chem. Eur. J.* **2004**, *10*, 3356 – 3362.
[4] P. Feng, X. Bu, N. Zheng, *Acc. Chem. Res.* **2005**, *38*, 293 – 303.
[5] M. G. Kanatzidis, *Adv. Mater.* **2007**, *19*, 1165 – 1181.
[6] S. Dehnen, M. Melullis, *Coord. Chem. Rev.* **2007**, *251*, 1259 – 1280.
[7] Q. Zhang, X. Bu, Z. Lin, T. Wu, P. Feng, *Inorg. Chem.* **2008**, *47*, 9724 – 9726.
[8] J. Zhou, J. Dai, G.-Q. Bian, C.-Y. Li, *Coord. Chem. Rev.* **2009**, *253*, 1221 – 1247.
[9] A. Rabenau, *Angew. Chem.* **1985**, *97*, 1017 – 1032; *Angew. Chem., Int. Ed. Engl.* **1985**, *24*, 1026 – 1040.
[10] W. S. Sheldrick, M. Wachhold, *Angew. Chem.* **1997**, *109*, 214 – 234; *Angew. Chem., Int. Ed. Engl.* **1997**, *36*, 206 – 224.
[11] T. Jiang, A. Lough, G. A. Ozin, R. L. Bedard, *J. Mater. Chem.* **1998**, *8*, 733 – 741.
[12] M. Schur, W. Bensch, *Z. Kristallogr.* **1997**, *212*, 305 – 307.
[13] M. Schur, W. Bensch, *Z. Anorg. Allg. Chem.* **1998**, *624*, 310 – 314.
[14] H. Rijnberk, C. Näther, M. Schur, I. Jeß, W. Bensch, *Acta Crystallogr.* **1998**, *C54*, 920 – 923.
[15] H. Rijnberk, C. Näther, W. Bensch, *Z. Anorg. Allg. Chem* **1999**, *625*, 1172 – 1176.
[16] X. Wang, F. Liebau, *Acta Crystallogr.* **1996**, *B52*, 7 – 15.
[17] X. Wang, F. Liebau, *Z. Kristallogr*. **1996**, *211*, 437 – 439.
[18] R. Stähler, W. Bensch, *Z. Anorg. Allg. Chem.* **2002**, *628*, 1657 – 1662.
[19] R. Kniep, D. Mootz, U. Severin, H. Wunderlich, *Acta Crystallogr.* **1982**, *B38*, 2022 – 2023.
[20] J. J. Vittal, P. A. W. Dean, *Acta Crystallogr.* **1996**, *C52*, 1180 – 1182.
[21] P. A. W. Dean, J. J. Vittal, N. C. Payne, *Can. J. Chem.* **1985**, *63*, 394 – 400.
[22] G. Barone, T. G. Hibbert, M. F. Mahon, K. C. Molloy, I. P. Parkin, L. S. Price, I. Silaghi-Dumitrescu, *J. Chem. Soc., Dalton Trans.* **2001**, 3435 – 3445.
[23] P. G. Harrison, B. J. Haylett, T. J. King, *Inorg. Chim. Acta* **1983**, *75*, 259 – 264.
[24] J. Potenza, D. Mastropaolo, *Acta Crystallogr.* **1973**, *B29*, 1830 – 1835.
[25] Q.-H. Wang, *Acta Crystallogr.* **2006**, *E62*, m1936–m1937.
[26] M. Schur, A. Gruhl, C. Näther, I. Jess, W. Bensch, *Z. Naturforsch.* **1999**, *54b*, 1524 – 1528.
[27] R. J. E. Lees, A. V. Powell, A. M. Chippindale, *Polyhedron* **2005**, *24*, 1941 – 1948.
[28] D.-X. Jia, Y. Zhang, J. Dai, Q.-Y. Zhu, X.-M. Gua, *J. Solid State Chem.* **2004**, *177*, 2477 – 2483.
[29] A. Bondi, *J. Phys. Chem.* **1964**, *68*, 441 – 451.
[30] K. Volk, P. Bickert, R. Kolmer, H. Schäfer, *Z. Naturforsch.* **1979**, *34b*, 380 – 382.
[31] H. A. Graf, H. Schäfer, *Z. Anorg. Allg. Chem.* **1975**, *414*, 211 – 219.
[32] G. Cordier, C. Schwidetzky, H. Schäfer, *J. Solid State Chem.* **1984**, *54*, 84 – 88.
[33] H.-O. Stephan, M. G. Kanatzidis, *Inorg. Chem.* **1997**, *36*, 6050 – 6057.
[34] R. Kiebach, F. Studt, C. Näther, W. Bensch, *Eur. J. Inorg. Chem.* **2004**, 2553 – 2556.
[35] W. Bensch, C. Näther, R. Stähler, *Chem. Commun.* **2001**, 477 – 478.
[36] L. Engelke, W. Bensch, *Acta Crystallogr.* **2003**, *E59*, m378 – m380.
[37] M. Schaefer, C. Näther, W. Bensch, *Monatsh. Chem.* **2004**, *135*, 461 – 470.
[38] M. Schur, W. Bensch, *Eur. J. Solid State Inorg. Chem.* **1997**, *34*, 457 – 466.
[39] A. Puls, M. Schaefer, C. Näther, W. Bensch, A. V. Powell, S. Boissière, A. M. Chippindale, *J. Solid State Chem.* **2005**, *178*, 1171 – 1181.
[40] A. M. Zhu, D. X. Jia, P. Wang, Y. Zhang, *Chin. J. Struct. Chem.* **2007**, *26*, 1296 – 1300.
[41] W. B. Wang, A. M. Zhu, D. X. Jia, Y. Zhang, *Chem. Res. Appl.* **2007**, *19*, 1017 – 1024.
[42] R. Kiebach, A. Griebe, C. Näther, W. Bensch, *Solid State Sci.* **2006**, *8*, 541 – 547.
[43] P. Vaqueiro, D. P. Darlow, A. V. Powell, A. M. Chippindale, *Solid State Ionics* **2004**, *172*, 601 – 605.
[44] V. Spetzler, C. Näther, W. Bensch, *Z. Naturforsch.* **2006**, *61b*, 715 – 720.
[45] H. Lühmann, Z. Rejai, K. Möller, P. Leisner, M.-E. Ordolff, C. Näther, W. Bensch, *Z. Anorg. Allg. Chem.* **2008**, *634*, 1687 – 1695.
[46] M. Zhang, T. L. Sheng, X. H. Huang, R. B. Fu, X. Wang, S. M. Hu, S. C. Xiang, X. T. Wu, *Eur. J. Chem.* **2007**, 1606 – 1612.
[47] J. Zhou, G. Q. Bian, Y. Zhang, J. Dai, N. Cheng, *Z. Anorg. Allg. Chem.* **2007**, *633*, 2701 – 2705.
[48] M. Schaefer, R. Stähler, W.-R. Kiebach, C. Näther, W. Bensch, *Z. Anorg. Allg. Chem.* **2004**, *630*, 1816 – 1822.
[49] A. V. Powell, R. J. E. Lees, A. M. Chippindale, *J. Phys. Chem. Solids* **2008**, *69*, 1000 – 1006.
[50] R. Stähler, C. Näther, W. Bensch, *J. Solid State Chem.* **2003**, *174*, 264 – 275.

[51] M. Schaefer, D. Kurowski, A. Pfitzner, C. Näther, W. Bensch, *Acta. Crystallogr.* **2004**, *E60*, m183 – m185.
[52] W. Bensch, M. Schur, *Z. Naturforsch.* **1997**, *52b*, 405 – 409.
[53] E. Quiroga-González, C. Näther, W. Bensch, *Z. Naturforsch*. **2009**, *64b*, 1312 – 1318.
[54] A. V. Powell, R. J. E. Lees, A. M. Chippindale, *Inorg. Chem.* **2006**, *45*, 4261 – 4267.
[55] J. B. Parise, Y. Ko, *Chem. Mater.* **1992**, *4*, 1446 – 1450.
[56] G. Dittmar, H. Schäfer, *Z. Anorg. Allg. Chem.* **1977**, *437*, 183 – 187.
[57] G. Dittmar, H. Schäfer, *Z. Anorg. Allg. Chem.* **1978**, *441*, 98 – 102.
[58] G. Dittmar, H. Schäfer, *Z. Anorg. Allg. Chem.* **1978**, *441*, 93 – 97.
[59] B. Eisenmann, H. Schäfer, *Z. Naturforsch.* **1979**, *34b*, 383 – 385.
[60] G. Cordier, H. Schäfer, C. Schwidetzky, *Z. Naturforsch.* **1984**, *39b*, 131 – 134.
[61] W. S. Sheldrick, H.-J. Häusler, *Z. Anorg. Allg. Chem.* **1988**, *557*, 105 – 111.
[62] J. B. Parise, *Science* **1991**, *251*, 293 – 294.
[63] L. Engelke, C. Näther, W. Bensch, *Eur. J. Inorg. Chem.* **2002**, 2936 – 2941.
[64] J. Rijnberk, C. Näther, W. Bensch, *Monatsh. Chem.* **2000**, *131*, 721 – 726.
[65] R. Stähler, C. Näther, W. Bensch, *Eur. J. Inorg. Chem.* **2001**, 1835 – 1840.
[66] A. Puls, C. Näther, W. Bensch, *Acta Crystallogr.* **2006**, *E62*, m674 – m676.
[67] V. Spetzler, R. Kiebach, C. Näther, W. Bensch, *Z. Anorg. Allg. Chem.* **2004**, *630*, 2398 – 2404.
[68] R. Kiebach, C. Näther, W. Bensch, *Z. Naturforsch.* **2004**, *59b*, 1314 – 1319.
[69] R. J. E. Lees, A. V. Powell, A. M. Chippindale, *J. Phys. Chem. Solids* **2007**, *68*, 1215 – 1219.
[70] X. Wang, A. J. Jacobson, F. Liebau, *J. Solid State Chem.* **1998**, *140*, 387 – 395.
[71] R. J. E. Lees, A. V. Powell, D. J. Watkin, A. M. Chippindale, *Acta Crystallogr.* **2007**, *C63*, m27 – m29.
[72] X. Wang, *Eur. J. Solid State Inorg. Chem.* **1995**, *32*, 303 – 312.
[73] A. Puls, C. Näther, R. Kiebach, W. Bensch, *Solid State Sci.* **2006**, *8*, 1085 – 1097.
[74] X. Wang, F. Liebau, *J. Solid State Chem.* **1994**, *111*, 385 – 389.
[75] Y. Ko, K. Tan, J. B. Parise, A. Darovsky, *Chem. Mater.* **1996**, *8,* 493 – 496.
[76] K. Tan, Y. Ko, J. B. Parise, *Acta Crystallogr.* **1994**, *C50*, 1439 – 1442.
[77] X. Wang, L. Liu, A. J. Jacobson, *J. Solid State Chem.* **2000**, *155*, 409 – 416.
[78] X. Wang, T.-L. Sheng, J.-S. Chen, S.-M. Hua, R.-B. Fu, X.-T. Wu, *J. Mol. Struct.* **2009**, *936*, 142 – 146.
[79] B. Seidlhofer, C. Näther, W. Bensch, to be published.
[80] R. Kiebach, C. Näther, C. P. Sebastian, B. D. Mosel, R. Pöttgen, W. Bensch, *J. Solid State Chem.* **2006**, *179*, 3082 – 3086.
[81] P. Vaqueiro, A. M. Chippindale, A. V. Powell, *Inorg. Chem.* **2004**, *43*, 7963 – 7965.
[82] R. L. Bedard, S. T. Wilson, L. D. Vail, J. M. Bennett, E. M. Flanigen, *Studies in Surface Science and Catalysis* **1989**, *49*, 375 – 387.
[83] R. L. Bedard, L. D. Vail, S. T. Wilson, E. M. Flanigen, *U. S. Patent* **1989**, 4880761.
[84] R. L. Bedard, L. D. Vail, S. T. Wilson, E. M. Flanigen, *U. S. Patent* **1990**, 4933068.
[85] J.-H. Liao, C. Varotsis, M. G. Kanatzidis, *Inorg. Chem.* **1993**, *32*, 2453 – 2462.
[86] J.-C. Jumas, E. Philippot, M. Maurin, *J. Solid State Chem.* **1975**, *14*, 152 – 159.
[87] T. Jiang, G. A. Ozin, *J. Mater. Chem.* **1998**, *8*, 1099 – 1108.
[88] A. K. Cheetham, G. Férey, T. Loiseau, *Angew. Chem.* **1999**, *111*, 3466 – 3492; *Angew. Chem. Int. Ed.* **1999**, *38*, 3268 – 3292.
[89] T. Jiang, G. A. Ozin, R. L. Bedard, *Adv. Mater.* **1994**, *6*, 860 – 865.
[90] H. Ahari, C. L. Bowes, T. Jiang, A. Lough, G. A. Ozin, R. L. Bedard, S. Petrov, D. Young, *Adv. Mater.* **1995**, *7*, 375 – 377.
[91] T. Jiang, A. Lough, G. A. Ozin, R. L. Bedard, R. Broach, *J. Mater. Chem.* **1998**, *8*, 721 – 732.
[92] Ö. Dag, H. Ahari, N. Coombs, T. Jiang, P. P. Aroca-Ouellette, S. Petrov, I. Sokolov, A. Verma, G. Vovk, D. Young, G. A. Ozin, C. Reber, Y. Pelletier, R. L. Bedard, *Adv. Mater.* **1997**, *9*, 1133 – 1149.
[93] J. B. Parise, Y. Ko, J. Rijssenbeek, D. M. Nellis, K. Tan, S. Koch, *J. Chem. Soc., Chem. Commun.* **1994**, 527.
[94] Y. Ko, K. Tan, D. M. Nellis, S. Koch, J. B. Parise, *J. Solid State Chem.* **1995**, *114*, 506 – 511.
[95] T. Jiang, A. Lough, G. A. Ozin, *Adv. Mater.* **1998**, *10*, 42 – 46.
[96] C. Näther, S. Scherb, W. Bensch, *Acta Crystallogr.* **2003**, *E59*, m280–m282.
[97] J. Li, B. Marler, H. Kessler, M. Soulard, S. Kallus, *Inorg. Chem.* **1997**, *36*, 4697 – 4701.
[98] M. Behrens, C. Näther, W. Bensch, *Z. Anorg. Allg. Chem.* **2002**, *628*, 2160.
[99] H. Pada Nayek, Z. Lin, S. Dehnen, *Z. Anorg. Allg. Chem.* **2009**, *635*, 1737 – 1740.
[100] A. Puls, C. Näther, W. Bensch, *Acta Crystallogr.* **2005**, *E61*, m868–m870.
[101] Y. Ko, C. L. Cahill, J. B. Parise, *J. Chem. Soc., Chem. Commun.* **1994**, 69 – 70.

[102] N. Pienack, C. Näther, W. Bensch, *Eur. J. Inorg. Chem.* **2009**, 937 – 946.
[103] Q. Zhao, D. Jia, Y. Zhang, L. Song, J. Dai, *Inorg. Chim. Acta* **2007**, *360*, 1895 – 1901.
[104] D. X. Jia, A. M. Zhu, J. Deng, Y. Zhang, *Z. Anorg. Allg. Chem.* **2007**, *633*, 1246 – 1250.
[105] M.-L. Fu, G.-C. Guo, B. Liu, A.-Q. Wu, J.-S. Huang, *Chin. J. Inorg. Chem.* **2005**, *21*, 25 – 29.
[106] D.-X. Jia, J. Dai, Q.-Y. Zhu, Y. Zhang, X.-M. Gu, *Polyhedron* **2004**, *23*, 937 – 942.
[107] D.-X. Jia, Y. Zhang, J. Dai, Q.-Y. Zhu, X.-M. Gu, *Z. Anorg. Allg. Chem.* **2004**, *630*, 313 – 318.
[108] M. Behrens, S. Scherb, C. Näther, W. Bensch, *Z. Anorg. Allg. Chem.* **2003**, *629*, 1367 – 1373.
[109] N. Pienack, C. Näther, W. Bensch, *Z. Naturforsch.* **2008**, *63b*, 1243 – 1251.
[110] N. Pienack, C. Näther, W. Bensch, *Eur. J. Inorg. Chem.* **2009**, 1575 – 1577.
[111] X. M. Gu, J. Dai, D. X. Jia, Y. Zhang, Q. Y. Zhu, *Cryst. Growth & Design* **2005**, *5*, 1845 – 1848.
[112] N. Pienack, K. Möller, C. Näther, W. Bensch, *Solid State Sci.* **2007**, *9*, 1110 – 1114.
[113] N. Pienack, C. Näther, W. Bensch, *Solid State Sci.* **2007**, *9*, 100 – 107.
[114] N. Pienack, W. Bensch, *Z. Anorg. Allg. Chem.* **2006**, *632*, 1733 – 1736.
[115] N. Pienack, A. Puls, C. Näther, W. Bensch, *Inorg. Chem.* **2008**, *47*, 9606 – 9611.
[116] M. Baiyin, L. Ye, Y. An, X. Liu, C. Jia, G. Ning, *Bull. Chem. Soc. Jpn.* **2005**, *78*, 1283 – 1284.
[117] Y. An, B. Menghe, L. Ye, M. Ji, X. Liu, G. Ning, *Inorg. Chem. Commun.* **2005**, *8*, 301 – 303.
[118] Y. Wang, M. Baiyin, S. Li, X. Liu, Y. An, G. Ning, *Chem. Res. Chinese U.* **2006**, *22*, 411 – 414.
[119] J. Zhou, G.-Q. Bian, J. Dai, Y. Zhang, A.-B. Tang, Q.-Y. Zhu, *Inorg. Chem.* **2007**, *46*, 1541 – 1543.
[120] N. Pienack, S. Lehmann, H. Lühmann, M. El-Madani, C. Näther, W. Bensch, *Z. Anorg. Allg. Chem.* **2008** , *634*, 2323 – 2329.
[121] R. Stähler, B.-D. Mosel, H. Eckert, W. Bensch, *Angew. Chem.* **2002**, *114*, 4671 – 4673; *Angew. Chem. Int. Ed.* **2002**, *21*, 4487 – 4489.
[122] R. Stähler, Dissertation Universität Kiel, Kiel **2003**.
[123] M. Schur, W. Bensch, *Z. Naturforsch.* **2002**, *57b*, 1 – 7.
[124] W. Bensch, M. Schur, *Eur. J. Solid State Inorg. Chem.* **1996**, *33*, 1149 – 1160.
[125] M. Schur, C. Näther, W. Bensch, *Z. Naturforsch.* **2001**, *56b*, 79 – 84.
[126] L. Engelke, R. Stähler, M. Schur, C. Näther, W. Bensch, R. Pöttgen, M. H. Möller, *Z. Naturforsch.* **2004**, *59b*, 869 – 876.
[127] M. Schaefer, C. Näther, N. Lehnert, W. Bensch, *Inorg. Chem.* **2004**, *43*, 2914 – 2921.
[128] A. Puls, C. Näther, W. Bensch, *Z. Anorg. Allg. Chem.* **2006**, *632*, 1239 – 1243.
[129] X. Wang, T.-L. Sheng, S.-M. Hu, R.-B. Fu, X.-T. Wu, *Inorg. Chem. Commun.* **2009**, *12*, 399 – 401.
[130] Z. Rejai, C. Näther, R. K. Kremer, W. Bensch, *Inorg. Chem.* **2010**, *49*, 1651 – 1657.
[131] R. J. Francis, S. J. Price, J. S. O Evans, S. O'Brien, D. O'Hare, S. M. Clark, *Chem. Mater.* **1996**, *8*, 2102 – 2108.
[132] R. Stähler, W. Bensch, *Eur. J. Inorg. Chem.* **2001**, 3073 – 3078.
[133] R. Kiebach, W. Bensch, R.-D. Hoffmann, R. Pöttgen, *Z. Anorg. Allg. Chem.* **2003**, *629*, 532 – 538.
[134] H.-O. Stephan, M. G. Kanatzidis, *J. Am. Chem. Soc.* **1996**, *118*, 12226 – 12227.
[135] R. Kiebach, R. Warratz, C. Näther, W. Bensch, *Z. Anorg. Allg. Chem.* **2009**, *635*, 988 – 994.
[136] M. Schur, H. Rijnberk, C. Näther, W. Bensch, *Polyhedron* **1998**, *18*, 101 – 107.
[137] R. Stähler, W. Bensch, *J. Chem. Soc.*, *Dalton Trans.* **2001**, 2518 – 2522.
[138] M. Schaefer, C. Näther, W. Bensch, *Solid State Sci.* **2003**, *5*, 1135 – 1139.
[139] K. Möller, C. Näther, A. Bannwarth, W. Bensch, *Z. Anorg. Allg. Chem.* **2007**, *633*, 2635 – 2640.
[140] J. Lichte, H. Lühmann, C. Näther, W. Bensch, *Z. Anorg. Allg. Chem.* **2009**, *635*, 2021 – 2026.
[141] J. Lichte, C. Näther, W. Bensch, *Z. Anorg. Allg. Chem.* **2010**, *636*, 108 – 113.
[142] P. Vaqueiro, A. M. Chippindale, A. V. Powell, *Polyhedron* **2003**, *22*, 2839 – 2845.
[143] N. Pienack, H. Lühmann, W. Bensch, to be published.
[144] M. G. Kanatzidis, N. C. Baenziger, D. Coucouvanis, *Inorg. Chem.* **1983**, *22*, 290 – 292.
[145] A. Puls, C. Näther, W. Bensch, *Acta Crystallogr.* **2006**, *E62*, m1045 – m1047.
[146] K. Tan, Y. Ko, J. B. Parise, J.-H. Park, A. Darovsky, *Chem. Mater.* **1996**, *8,* 2510 – 2515.
[147] R. J. E. Lees, A. V. Powell, A. M. Chippindale, *Acta Crystallogr.* **2005**, *C61*, m516–m518.
[148] A. V. Powell, S. Boissiere, A. M. Chippindale, *Chem. Mater.* **2000,** *12,* 182 – 187.
[149] A. Müller, J. Schimanski, M. Römer, H. Bögge, F.-W. Baumann, W. Eltzner, E. Krickemeyer, U. Billerbeck, *Chimia* **1985**, *39*, 25 – 27.
[150] W. Bubenheim, U. Müller, *Z. Naturforsch.* **1995**, *50b*, 1135 – 1136.
[151] J. B. Parise, Y. Ko, *Chem. Mater.* **1994**, *6*, 718 – 720.
[152] V. Spetzler, H. Rijnberk, C. Näther, W. Bensch, *Z. Anorg. Allg. Chem.* **2004**, *630*, 142 – 148.
[153] V. Spetzler, C. Näther, W. Bensch, *Inorg. Chem.* **2005**, *44*, 5805 – 5812.
[154] A. V. Powell, S. Boissiere, A. M. Chippindale, *Dalton Trans.* **2000**, 4192 – 4195.

[155] A. V. Powell, R. Paniagua, P. Vaqueiro, A. M. Chippindale, *Chem. Mater.* **2002**, *14*, 1220 – 1224.
[156] M. Zhang, T. Sheng, X. Wang, S. Hu, R. Fu, J. Chen, Y. He, Z. Qin, C. Shen, X. Wu, *Cryst. Eng. Comm.* **2010**, *12*, 73 – 76.
[157] V. Spetzler, C. Näther, W. Bensch, *J. Solid State Chem.* **2006**, *179*, 3541 – 3549.
[158] P. Vaqueiro, A. M. Chippindale, A. R. Cowley, A. V. Powell, *Inorg. Chem.* **2003**, *42*, 7846 – 7851.
[159] A. V. Powell, J. Thun, A. M. Chippindale, *J. Solid State Chem.* **2005**, *178*, 3414 – 3419.
[160] M. Jansen, *Angew. Chem.* **1987**, *99*, 1136 – 1149; *Angew. Chem., Int. Ed. Engl.* **1987**, *26*, 1098 – 1110.
[161] M. Schaefer, L. Engelke, C. Näther, W. Bensch, *Z. Anorg. Allg. Chem.* **2003**, *629*, 1912 – 1918.
[162] D. Jia, Q. Zhao, Y. Zhang, J. Dai, J. Zuo, *Inorg. Chem.* **2005**, *44*, 8861 – 8867.
[163] D.-X. Jia, Q.-Y. Zhu, J. Dai, W. Lu, W.-J. Guo, *Inorg. Chem.* **2005**, *44*, 819 – 821.
[164] L. Engelke, C. Näther, P. Leisner, W. Bensch, *Z. Anorg. Allg. Chem.* **2008**, *634*, 2959 – 2965.
[165] R. Stähler, W. Bensch, *Acta Crystallogr.* **2002**, *C58*, m537–m538.
[166] M. Poisot, C. Näther, W. Bensch, *Acta Crystallogr.* **2007**, *E63*, m1751–m1752.
[167] P. Norby, J. Hanson, *J. Catal. Today* **1998**, *39*, 301 – 309.
[168] S. O'Brien, R. Francis, A. Fogg, D. O'Hare, N. Okazaki, K. Koruda, *Chem. Mater.* **1999**, *11*, 1822 – 1832.
[169] A. Christensen, T. Jensen, P. Norby, J. Hanson, *J. Chem. Mater.* **1998**, *10*, 1688 – 1693.
[170] C. L. Cahill, Y. Ko, J. C. Hanson, K. Tan, J. B. Parise, *Chem. Mater.* **1998**, 1453 – 1458.
[171] L. Engelke, M. Schaefer, M. Schur, W. Bensch, *Chem. Mater.* **2001**, *13,* 1383 – 1390.
[172] L. Engelke, M. Schaefer, F. Porsch, W. Bensch, *Eur. J. Inorg. Chem.* **2003**, 506 – 513.
[173] R. Kiebach, N. Pienack, M.-E. Ordolff, F. Studt, W. Bensch, *Chem. Mater.* **2006**, *18,* 1196 – 1205.
[174] R. Kiebach, M. Schaefer, F. Porsch, W. Bensch, *Z. Anorg. Allg. Chem.* **2005**, *631*, 369 – 374.
[175] A. Michailovski, J.-D. Grunwaldt, A. Baiker, R. Kiebach, W. Bensch, G. R. Patzke, *Angew. Chem.* **2005**, *117*, 5787 – 5792; *Angew. Chem. Int. Ed.* **2005**, *44*, 5643 – 5647.
[176] A. Michailovski, R. Kiebach, W. Bensch, J.-D. Grunwaldt, A. Baiker, S. Komarneni, G. R. Patzke, *Chem. Mater.* **2007**, *19*, 185 – 197.
[177] R. Kiebach, N. Pienack, W. Bensch, J.-D. Grunwaldt, A. Michailovski, A. Baiker, T. Fox, Y. Zhou, G. R. Patzke, *Chem. Mater.* **2008**, *20*, 3022 – 3033.
[178] Y. Zhou, N. Pienack, W. Bensch, G. R. Patzke, *Small* **2009**, *5*, 1978 – 1983.
[179] H. Ahari, G. A. Ozin, R. L. Bedard, S. Petrov, D. Young, *Adv. Mater.* **1995**, *7*, 370 – 374.